Optimization of Thin-Walled Packaging

Ronald van Dijk

Optimization of Thin-Walled Packaging

Optimalisatie van dunwandige verpakkingen

Proefschrift
ter verkrijging van de graad van doctor
aan de Technische Universiteit Delft,
op gezag van de Rector Magnificus prof. ir. K. F. Wakker,
voorzitter van het College voor Promoties,
in het openbaar te verdedigen op
op maandag 8 oktober 2001 om 13.30 uur
door

Ronald VAN DIJK

ingenieur industrieel ontwerpen,
geboren te Maassluis.

Dit proefschrift is goedgekeurd door de promotor:
Prof. dr. ir. A. van Keulen

Samenstelling van de promotiecommissie:

Rector Magnificus,	Voorzitter
Prof. dr. ir. A. van Keulen,	Technische Universiteit Delft, promotor
Prof. dr. V.V. Toropov	University of Bradford, Verenigd Koninkrijk
Prof. dr. W.G.M. Agterof	Unilever Research / Universiteit Twente
Prof. dr. ir. A. de Boer	Universiteit Twente
Prof. ir. J.L. Spoormaker	Technische Universiteit Delft
Prof. dr. ir. L.J. Ernst	Technische Universiteit Delft

ISBN 90-9015084-6

Printed by Shaker Publishing BV, Maastricht, The Netherlands

Propositions

accompanying the thesis
Optimization of Thin-Walled Packaging
R. van Dijk

1. The success of optimization relies more on the requirement to quantify previously undefined quality than on the actual optimization.
2. Innovation is an art and can therefore not be automated.
3. An environmental tax on packages which depends on the weight percentage of the package could be advantageous for packaging waste reduction.
4. When governments are technically able to buy the waste generated by the consumer then they can directly regulate this waste stream.
5. Scientific research sponsored by industry is a challenge for all partners involved.
6. Regulations should apply to everyone.
7. 1984* is yet to come. (*George Orwell)
8. Green energy does not exist.
9. It would be very advantageous if we could gain energy out of traffic jams.

Stellingen

behorende bij het proefschrift
Optimization of Thin-Walled Packaging
R. van Dijk

1. Het succes van optimalisatie is eerder te danken aan de noodzaak voorheen vaak ongedefinieerde kwaliteit te kwantificeren dan aan de daadwerkelijke optimalisatie.
2. Innoveren is een kunst en kan hierdoor niet worden geautomatiseerd.
3. Een milieubelasting op verpakkingen welke afhankelijk is van het gewichtspercentage van de verpakking zou afvalverminderend kunnen werken.
4. Op het moment dat de overheid het door de consument gegenereerde afval technisch gezien op kan kopen heeft zij het in haar macht deze afvalstroom direct te reguleren.
5. Wetenschappelijk onderzoek gesponsord door de industrie is een uitdaging voor alle betrokken partners.
6. Regelgeving dient voor iedereen te gelden.
7. 1984* ligt nog voor ons. (*George Orwell)
8. Groene energie bestaat niet.
9. Het zou zeer aantrekkelijk zijn wanneer we energie kunnen winnen uit files.

Aan Olga, Sasha & · · ·

Aan mijn ouders

Contents

Symbol listing

The following notations have been used:

$\mathbf{a}$	=	$\frac{\partial \mathbf{v}}{\partial \mathbf{u}}$
A	=	surface area exposed to permeation
B_a	=	axial blow-up ratio
B_c	=	circumferential blow-up ratio
$\mathbf{D}$	=	mapping between nodal degrees of freedom and generalized strain rates
D_i	=	dissolved amount of gas i
D_i^f	=	initial dissolved amount of gas i at filling temperature
E_a	=	axial Young's modulus
E_c	=	circumferential Young's modulus
f	=	initial fluid fraction
$\mathbf{f}$	=	load vector
$\mathbf{f}^p$	=	load vector due to the gas
f_V^g	=	function which describes the volume change of the structure for internal pressure changes
$\mathbf{G}$	=	geometric stiffness matrix
$\mathbf{G}'$	=	geometric stiffness matrix differentiated to the design variable
$\mathbf{G}_p$	=	gas pressure contribution in geometric stiffness matrix
$\mathbf{G}_{fluid}$	=	hydrostatic pressure contribution in geometric stiffness matrix
h	=	wall thickness of the package
h_f	=	final global wall thickness
h_p	=	preform wall thickness
H	=	height of the air spring
$\mathbf{J}$	=	tangent matrix
$\mathbf{K}$	=	tangent operator
$\mathbf{K}'$	=	tangent operator differentiated to the design variable
l	=	bottle length
L	=	preform length
m	=	number of gases
M	=	mass
n	=	amount of gas (in mol, not dissolved in the fluid)
n^{cr}	=	amount of gas for $p = p^{cr}$
n_i	=	actual amount of gas i (in mol, not dissolved in the fluid)
n_i^f	=	amount of gas i during filling (in mol)
N_i	=	total amount of component i (note:dissolved in the fluid and as gas, N_i is not constant in time)
N_i^0	=	initial total amount of component i (dissolved in the fluid and as gas)

p	=	gas pressure
$\mathbf{p}$	=	reference point for calculation of the enclosed volume
p^*	=	critical pressure load
p_i	=	actual partial gas pressure
p_i^0	=	initial partial gas pressure
p^a	=	ambient pressure
p_i^a	=	partial ambient pressure
p^{equi}	=	post-oxidation equilibrium pressure
p_i^f	=	partial pressure during filling
p^{cr}	=	critical pressure, *i.e.* the internal pressure at which buckling occurs
p_i^{cr}	=	critical partial pressure of gas i
P_i	=	permeability of the structure for gas i
$\mathbf{r}_i$	=	element corner node vectors with respect to reference point $\mathbf{p}$ (i refers to the corner number)
$r_i(p_i)$	=	reaction speed of gas i as function of the its partial pressure per unit volume
r_{max}	=	maximum bottle radius
r_{loc}	=	local bottle radius
R	=	internal preform radius (note: that R is also used as the universal gas constant)
R	=	universal gas constant (note: see above)
$\mathbf{S}$	=	generalized elasticity matrix
s	=	fluid compressibility
s_i	=	initial 'saturation' of the fluid for gas i
$\mathbf{S}$	=	matrix depending on elastic material properties and element definition
S_i	=	solubility of gas i
t	=	time
T	=	actual temperature
$\mathbf{T}$	=	pre-multiplication matrix
T^0	=	initial temperature
T^a	=	ambient temperature
T^f	=	temperature during filling
$\mathbf{u}$	=	nodal degrees of freedom
$\mathbf{u}_i$	=	nodal displacement vector
$\mathbf{v}$	=	buckling mode
v	=	actual volume fraction
v_c	=	critical volume ratio
V	=	total enclosed volume
V^0	=	initial enclosed volume
V_b	=	brimful volume at the onset of paneling
V_i	=	undeformed brimful volume
V^a	=	initial enclosed volume at ambient temperature
V^f	=	total enclosed volume at filling temperature
V_g^f	=	gas volume during filling
V_g^a	=	initial gas volume at ambient temperature
V_g^0	=	initial gas volume
V_g	=	actual gas volume
V_f^f	=	fluid or contents volume at filling temperature
V_f	=	fluid or contents volume at ambient temperature
V_k	=	tetraedrical volume contribution of a single element k

δW^{int}	=	internal virtual work of deformation
δW^{ext}	=	virtual work carried out by external load
δW_p^{ext}	=	virtual work corresponding to the pressure difference
$\mathbf{x}_i$	=	initial corner node location vector
$\boldsymbol{\varepsilon}$	=	generalized deformations
λ	=	load factor
$\boldsymbol{\sigma}$	=	generalized stresses
τ	=	relative temperature
γ	=	volumetric expansion coefficient of the contents
λ	=	linear expansion coefficient of the structure (note: see also below)
λ	=	load factor (note: see also above)
η_i	=	change of the internal amount of gas
Φ_i	=	reacted amount of gas i
Ψ_i	=	permeated amount of gas i
Γ	=	matrix used for description of the second order derivative of the volume
κ	=	$-\frac{dp}{dV}$
ϖ_i	=	reaction or oxidation factor (when i is omitted oxidation is meant)
α	=	volume-pressure compliance of a package
ι	=	design variable
ζ	=	percentage change of the design variable

Chapter 1

Introduction

The yearly produced amount of waste (including separated components) produced per Dutch person increased from 420 kg in 1990 to 512 kg in 1998 [77]. In the same period the percentage of green waste (vegetables, fruit and garden waste) as thrown away in packets reduced from 47% to 33%. While the amount of plastic waste increased from 8.1% to 12% and the amount of un-separated paper waste increased from 25% to 32%. These numbers clearly illustrate the importance of waste and weight reduction. Moreover weight reduction of packaging can lead to significant cost savings. The latter is of more direct importance to industry and has been the actual reason for Unilever Research to pursue the present research.

In near future, governments will put more emphasis on material reduction by taxing the pollution and recycling of plastic packaging is currently a 'hot topic'. It can therefore be expected that waste management for packaging will play even a more prominent role. A typical package is the plastic bottle which is commonly used for food and non-food products. In 1995, generally three types of manufacturing techniques for plastic bottles could be distinguished [55]: extrusion blow molding, extrusion stretch blow molding and injection stretch blow molding as depicted in Figure 1.1. From which extrusion blow moulding belongs to the older techniques and injection stretch blow moulding to the latest technology.

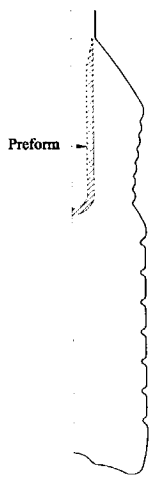

Figure 1.1: *During injection stretch blow moulding a preform is heated and respectively stretched with a rod and blown to its final bottle shape.*

However depending on the contents of the package and the packaging material all techniques are currently still in use.

In 1995 many bottles were made from PVC, since the material properties of PVC with respect to its chemical inertness and permeability are excellent. The introduction of extrusion stretch blow molding allowed weight savings of approximately 16 % for a 1 litre bottle using the same source material. Currently, PVC favours a bad public opinion which is one of the reasons that many bottles are made of PET using the injection stretch blow molding technique. Additionally this technique reduced the weight of a 1 litre bottle further with 13–25%. The previously mentioned weight changes were mainly due to new manufacturing techniques while only little attention has been paid to the real requirements for packaging and the design of packaging. It is here where the actual problem occurs. The development of packaging is still based for a large extent on experience and trial and error. Therefore, most requirements for packages are historical and in some cases the origin of these requirements can not be determined, while others are applied without thorough examination how the involved process interacts with the package. An example of the latter is permeation. Permeation is commonly blamed for the occasionally disappearing of the complete initial gas volume in the package. However, as shown in this thesis, permeation has almost a negligible affect on the behavior of the structure and the quality of the contents for the package studied here. It should therefore be considered if the permeability requirement should be maintained. In the present thesis the relevant processes will be examined. Consequently, examination of these processes leads to the definition of more realistic requirements. Finally, these requirements can be used as constraints during optimization of the package. Only the above described method leads to significant potential material savings without affecting the quality of the package.

The present thesis describes the optimization of thin walled packages. This thesis is for a large extent based on papers and conference proceedings published during the duration of this research. In each chapter new aspects required for a complete description of the involved problems are introduced. The synthesis takes place in the before last chapter where the optimization problem is concluded with a significantly lighter bottle. Moreover, the last chapter describes an optimization methodology which can be applied for many similar packages.

In Figure 1.2 two bottles are depicted which have been used throughout this thesis to study the relevant processes. In Chapter 2 two tests are described which are currently carried out for this type of package: empty top load testing and vacuum resistance testing. Each bottle has to meet a specified empty compression strength and a certain vacuum resistance (see also Chapter 2). The empty compression strength is motivated by the required resistance during stacking while a certain vacuum resistance is required to prevent paneling. Paneling has been described earlier by Penzkofer [50] and Tsiourvas *et al.* [64]. Tsiourvas *et al.* indicated that the paneling can be prevented by applying a circumferential ribbing such that the bottle can deform like a 'harmonica'. The latter was emphasized with experimental work. Similar attempts where paneling is controlled in such a way that it is invisible to the customer are described in many patents [2,3,12,16–19]. Penzkofer [50] quantified paneling for cylindrical (not ribbed) bottles as a function of oxidation of the contents and permeation. Since, we would like to optimize this type of package prior manufacturing a start has been made to simulate the behavior of these bottles using FEA (Finite Element Analysis).

The empty compression strength is a measure which still dates from the past where plastic bottles did not have a neck support ring, similar to glass bottles. In such cases the force required to apply a snap–on cap had to be carried by the complete bottle since it was only supported at its base. Currently, a neck support ring replaces this function. However, requirements with respect to the empty compression strength are still being used. The compression strength has been investigated in Chapter 3 which showed a large difference between empty and filled bottles. One can therefore conclude that rejecting the empty compression strength gives potential material savings. Rejecting of the empty top load requirements should however be accompanied by additional specifications for the closure of the package. Simulation of gas-fluid filled structures also introduced numerical problems. These problems have been discussed and solved in this chapter. However, still there was a discrepancy between numerical and simulated results for gas-fluid filled structures. Investigation of this problem led to the implementation of solubility

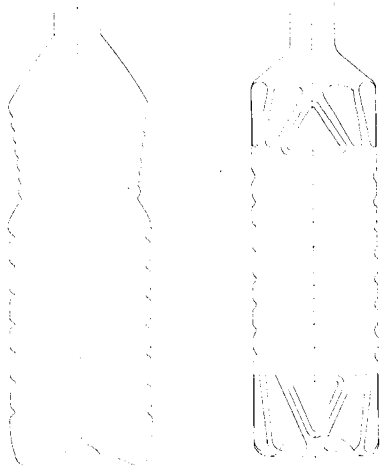

(a) (b)

Figure 1.2: *a) Round bottle for 750 ml of vegetable oil. b) Square bottle for 1000 ml of olive oil.*

effects, which are rarely investigated [37, 38], in the simulations as described in Chapter 4. Hereafter, a remarkable match between numerical and experimental results has been obtained.

Design sensitivities [14] are a way to investigate how a structure responds to small design changes. The deformation induced pressure influences on the calculation hereof. How the latter has been implemented numerically is described in Chapter 5 and illustrates once more the relevance of solubility effects.

For a complete optimization of the involved bottle as depicted in Figure 1.2a, further examination of the involved processes is described in Chapter 6. Here, the optimization of the bottle will be progressed while neglecting empty compression strength requirements. Moreover, it will be assumed that the filled compression strength is sufficient. In Chapter 6 distinction is made between three types of packaging: rigid, non-resistant and flexible packages. For these packages all the processes acting on the package have been taken into account. Similar studies were carried out by Talasila *et al.* [61] and Herlitze [34]. However both examined only rigid and non-resistant packages. Effects of oxidation and permeation are more often subject of research for very thin–walled packages *e.g.* pouches or films [41, 45, 49]. The latter fall in the non-resistant (pouches) and rigid category (tubs sealed with a film). Simulations which examined all the relevant effects let to a simplification by neglecting the permeability effects. In Chapter 7 the problem is narrowed down even further by the introduction of a new parameter in the design of plastic bottles, the volume-pressure compliance. Moreover, it has been illustrated that the behavior of the structure is mainly determined by the nitrogen gas. This observation created the capability to predict the internal pressure easily. During this prediction only a small error is introduced due to a piece-wise linearization of the bottle-behavior.

In Chapter 8 optimization of the whole bottle is discussed while taken into account the simplifications as described in the earlier chapters. This chapter illustrates that the optimal bottle design can be determined automatically if the constraints are available. Therefore future geometrical changes in the bottle-design can be followed by an optimization which determines the optimal ribbing. The latter takes care that the optimality of the bottle is maintained for each design change. This also prevents excessive material usage in current and future designs.

Combination of all involved processes in an optimization problem where the design of the bottle is determined automatically has not been carried out before. The present thesis describes an attempt to approach this optimization problem leading to significant material savings. However, the described approach has its limitations. It has not been described how the oxidation process takes place exactly. The latter might be of interest for products with a short shelf life and in a situation where one wants to cut down the packaging costs as far as possible. Another limitation is the time dependent behavior of the package. If a certain under-pressure exists for a long period of time then the package will not return to its initial shape after unloading. This might cause a complete disappearing of the initial gas volume depending on the initial gas-fluid ratio and the saturation of the contents. This effect has not been studied in this thesis.

Finally, in Appendix A application of optimization methods on another application, namely a tub, has been discussed. Here a plastic tub is optimized with respect to its weight. The initial set of design variables has been reduced with the help of sensitivity analysis which indicated the most relevant variables. Hereafter, the more expensive optimization tool Multi-point Approximation Method [76] (MAM) was used to determine the optimal tub design.

Based on: R. van Dijk, J.C. Sterk, D. Sgorbani and F. van Keulen, Lateral Deformation of Plastic Bottles Experiments, Simulations and Prevention, Packaging Technology and Science, 11, 91–117 (1998).

Chapter 2

Lateral Deformation of Plastic Bottles

Mass reduction of plastic bottles containing non-carbonated liquids calls for advanced design approaches. Weight reduction of bottles consequently influences the mechanical performance of the bottle. This performance involves top load, vacuum and impact resistance. This chapter studies the lateral deformation of a bottle due to an internal vacuum. Similar studies have been carried out before, but till so far the allowable deformation has never been related to the initial headspace of the bottle. If a bottle design is able to compensate for a potential vacuum in an aesthetic manner, then paneling will not occur. Changing the vacuum resistance of a bottle will result in a different top load. Current computational techniques enhance the understanding of the problem and provide tools to achieve solutions for the described above.

2.1 Introduction

The use of lightweight plastic bottles in the foods industry is still growing. It is commonly accepted that plastic packs have a number of advantages over glass packaging, namely, they are lighter, almost unbreakable and cheaper [55]. Furthermore, if the plastic pack is properly recycled it is more environmental friendly, as less energy is required to produce a bottle. Of course the plastic pack is also accompanied with disadvantages. These involve the top load strength, vacuum resistance and permeability, which are superior for the glass bottle. A severe complication is that a sufficient underpressure in the plastic bottle will finally result in a substantial deformation [66]. This phenomenon is often denoted as paneling and results in an unaesthetic pack that gives the consumer the impression that something happened with the contents. Plastic containers are sensitive to this type of deformation due to the relatively low bending stiffness of the bottle wall. This is the result of a relatively lower Young's modulus (approximately 30 times less) and much thinner walls in comparison with glass bottles. Paneling is currently an important factor that hinders further weight reduction of plastic bottles.

Paneling of a bottle is caused by an underpressure that can arise due to one or more of the following factors:

1. altitude differences (e.g. filling at high altitude followed by transportation to lower level);
2. temperature differences (filling at higher than ambient temperature will result in a contraction of the oil volume and a reduction of the headspace pressure);
3. chemical (e.g. oxidation) or physical (solubility) processes between the contents and the air in the headspace of the bottle. In due time these factors can cause enough underpressure to initiate paneling.

In case the content of the pack is sensitive to oxidation then this is generally the most important factor of the potential occurring of paneling. The oxidation is a progressive process that in most cases will cause a, nearly, complete disappearing of the oxygen in the headspace, consequently leading to an underpressure in the bottle. Long term, one year, experiments on bottles containing edible oil also showed that the

complete headspace can disappear [65]. This effect is related to the permeability of the plastic container and the non-rigidity of the bottle. If the bottle contains a vacuum and is not rigid or has collapsed then there is no equilibrium nitrogen pressure inside and outside the pack, causing the nitrogen to permeate.

The requirements for a good bottle design are often conflicting each other. Where a certain design is good with respect to paneling it might be unacceptable for top load strength and impact resistance and *visa versa.*

Penzkofer [50] presented formulas to describe the paneling of cylindrical HDPE bottles. Rosato [55], Ryder and Buttermore [56], and Szanja [59], describe guidelines, based on experience, for round as well as non-round bottles with respect to top load strength and vacuum resistance. By identifying the important design parameters of a bottle (e.g. shoulder design, label area, rigidizing the body) they advise how to design plastic bottles. Rosato [55] describes a solution to prevent paneling in round hot-fill bottles by applying vertical panels circumferential. However, most of their advises do not give a solution for the paneling phenomena as observed for round, axial symmetric, bottles.

Tsiourvas *et al.* [64] also investigated the paneling phenomena and proposed solutions in the form of easily deformable bottles. Tsiourvas *et al.* [64] tested different round bottle designs and a bottle with different wall thickness distributions. One of the bottles was designed with a circumferential ribbing such that it is able to deform locally in vertical direction, in such a way preventing the creation of an underpressure. Another solution to prevent paneling is given in Food Marketing & Technology [5] in which a bottle for hot filling is described. Several vertical membrane panels have been designed in this bottle. These panels can move inwards and therefore reduce or eliminate the occurring of an underpressure. The last is similar to the effect that can be observed for square bottles where no 'circumferential' ribbing has been applied.

When paneling plays an important role, there are basically three design alternatives:

1. rigid bottle approach, i.e. trying to make the bottle as rigid as possible by either increasing the wall thickness and/or stiffening the bottle by adding ribs;

2. flexible bottle approach, i.e. to allow global deformation of the bottle and to 'control' this deformation;

3. mixed approach, in this case the bottle as a whole is rigid but locally it is able to deform substantially, e.g. due to the vertical membranes as described in Food Marketing & Technology [5] and various patents [2, 3, 12, 16–19].

A significant increase of the wall thickness, and therefore a significant increase in material costs, is necessary to prevent paneling and to obtain a rigid bottle. Therefore a solution needs to be found in the flexible bottle or mixed approach as described by Tsiourvas *et al.* [64] and Food Marketing & Technology [5]. However, the deformation should be related to the initial headspace of the bottle. If the bottle is not able to compensate the headspace volume then this will still result in paneling. Consequently, a reliable way of designing a bottle, such that a specified volume change can be compensated, is demanded for. This means that we should find a way to quantify the volume absorption of the bottle beforehand. One way of doing this is by using the Finite Element Method (FEM). With the FEM a bottle can be analyzed numerically in the design stage. Furthermore, all relevant factors (e.g. material data, wall thickness distribution etc.) can be changed and evaluated for their influence, easily.

Finally it needs to be mentioned that there are more solutions to prevent paneling than the one described in this chapter. Many solutions have been developed and are available: adding a drop of liquid N_2 to the contents to increase internal bottle pressure [5] , other packaging concepts (e.g. bag in box packaging), using vent caps, filling at low temperatures, heat treatment of the container [52] and using specially designed caps that can deform [4] are other, more costly, solution examples to the paneling phenomena.

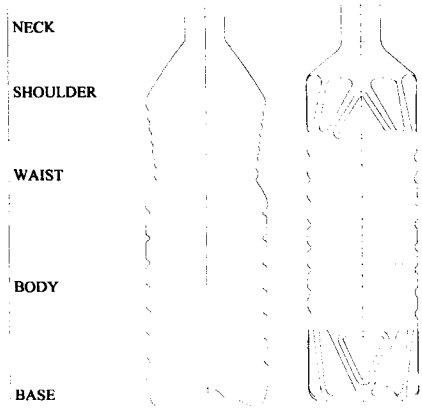

Figure 2.1: *a) Round PET bottle (750 ml). b) Square PVC bottle (1000 ml).*

The present work can be divided in different parts. First of all a number of laboratory tests have been carried out to determine the critical top load and critical internal underpressure. Secondly, FEM has been used to simulate the laboratory tests. The results from these simulations let to the question whether the critical top load and critical underpressure are sufficient design criteria. It turned out that the use of an additional constraint, the critical volume ratio, during 'vacuum' resistance testing could lead to a complete prevention of paneling. If a bottle can be designed using this design criterion then underpressure buckling, paneling, will not occur. The top load buckling can be potentially prevented by introducing the critical vertical compression of a bottle, provided that after a specified deformation additional load is carried by the secondary package. Finally, we will discuss how we can quantify these additional constraints.

2.2 Laboratory testing

The bottles that were used during this study are depicted in the Figure 2.1. In Section 2.2.1 top load tests will be described, whereas 'vacuum' resistance tests will be the subject of Section 2.2.2.

2.2.1 Top load testing

During top load testing the bottle was compressed between two horizontal plates with a speed of 100 mm/min. The internal pressure was kept constant during testing. Figure 2.2 depicts the deformed round and square bottle, respectively. As denoted in Table 2.1 and Figure 2.3 the critical top load as well as the critical compression have been evaluated during testing. The critical vertical compression is the shortening of the bottle at the point of buckling and is in this chapter expressed as a percentage of the bottle height. As can be seen from Figure 2.3, initially, the square bottle's response to the applied deformation is nearly linear. At a certain compression the force no longer increases linearly with the applied deformation. This is the point were the actual buckling starts. In practice the maximum load that can be applied on the bottle is used as a constraint. In Table 2.1 we observe that the actual buckling load is 13% less than the maximum load and the critical deformation is 32% less than the deformation at

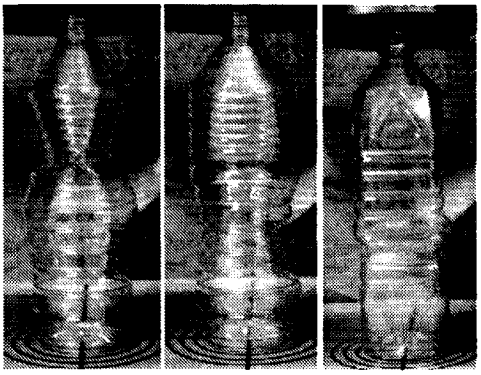

(a) (b)

Figure 2.2: *Experimental deformation during top load testing. a) Front and side view of the round bottle. b) Square bottle*

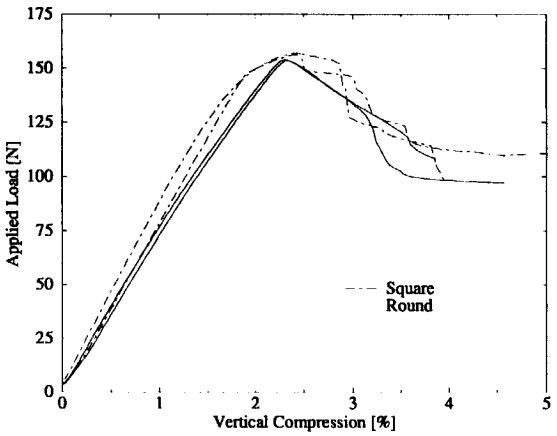

Figure 2.3: *Top load test curves for round and square bottles. Two test curves for each bottle type have been depicted. The non-zero onset of the applied load is caused by pre-loading during testing.*

	Onset of Buckling [N]	Max. Load [N]	Onset of Buckling Compression [%]	Critical Vertical Compression [%]
Round	n.a.	156.8	n.a.	2.3
Square	136	156	1.6	2.4

Table 2.1: *Average top load test results. Six round and four square bottles have been tested.*

maximum load. Thus, by using the maximum load as constraint, the top load and critical deformation of the bottle are significantly overestimated.

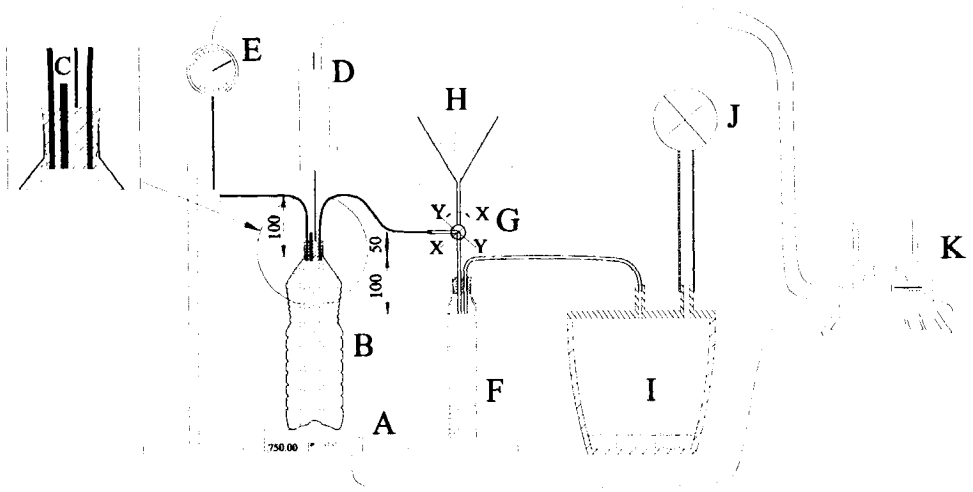

Figure 2.4: *Experimental setup to measure the critical volume and corresponding underpressure (all dimensions are in mm).*

2.2.2 'Vacuum' resistance testing

Commonly the critical internal underpressure is denoted as the vacuum resistance of a bottle. Paneling can be observed when the internal underpressure exceeds the 'vacuum' resistance.

A convenient quantity for bottles is the *critical volume ratio* which will be defined as:

$$v_c = \frac{V_i - V_b}{V_i}, \tag{2.1}$$

where v_c, V_i and V_b are the critical volume ratio, the undeformed brimful volume and the brimfull volume at the onset of paneling, respectively. In Figure 2.4 the experimental setup to determine the critical volume ratio is depicted. This setup consists of a bottle brimfull filled with water (B), which is placed on a balance (A). The vertical displacement caused by the balance can be neglected. The balance has an accuracy of $\pm$ 32 mg. The bottle is closed with a rubber plug with 3 openings, one opening is connected with a tube to the barometer (E), the other opening is connected to a valve (G) and in the last opening a ventile (C) is placed. The accuracy of the barometer is $\pm$ 0.1 kPa. The length of the bottle is continuously measured with a displacement measuring device, an LVDT, (D). At the start of the experiment, valve (G) is in such position (X-X) that water can enter the bottle from funnel (H). Any air in the bottle or tube between (H) and (B) can leave the bottle through ventile (C). After filling the bottle to the brim with water, ventile (C) is closed and valve (G) will be turned into Y-Y position such that the connection with the vacuum-pump (J) is made and the connection with (H) is closed. Between the vacuum pump (J) and valve (G) two capacities are positioned. Capacity (F) will contain all water that will be removed from the bottle. The function of capacity (I) is solely to protect water from entering the vacuum pump. Barometer (E), displacement measuring device (D) and balance (A) are connected to the computer (K). Since the volume change of the bottle is directly related to the change in weight of the bottle, the required volume-pressure relation can be obtained. In addition the length is known with respect to the volume and internal pressure. One might question the 100 mm height difference in the system between (B) and (E). Since this has a constant pressure influence of approximately 1 kPa this

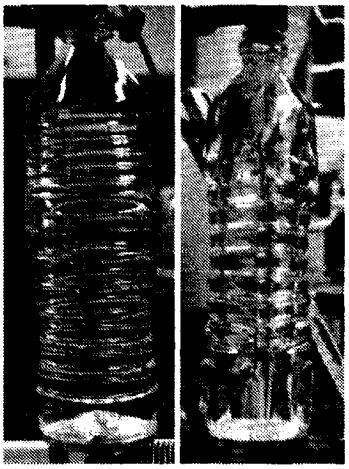

(a) (b)

Figure 2.5: *Paneling of the round and square bottle.*

has been neglected for the round bottle. It might be necessary to take this influence into account for the square bottle, due to it's low vacuum resistance.

On the test-setup, as depicted in Figure 2.4, full as well as empty bottles have been tested. During the empty bottle testing, length and internal pressure changes were evaluated. Comparing empty and full bottle test results gives an insight in the relation between length and volume change. Full as well as empty round bottles give similar results, however, for the square bottle a significant difference was found. The buckled configurations for full and empty, round as well as square, bottles were similar, and are depicted in Figure 2.5.

Typical results of the pressure versus time of empty round and square bottles are depicted in Figure 2.6. Due to the fact that we intend to simulate the deformation of the bottle with Finite Element Analyses as a time independent process, we prefer to exclude time. From Figure 2.7 we may conclude that the length of an empty round bottle does not change significantly after buckling. However, the square bottle starts to deform significantly in vertical direction after the buckling load has been reached. Since we do not know yet how the length change relates to the volume change, we should carry out tests on full bottles to determine the critical volume of the bottle. In the Figures 2.8–2.10 the results from tests on a full bottle are depicted. Figure 2.8 depicts the result of repeated measurements on one sample. This means that one round bottle was repeatedly tested not exceeding the critical underpressure except for the last test (test 6). The square bottle was repeatedly tested exceeding its critical underpressure. Both, round and square bottles fully recovered after unloading, even if the loading led to buckling. The latter implies an absence of global permanent deformation. Therefore, initial simulations make use of linear material behavior. If the latter produces inadequate results then the material description should be refined.

As can be seen in Figure 2.9 and Figure 2.10 the round bottle deforms significantly in axial direction (approximately 1.4 %) while the square bottle does not significantly deform in axial direction (approximately 0.070 %). However, the volume decreases significantly (approximately 1.45 %) for the square bottle. Also we can observe that the volume decrease of the round bottle has a much wider variance than the change in length. Reasons for the variance in the volume measurements, for round as well as square bottles, can be due to:

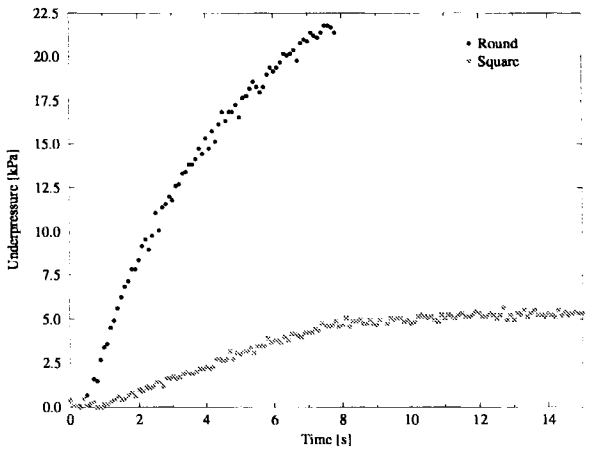

Figure 2.6: *Vacuum resistance testing of empty bottles.*

Bottle type	Critical Underpressure [kPa]	Critical Volume Ratio [%]	Critical Bottle Shortening [%]
Round	21.5-23.2	1.76-1.97	1.35-1.43
Square	5.8-6.9	1.39-1.53	0.065-0.076

Table 2.2: *Vacuum test results. From each type 4 bottles were tested.*

- accelerating water in the system, water in the tube between (E) and (B), and the tube between (F) and (G) might cause fluctuations in pressure and weight measurements;
- any moving of air in the test room can influence on the pressure measurements;
- small, invisible, changes in bottle geometry and stability of the bottle can result in accelerations that are again passed through to the balance;
- noise in the measurements.

Since we are not able to determine the critical volume ratio precisely, a range is given for the critical volume ratio and the critical underpressure in Table 2.2. Further, we can observe from the Figures 2.7–2.10 that the critical underpressure of a full round bottle differs slightly from an empty round bottle, which has a critical underpressure of approximately 21.7 kPa. For the square bottle the influence of the hydrostatic fluid pressure has a significant influence. An empty square bottle has a critical underpressure in the range of 4.5–5.2 kPa while a full bottle has a critical underpressure in the range of 5.8–6.9 kPa.

2.3 Simulation

Finite Element Analysis [6, 79] allows us to simulate structural behavior prior to manufacturing. In the present chapter two approaches have been used to determine the critical load of the structure: linearized buckling analyses and geometric non-linear analyses. Linearized buckling analysis predicts the buckling load and the corresponding buckling mode assuming a fully linear fundamental or pre-buckling solution. In a non-linear analysis the load is applied gradually. Bifurcation points can be estimated by

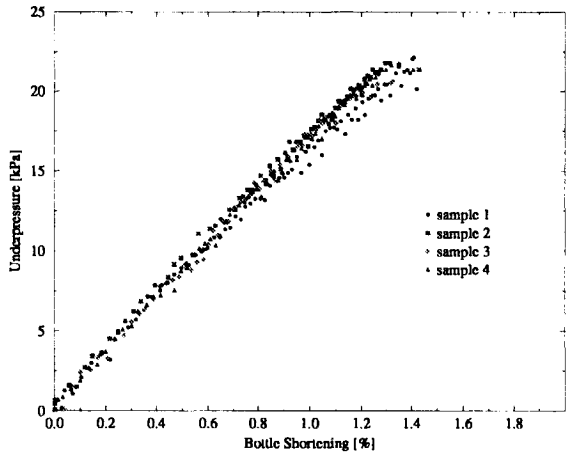

(a) *Round*

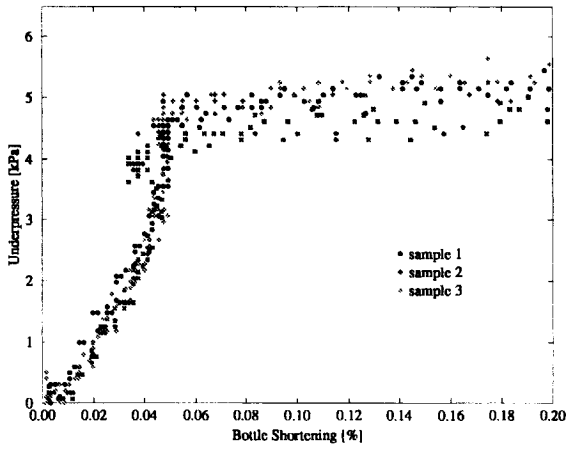

(b) *Square*

Figure 2.7: *Results of 'vacuum' resistance testing on empty bottles.*

monitoring the lowest eigenvalues of the tangent stiffness matrix. Limit points become apparent from the corresponding load-deflection curves [54]. In this kind of analysis it is also possible to account for imperfections. Obviously this type of analysis is more close to the actual tests described in the previous section.

If the deformed and undeformed structure are symmetric, then use of symmetry can be made and, consequently, only a part of the structure has to be modeled. This results in a significant reduction of computing time.

The element that was used in all the analyses was a triangular shell element with 12 degrees of

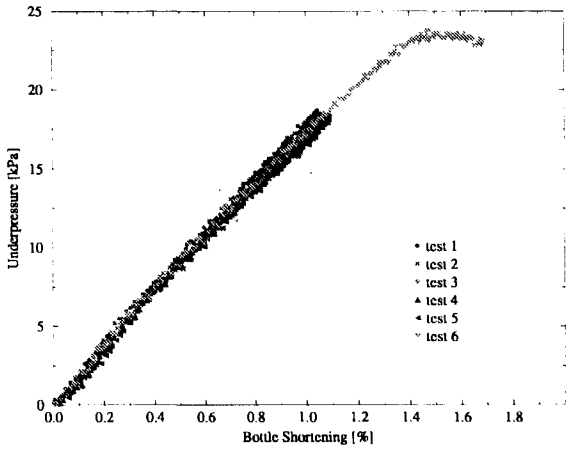

(a) *Round*

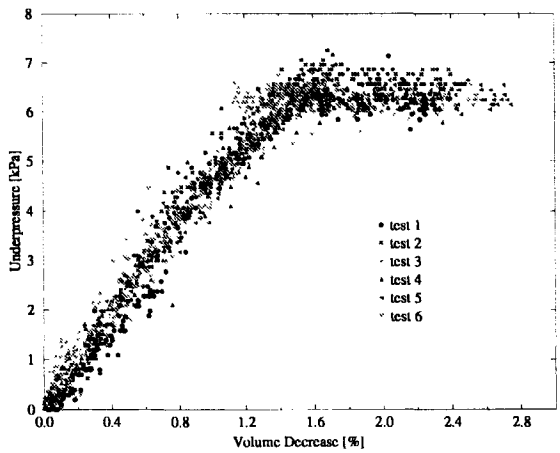

(b) *Square*

Figure 2.8: *Results of repeated 'vacuum' resistance testing on one sample.*

freedom (DOF) from which 3 displacements at each corner node and a rotation along each side of the element [72, 73]. In all the analyses linear material behavior has been used.

A number of simplifications have been adopted for the round as well as for the square bottle. The wall thickness has been approximated using

$$h = ar_{loc}^2 + br_{loc} + c \quad , 0 \leq r_{loc} \leq r_{max}, \tag{2.2}$$

where h, r_{loc} and r_{max} are the wall thickness at a certain point, the local radius of the bottle and the maximum bottle radius, respectively (see also Figure 2.11 and 2.12). The values a, b and c can be

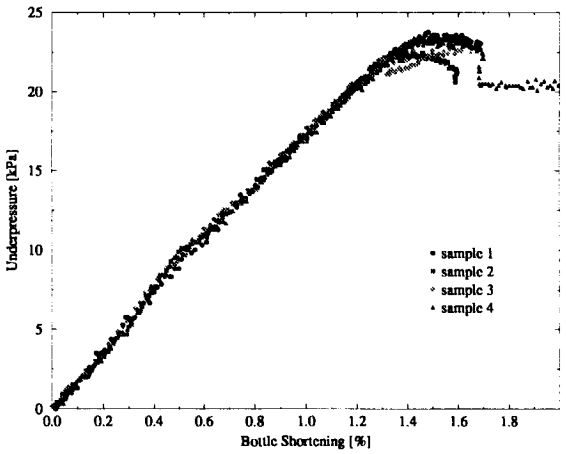

(a) *Underpressure versus bottle shortening during 'vacuum' testing.*

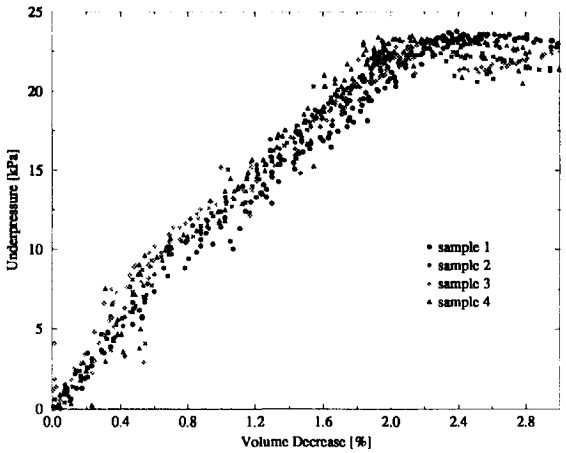

(b) *Underpressure versus volume decrease during 'vacuum' testing.*

Figure 2.9: *Results of 'vacuum' resistance testing of full round bottles. Four round bottles were tested.*

determined on the basis of wall thickness measurements. This description gives an approximation of the axial wall thickness distribution for round as well as square bottles. Maximum deviations of 10 % of the approximated value have been found for round bottles, while locally deviations up to 40 % were found for the square bottle. The last has not been examined more thoroughly.

Due to the nature of the stretch blow molding process the neck and bottom areas of a bottle are significantly thicker than the body. The neck of a bottle requires a high dimensional accuracy, which may not be distorted during the heating in the stretch blow molding process. The base needs to be thicker to prevent the stretch rod from pinching through the material during the stretching stage. Therefore the

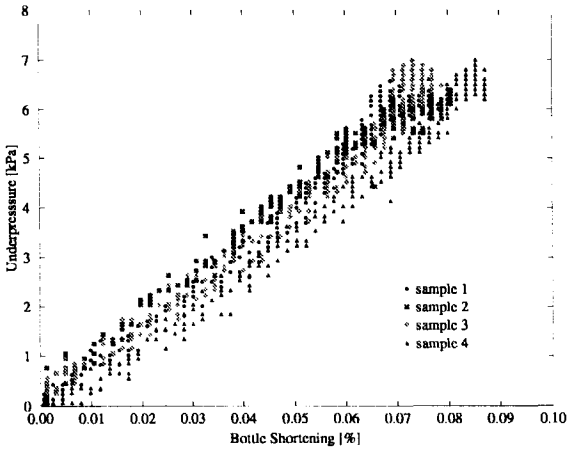

(a) *Underpressure versus bottle shortening during 'vacuum' resistance testing.*

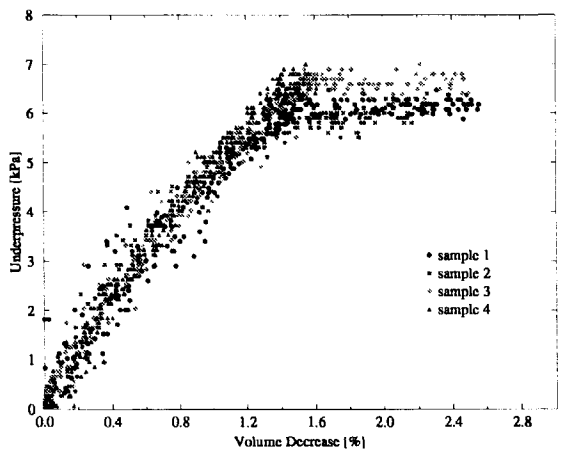

(b) *Underpressure versus bottle shortening during 'vacuum' resistance testing.*

Figure 2.10: *Results of 'vacuum' resistance testing of full square bottles. Four square bottles were tested.*

wall thickness in these areas cannot be approximated and (2.2) can only be used for the shoulder, waist and body areas of a bottle. For this reason a constant wall thickness has been assigned to the neck and base area.

As can be seen in Table 2.3, a difference of 4 % was found for bottles with a varying wall thickness in comparison with bottles with a constant wall thickness (based on linearized buckling simulations). The thickness of the bottle with a constant wall was based on (2.2) with r_{loc} taken as the maximum bottle radius and a wall thickness in the neck and base equivalent to the bottle with a varying thickness.

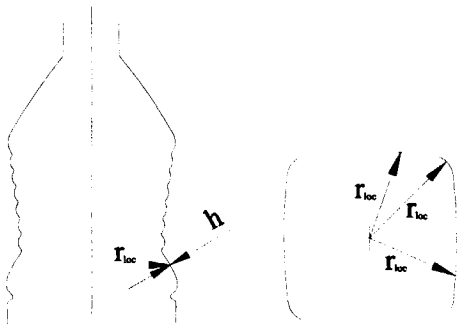

Figure 2.11: *Local radius of the bottle. For non-axial symmetric bottles the local radius can vary in a cross section.*

	Critical Top Load [N]	'Vacuum' resistance [kPa]
Varying wall thickness	165.9	23.62
Constant wall thickness	160.0	22.66

Table 2.3: ***Comparison of the results of a round bottle with varying wall thickness (minimum thickness is 0.235 mm) and a round bottle with a constant wall thickness (wall thickness is 0.235 mm). The results are based on linearized buckling analyses.***

The simulations that will be further described in this chapter have been carried out with a constant wall thickness. Due to the non-axial symmetry of the square bottle, the wall thickness has not been simplified with a constant value but has been approximated using (2.2).

Due to a biaxial stretching of the bottle during the forming process the bottle is orientated. The Young's moduli in circumferential and axial direction depend on the blow-up ratio's (also called stretch ratio's) of the bottle [15,44]. The axial blow-up ratio is defined as [15,44]

$$B_a = \frac{l}{L}, \tag{2.3}$$

where B_a, l and L are the axial blow-up ratio, the bottle 'length' and the preform 'length', respectively (see Figure 2.12). The global circumferential blow-up ratio is defined as [15,44]

$$B_c = \frac{r_{max}}{R}, \tag{2.4}$$

where B_c, r_{max} and R are the circumferential blow-up ratio, the maximum bottle radius and the internal preform radius, respectively. The final global wall thickness in the bottle can be estimated with the help of the blow-up ratio's [15,44]. This results in

$$h_f = \frac{h_p}{B_a B_c}, \tag{2.5}$$

where h_f and h_p are the final global wall thickness and preform wall thickness, respectively. If we apply (2.3) till (2.5) on the round bottle then the final global wall thickness would be 0.237 mm, which comes close to the thickness as found in the actual bottle (0.235–0.240 mm).

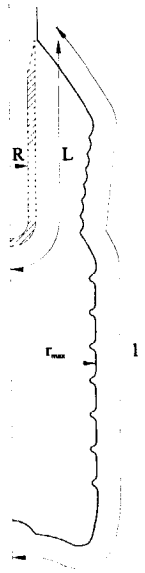

Figure 2.12: *Blow-up ratio terminology.*

The circumferential Young's modulus can be obtained with the help of experiments. Test specimens in this direction are easy to obtain. Test specimens in axial direction are practically impossible to get. The axial Young's modulus can be roughly estimated according [44]

$$E_a = \frac{E_c B_a}{B_c}, \tag{2.6}$$

where E_a and E_c are the axial and circumferential Young's modulus, respectively. The circumferential Young's modulus has been determined experimentally, while the axial Young's modulus has been estimated using (2.6). A slight orthotropy of 1.03 was found (E_c / E_a = 1.03). The Poisson's ratio and shear modulus for the stretched material were taken from supplier data sheets.

The equations (2.3)–(2.6) are easily applied to the round bottle. Due to the non-axial symmetry of the square bottle, the axial blow-up ratio (see also Figure 2.12) can not be defined uniquely. Therefore there is more than one global axial stretch ratio. Also the circumferential stretch ratio can vary in a single horizontal cross section. However, experiments on the square PVC bottle showed that the material is by good approximation isotropic. Isotropic material properties have therefore been used in the simulations for the square bottle.

2.3.1 Top load simulation

Due to the axial-symmetry of the undeformed structure and the two planes of symmetry in the deformed structure only a quart of the round bottle has been modeled. This significantly reduces computing time. Consequently, this simplification excludes non-symmetric deformation modes. If there is a small chance that the deformation mode is non-symmetric then this should be verified on the hand of an analysis of a complete bottle model. Since the deformed structure of the square bottle under top load contains no planes of symmetry, the whole structure had to be modeled. The last resulted in long computing times

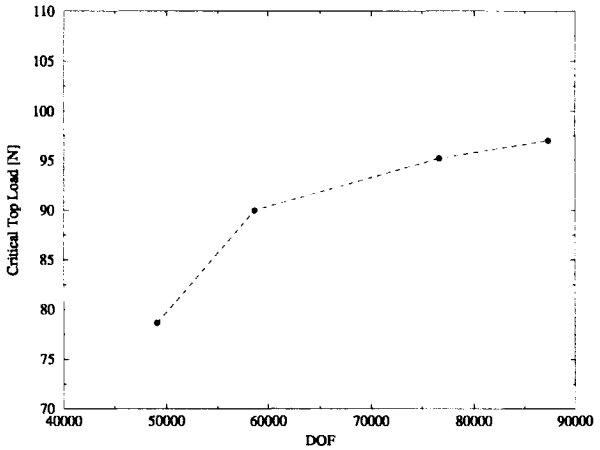

Figure 2.13: *Simulated top load of the square bottle versus degrees of freedom. The results from linearized buckling analyses have been depicted.*

and therefore all computations on the square bottle under top load are restricted to linearized buckling analyses.

As described earlier, the paneling in square bottles can easily be camouflaged by design features (e.g. square panels that are able to deform). Due to their geometry round bottles are more prone to paneling and need a different design strategy. Therefore, in this chapter the paneling of round bottles is emphasized.

The deformed configuration of the round bottles and the buckling mode of the square bottle are depicted in Figure 2.14 and resemble the experimentally deformed structures. As can be seen in Table 2.4 the top load of the round bottle is reasonably well predicted in the present setting (with only 2 % difference from the experimental value). The simulated top load of the square bottle differs approximately 30% from experimental values. One reason for this is that the applied mesh density is not sufficient to describe the bottle geometry, accurately. For an accurate description of the geometry a large number of Degrees Of Freedom (DOF) was required, consequently increasing computing costs and effort. As can be seen from Figure 2.13, a rough mesh of approximately 50.000 DOF, where the mesh density near the ribs is far insufficient, leads to a top load of 79 N while more refined meshes lead to significantly higher top loads. Other reasons for this can be local wall thickness variations and material property variations.

Figure 2.15 depicts the simulated load-displacement curves (non-linear analyses) for round bottles with a different wall thickness. The critical top load is reached at the onset of buckling which is indicated by a dashed vertical line. The critical vertical compression is more or less the same for bottles with a different wall thickness. The top load at the onset of buckling is reasonably predicted in comparison with experiments. The critical vertical deformation as found in non-linear analysis still differs significantly. The critical vertical deformation was predicted more accurately with the linearized buckling analysis.

As can be seen in Figure 2.15, the post-buckling path of the experimental results differs significantly from the simulated results. The last can possibly be explained by two effects. Firstly, during experiments local plastic deformation was found immediately after the buckling occurred while for the simulations linear material has been used. Secondly, the bottle was simulated assuming symmetric buckling. During experiments the buckling was also symmetric but in the post buckling region the bottle snapped in a non-symmetric buckling shape, as can be seen from Figure 2.16.

Figure 2.17 depicts the significant effect from different uniform wall thickness distributions on the

Bottle type	Critical Top Load		Critical Vertical Compression	
	Numerical	Experimental	Numerical	Experimental
	[N]	[N]	[%]	[%]
Round	160.0	156.8	2.2	2.3
Square	96	136	0.72	1.6

Table 2.4: *Simulated (linearized buckling analyses) versus measured top load results. The round bottle had a 0.235 mm overall wall thickness.*

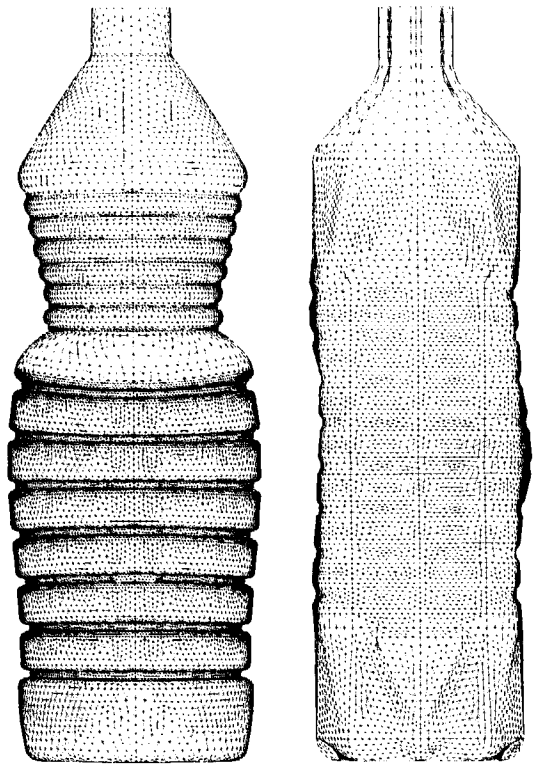

(a) *Round* (b) *Square*

Figure 2.14: *Deformed configuration of the round bottle based on a quart model (a) and buckling mode of the square bottle under top load (b). For the square bottle a complete model has been used.*

critical top load, while the critical vertical deformation changes only slightly. For example 14 % increase of the wall thickness from 0.22 mm to 0.25 mm will result in 33 % increase in critical top load and only 1 % increase of critical compression.

2.3.2 'Vacuum' resistance simulation

The round as well as the square bottle contain two planes of symmetry in undeformed and deformed, paneled, configuration. Therefore all the 'vacuum' resistance simulations have been carried out on a

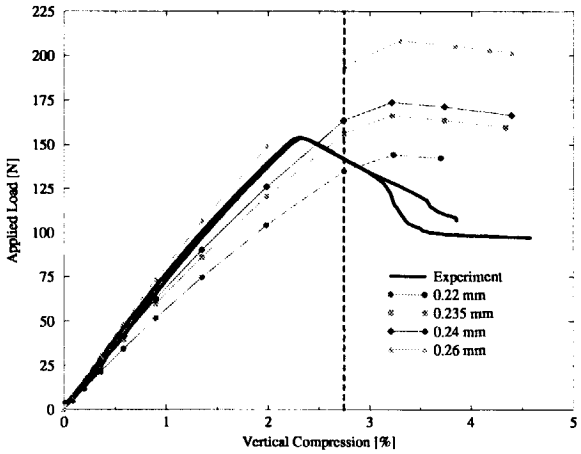

Figure 2.15: *Simulated and experimental results for the round bottle under top load for different wall thickness. The dashed line indicates the onset of buckling during simulations.*

Figure 2.16: *Experimental post-buckled configuration for a round bottle under top load. Note that this configuration is not symmetric.*

quart bottle. As can be seen from Figure 2.18 the deformed configurations are in good agreement with the experiments. The round and the square bottle have both been analyzed empty and full. Analyzing a full bottle implies that the influence of the hydrostatic pressure caused by the containing liquid should be considered. Non-linear analyses where the hydrostatic pressure was taken into account have been carried out for the round bottle. The vacuum simulation is in good resemblance with the experiments as can be seen from Figure 2.19, also it can be seen that the influence of the liquid pressure is not significant for the round bottle. During non-linear analysis the deformation of the square bottle was not conform the linearized buckling mode and the experimental deformation. Several reasons can be appointed for this. Firstly, the mesh is not fine enough to follow all geometric details of the bottle. Secondly, initial

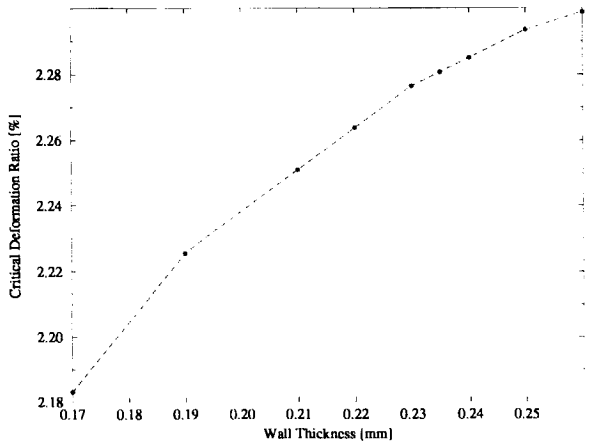

(a) *Critical vertical compression versus wall thickness.*

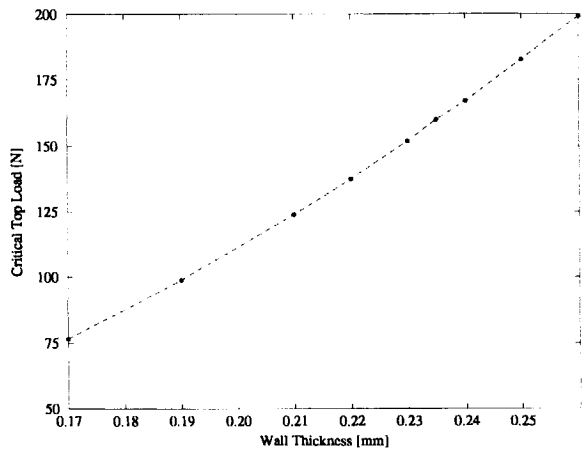

(b) *Critical top load versus wall thickness.*

Figure 2.17: ***Linearized buckling load and its relation to wall thickness.***

imperfections in geometry and thickness and varying material properties can be present and need to be considered in the non-linear analyses. However, the linearized buckling mode predicts the critical underpressure accurately and can also be used to determine the critical underpressure of a full bottle.

The linearized buckling analysis is based on the solution of

$$[\mathbf{K} + \mathbf{G}]\mathbf{v} = \mathbf{0}, \tag{2.7}$$

where $\mathbf{K}$, $\mathbf{G}$ and $\mathbf{v}$ are the structure's stiffness matrix, the geometric stiffness matrix and the buckling

Critical Underpressure		Critical Bottle Shortening	
Numerical [kPa]	Experimental [kPa]	Numerical [%]	Experimental [%]
23.0	21.5-23.2	1.40	1.35-1.43

Table 2.5: *Simulated versus measured results for the round bottle containing an underpressure. The simulated bottle had a 0.235 mm wall thickness. The numerical results were obtained from non-linear analyses on a full bottle.*

Critical Underpressure (Empty Bottle)		Critical Underpressure (Full Bottle)	
Numerical [kPa]	Experimental [kPa]	Numerical [%]	Experimental [%]
4.5	4.5-5.2	6.2	5.8-6.9

Table 2.6: *Simulated versus measured results for the square bottle containing an underpressure.*

mode, respectively. For a full bottle (2.7) changes to

$$[\mathbf{K} + \mathbf{G}_p + \mathbf{G}_{fluid}]\mathbf{v} = \mathbf{0}, \tag{2.8}$$

where the matrix $\mathbf{G}_p$ is the contribution to the geometric stiffness matrix due to the gas pressure. The matrix $\mathbf{G}_{fluid}$ is the contribution of the hydrostatic pressure to the geometric stiffness matrix and is constant. With

$$\mathbf{G}_p = \mathbf{G}_p(p) = \lambda \mathbf{G}_p(\hat{p}), \qquad p = \lambda \hat{p}$$

where p, $\hat{p}$, λ, are the critical buckling pressure, the initial applied pressure and the load parameter, respectively, the eigenvalue problem (2.8) can be written as

$$[\mathbf{K} + \lambda \mathbf{G}_p(\hat{p}) + \mathbf{G}_{fluid}]\mathbf{v} = \mathbf{0}. \tag{2.9}$$

Replacing (2.9) by

$$[\mathbf{K} + \mu\{\mathbf{G}_p(p^*) + \mathbf{G}_{fluid}\}]\mathbf{v} = \mathbf{0},$$

and searching for $\mu(p^*) = 1$ leads to

$$[\mathbf{K} + \mathbf{G}_p(p^*) + \mathbf{G}_{fluid}]\mathbf{v} = \mathbf{0},$$

which is equivalent to (2.8), with p^* the critical pressure load. The function $\mu(p^*)$ is depicted in Figure 2.20, where p^* has been varied from 2–10 kPa. The critical pressure load, p^*, was found at 6.2 kPa when $\mu(p^*)$ equals 1.

From Figure 2.19, Figure 2.20 and Table 2.6 we can conclude that the fluid has a significant influence for the square bottle but a negligible influence for the round bottle. Further we can see from Figure 2.19(a) that the critical bottle shortening of the round bottle seems not to depend significantly on the wall thickness. The simulated critical underpressure is nearly linear dependent on the overall wall thickness in a range as depicted in Figure 2.21.

2.4 Discussion

The critical deformation that occurs during vacuuming of a round bottle does not significantly depend on the wall thickness. This deformation can well be determined with the help of finite element analysis. If care is taken that this deformation is invisible for the customer, then a bottle can be designed such that the deformation can compensate for the complete headspace. Paneling is inclined to occur as long as this deformation is not able to compensate for the headspace volume.

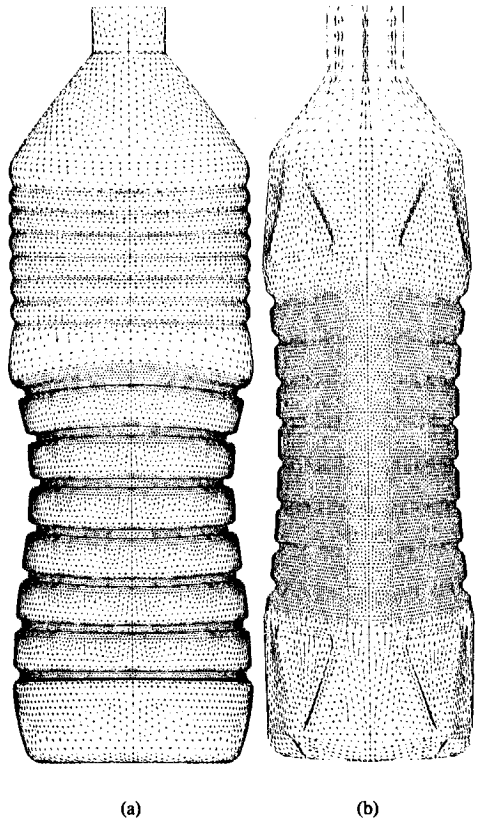

Figure 2.18: *Deformed structure for the round bottle (a) and buckling mode (b) of the square bottle during vacuum resistance simulations.*

The circumferential ribbing as applied for most axial-symmetric bottles gives a high vacuum resistance and allows the bottle a certain axial contraction. When this contraction is not sufficient to compensate the headspace volume then paneling can still occur. Many bottles with a high vacuum resistance in order to resist paneling can still be found, consequently using excessive material. In most cases these bottles still buckle in due time. If these bottles would allow controlled paneling such that the complete headspace can be compensated then the excessive material preventing paneling can be removed.

Although paneling is a phenomena that occurs for round and non-round bottles, the effects of it on square bottles can easily be eliminated. As depicted in Figure 2.18(b) a square bottle will deform parallelogram like if the bottle contains an internal underpressure. However, the latter will only occur if a 'circumferential' ribbing was applied on the container. If no ribbing would have been applied then the sidewalls of the bottle will move inwards, absorbing sufficient volume to eliminate paneling.

Finite element calculations depend very much on the input of material data and in the case of thin walled structures also on accurate data of the local thickness. The thickness can be easily evaluated for existing structures. Material properties, on the contrary, are hard to get. However, some aspects of the behavior of a bottle, here paneling, seem to depend less on the wall thickness distribution and the material properties. The un-sensitivity to these properties can in certain cases be exploited during the design process.

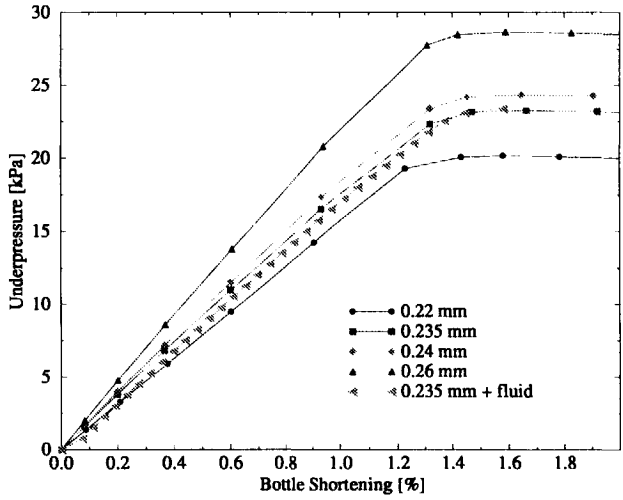

(a)

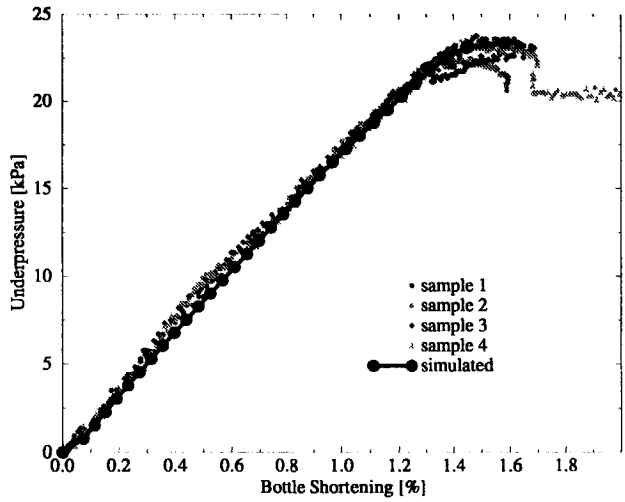

(b)

Figure 2.19: *Results of non-linear 'underpressure' analyses on the round bottle. a) Results of empty bottle simulations with different wall thickness. b) Experimental and simulated results of full bottles.*

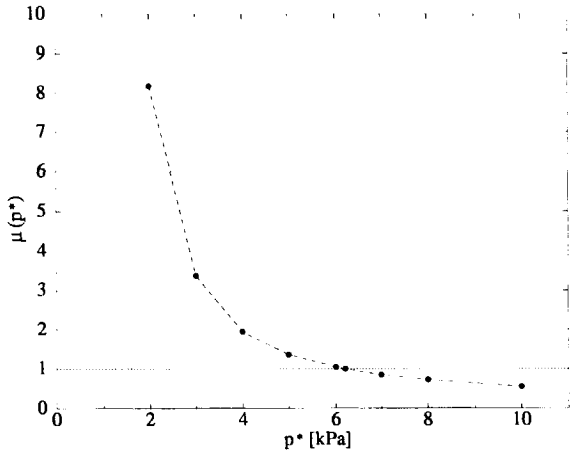

Figure 2.20: *Determination of the critical underpressure of a full square bottle using linearized buckling analyses. The critical underpressure for the filled bottle is found for* $\mu(p^*) = 1$.

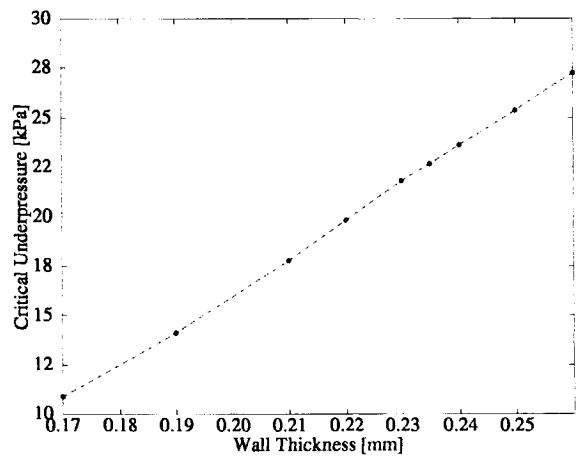

Figure 2.21: *Linearized buckling load during 'vacuum' simulations and its relation to wall thickness (empty round bottle).*

Based on: R. van Dijk, F. van Keulen and J.C. Sterk, Simulation of Closed Thin-Walled Structures Partially Filled with Fluid, Int. J. of Solids and Structures, 37, 6063–6083, (2000).

Chapter 3

Pressure Effects in Closed Structures

For closed structures, the enclosed gas volume can contribute significantly to the strength and stiffness of a structure. The present chapter describes the use of a gas element which is incorporated into finite elements for shells. In addition, a method to solve the governing set of equations efficiently is described. The method has been applied to a typical packaging example, namely a closed filled bottle. To validate the proposed method, numerical studies have been compared with experiments.

3.1 Introduction

Many thin-walled structures surround a volume. Typical examples are filled bags, bottles, soft drink cans, tires, balloons, athletic shoes with air compartments, *etc.* Deformation of such structures causes internal pressure changes and may therefore influence the mechanical properties significantly. For example, a buckling load can increase.

The present research originates from the fact that it was desirable for Unilever, a large manufacturer of food products, to determine the compression strength of closed filled bottles for edible oil. Effective tools for simulation of the filled packages makes it possible to achieve more competitive designs at acceptable design or reduced design costs.

In many Finite Element(FE) programs it is not possible to include this pressure effect easily. However the FEA program Abaqus [36] contains elements for solving problems involving fluid-filled cavities under hydrostatic conditions. Among others [10, 20, 25, 29, 33, 58, 78], Berry [7] investigated internal pressure effects. The modelling was done using a pneumatic element which relates the pressure to the internal enclosed volume. Applications that were considered are pressurized soft drink cans and an air spring. The formulation of the pneumatic element is started from the virtual work principle. The virtual work equation is augmented to account for the virtual work corresponding to the pressure of the enclosed gas. The latter can easily be determined using the corresponding gas law. The solution of the governing set of equations has not been addressed by Berry [7]. Due to the fact that the pressure causes the system matrix to be non-sparse, solving the set of equations, using a direct solver, is not obvious and will be described in this chapter. The results of the described method have been compared with experimental and numerical results reported by Berry [7].

Other complications that were encountered involved a reversing of the pressure. If during an incremental iterative solution procedure the incremental volume change of the structure is larger than the remaining gas volume, then the new gas volume becomes negative, consequently leading to a negative pressure. Obviously, this situation is physically infeasible. This effect manifests itself mainly for relatively small enclosed gas volumes which is typical for many packages. By introducing a fluid compliance, this numerical complication has been circumvented.

The present work can be divided in different parts. Firstly, a theoretical description is given which describes how the contents, gas and fluid, influence on the internal gas pressure. Furthermore, this section describes the prevention of the pressure reverse as discussed earlier. Secondly, implementational issues and solution of the non-sparse stiffness matrix are addressed. Thereafter, some examples have

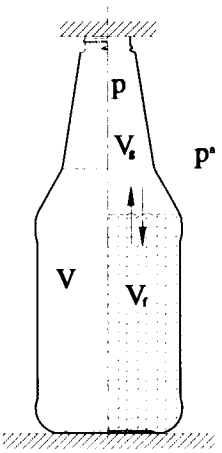

Figure 3.1: *Situation sketch, V, V_g, V_f, p and p^a are the total enclosed volume, the gas volume, the actual fluid volume, the internal pressure and the ambient pressure, respectively.*

been presented. The examples compare analytical and simulated results and illustrate the benefits of a fluid compliance. Finally, two applications, an airspring [7] and a plastic bottle for edible oil, have been studied.

3.2 Influence of the gas and fluid

In Figure 3.1, a typical closed-filled structure has been depicted. The figure displays a closed bottle which contains both gas and fluid and is being compressed.

In the sequel, the following assumptions have been made:

- hydrostatic pressure effects of the liquid are negligible in comparison with the pressure effects of the gas;
- the gas behaves as an ideal gas;
- the temperature is constant;
- a constant amount of enclosed gas.

The virtual work corresponding to the pressure difference, can be expressed as

$$\delta W_p^{ext} = (p(V_g) - p^a)\ \delta V_g, \tag{3.1}$$

where $p(V_g)$ represents the internal pressure which is a function of the gas volume, V_g. In case of a constant amount of ideal gas and at constant temperature the gas law simplifies to

$$pV_g = p^0 V_g^0 = C_g\ , \tag{3.2}$$

where p^0, V_g^0 and C_g are the initial gas pressure, the initial gas volume and a constant, respectively (see also Figure 3.1). In the present setting, it is more convenient to express the gas law in terms of the enclosed volume, V. In case the gas is governed by (3.2), then the pressure is determined by

$$p = \frac{p^0(V^0 - V_f^0)}{V - V_f^0}\ , \tag{3.3}$$

where V_f^0 and V^0 are the initial fluid volume and the initial enclosed volume, respectively (see also Figure 3.1). Introducing

$$f = \frac{V_f^0}{V^0}, \qquad v = \frac{V}{V^0}, \qquad r = \frac{p}{p^0}, \tag{3.4}$$

where f, v, r are the initial fluid fraction, the actual volume fraction and a normalized pressure, respectively, (3.3) can be rewritten as

$$r = \frac{1-f}{v-f}. \tag{3.5}$$

As will be shown later, also the derivative of the pressure with respect to the volume will be required. This derivative can be found by differentiation of (3.5), giving

$$\frac{dp}{dV} = \frac{dr}{dv}\frac{p^0}{V^0} = -\frac{r}{v-f}\frac{p^0}{V^0}.$$

During a FE calculation it can occur that $v < f$, *i.e.* compression of the fluid volume. This happens when the volume change caused by a linearized step of the analysis is larger than the current gas volume leading to a new gas volume, $v - f$, which is negative. This will consequently result in a negative pressure. This effect has been illustrated in Figure 3.2a where (3.5) has been plotted. Complications due to a negative pressure can be circumvented by introducing a penalty factor [39, p.196–197] for the fluid compressibility. The penalty factor is defined as

$$c = (p - p^0)\frac{V_f^0}{V_f^0 - V_f}, \tag{3.6}$$

where c is the compressibility of the fluid. In case of an incompressible fluid, the compressibility c becomes infinite and consequently $V_f = V_f^0$. The total volume V is given by $V_g + V_f$ and can be expressed in terms of the internal pressure using (3.2) and (3.6). This gives

$$V = \frac{p^0}{p}V_g^0 + \left(1 - \frac{p-p^0}{c}\right)V_f^0.$$

Similar to (3.4) the pressure, volume and fluid volume can be normalized. Furthermore, $f = V_f^0/V^0$ and $V^0 = V_g^0 + V_f^0$ can be combined to $(1-f) = V_g^0/V^0$.

With the introduction of a normalized compliance for the fluid, $s = p^0/c$, the normalized pressure can be written as

$$1 - f - rv + rf - sf(r^2 - r) = 0. \tag{3.7}$$

Solving of (3.7) for r is straightforward. However, only the positive solution is relevant, which reads

$$r = \frac{1}{2}\frac{f - v + sf + q}{sf}, \tag{3.8}$$

where $q = \sqrt{(f - v + sf)^2 - 4sf^2 + 4sf}$.

Similar to (3.5) the derivative of the pressure with respect to the volume can be evaluated, which becomes

$$\frac{dp}{dV} = -\frac{r}{q}\frac{p^0}{V^0}.$$

In Figure 3.2b, the pressure fraction, r, has been depicted for various values of s. This figure shows that s should be chosen small such that the behavior of the structure is similar when containing an incompressible fluid. In Section 3.4, the effectiveness of the above approach will be illustrated on the basis of several numerical examples.

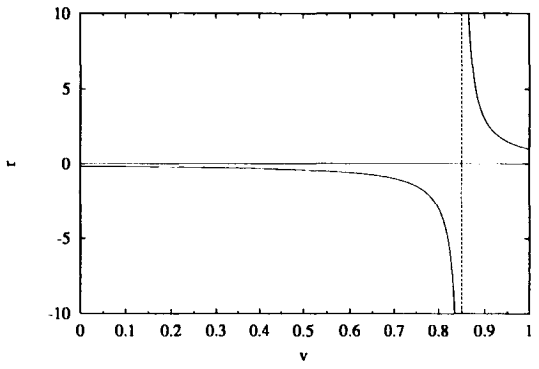

(a)

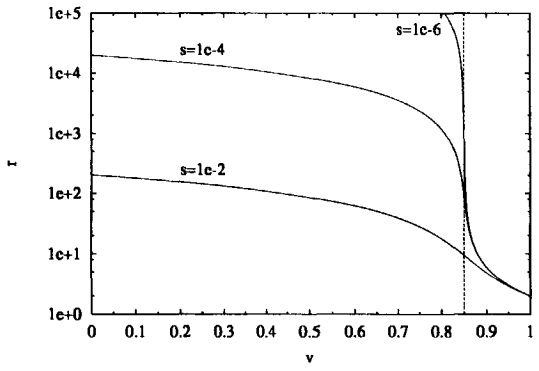

(b)

Figure 3.2: *The influence of fluid compressibility for a structure filled for 85% with fluid. Analytical results are depicted. The horizontal and vertical axes refer to the normalized volume and the normalized pressure, respectively. (a) Due to an incremental-iterative solution procedure the gas pressure can become negative. (b) The introduction of a nearly incompressible fluid with a fluid compliance* s*, prevents the gas pressure from becoming negative for the full range of* v*. The pressure fraction* r *has been depicted for various values of* s*.*

3.3 Finite element approach

In a general FE setting [6, 79] we often start from the principal of virtual work which reads

$$\delta W^{int} = \delta W^{ext}, \tag{3.9}$$

where δW^{int} and δW^{ext} are the internal and external virtual work, respectively.

Assuming linear elastic material behavior the internal virtual work for the entire structure can be formally described as

$$\delta W^{int} = \delta \boldsymbol{\varepsilon}^T \boldsymbol{\sigma} = \delta \boldsymbol{\varepsilon}^T \mathbf{S} \boldsymbol{\varepsilon}(\mathbf{u})$$

where $\varepsilon, \sigma, \mathbf{u}$ and $\mathbf{S}$ are the generalized deformations, the generalized stresses, the nodal degrees of freedom and a symmetric matrix which depends on the elastic material properties and the precise element definitions, respectively. The corresponding rate equations become

$$\left(\mathbf{D}^T\mathbf{S}\mathbf{D} + \mathbf{G}\right)\frac{d\mathbf{u}}{d\lambda} = \frac{d\mathbf{f}}{d\lambda}.$$

The matrix $\mathbf{G}$ represents the geometric stiffness matrix. The matrix $\mathbf{D}$ gives the relations between the deformation rates and the nodal velocities. The last term, the load vector $\mathbf{f}$, can in the present setting be described by two terms

$$\mathbf{f} = \lambda\mathbf{f}^\lambda + \mathbf{f}^p,$$

where $\lambda\mathbf{f}^\lambda$ is an external load vector, independent of $\mathbf{u}$, which can be scaled with the load factor λ. The vector $\mathbf{f}^p$ is the external load due to the gas which, with the help of (3.1), can be written as

$$\mathbf{f}^p = (p(V_g) - p^a)\frac{\partial V}{\partial \mathbf{u}} \tag{3.10}$$

The way the enclosed volume of the structure is calculated, is described in Appendix 3.A. During a FE analysis the external load will be incremented by changing the factor λ. The corresponding rate equations become

$$\left[\left(\mathbf{D}^T\mathbf{S}\mathbf{D} + \mathbf{G}\right) - \frac{\partial \mathbf{f}^p}{\partial \mathbf{u}}\right]\frac{d\mathbf{u}}{d\lambda} = \mathbf{f}^\lambda\,. \tag{3.11}$$

With (3.10) it follows that

$$f^p_{i,j} = \frac{dp(V_g)}{dV}V_{,i}V_{,j} + (p(V_g) - p^a)V_{,ij}, \tag{3.12}$$

where $\cdots_{,i}$ refers to $\frac{\partial \cdots}{\partial u_i}$.

It may be clear, that V is a function of nearly all nodal degrees of freedom. Therefore, the first term in the r.h.s. of (3.12) yields a *non-sparse* contribution to the system matrix. The contribution $f^p_{i,j}$ is symmetric and has previously been examined by many investigators [35, 46, 47, 57, 78](the reader is also referred to Appendix 3.A). The non-sparse system matrix requires a special method to solve the set of equations using a direct method. Combining (3.11) and (3.12) in such a way that the sparse and non-sparse components are separated leads to

$$[\mathbf{K} + \kappa\mathbf{a}\mathbf{a}^T]\frac{d\mathbf{u}}{d\lambda} = \mathbf{f}^\lambda, \tag{3.13}$$

with

$$\mathbf{K} = \mathbf{D}^T\mathbf{S}\mathbf{D} + \mathbf{G} - (p - p^a)\frac{\partial^2 V}{\partial \mathbf{u}\partial \mathbf{u}}$$

$$\kappa = -\frac{dp}{dV}, \qquad \mathbf{a} = \frac{\partial V}{\partial \mathbf{u}}.$$

As can be seen from (3.13), $\mathbf{K}$ is still sparse, whereas the non-sparse contribution has been described by $\kappa\mathbf{a}\mathbf{a}^T$. A technique to solve (3.13) has been found by trying

$$\frac{d\mathbf{u}}{d\lambda} = \mu\mathbf{a} + \mathbf{b}, \qquad \mathbf{a}\cdot\mathbf{b} = 0.$$

This results in

$$\mathbf{b} = \mathbf{K}^{-1}\mathbf{f}^\lambda - \mu\left(\mathbf{a} + \kappa a^2\mathbf{K}^{-1}\mathbf{a}\right)$$

with

$$\mu = \frac{\mathbf{a}^T\mathbf{K}^{-1}\mathbf{f}^\lambda}{a^2(1 + \kappa\mathbf{a}^T\mathbf{K}^{-1}\mathbf{a})}, \qquad a^2 = \mathbf{a}^T\mathbf{a}.$$

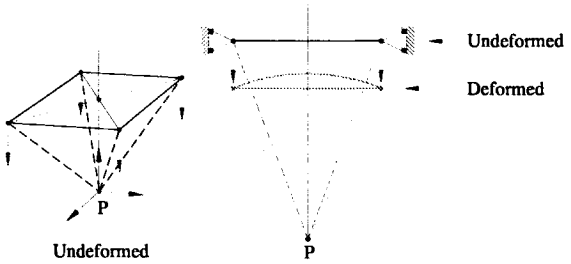

Figure 3.3: *Square plate that determines a pyramid shaped reference volume. The reference volume can contain a combination of fluid and gas.*

This way of solving turn out to be similar to the Sherman-Morrison formula [1,27,31] where the inverse of a modified matrix is related to the original matrix. Akgün *et.al.* [1] uses the Sherman-Morrison formulas for fast static reanalysis in order to find the response of a structure after modifications by using the original response of the structure. The required computional effort for this is much less than the effort required by a complete analysis. The Sherman-Morrison formulas utilize the property that the solution of a system of linear equations can be updated inexpensively when the matrix is changed by a low-rank increment [1].

More details and a slightly modified formulation, which is also applicable when the matrix $\mathbf{K}$ is singular, are given in Appendix 3.B. It is noted, that the problem of a non-sparse matrix could also be circumvented using a Lagrange multiplier formulation. In that case the formulation starts of from the introduction of an additional kinematic variable, being the volume of the structure. This approach will lead to governing equations which are similar to the ones described here.

3.4 Examples

In this section the effectiveness of the penalty method as defined by (3.6) will be examined by four examples, namely:

- an undeformable structure containing an incompressible fluid;
- an undeformable structure that contains a nearly incompressible fluid;
- a flexible structure containing an incompressible fluid;
- a flexible structure that contains a nearly incompressible fluid.

All four examples are based on the same problem definition. The structure that has been considered is depicted in Figure 3.3, which shows a square plate that determines a pyramid shaped reference volume. The reference volume is filled for 85% with fluid. A displacement in downward direction has been prescribed along all sides. The in-plane displacement components and all the rotations about the sides have been set to zero. During the downward movement of the plate the internal pressure will increase and causes deformation of the flexible plate. If during an FE analysis the volume change of the structure is larger than the remaining gas volume and the fluid is incompressible then the pressure becomes negative as discussed in section 3.2. This is more prone to happen with stiff structures and can be circumvented by application of the penalty method.

The undeformable structure consists of a square plate modeled by only two triangular elements [9, 72,73]. The used element has a rotational degree of freedom about each element side and 3 translational degrees of freedom at each corner node. Since, the rotations about the sides of the structure have been

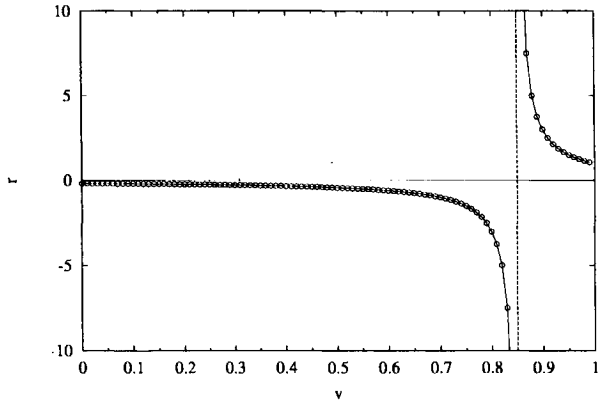

(a)

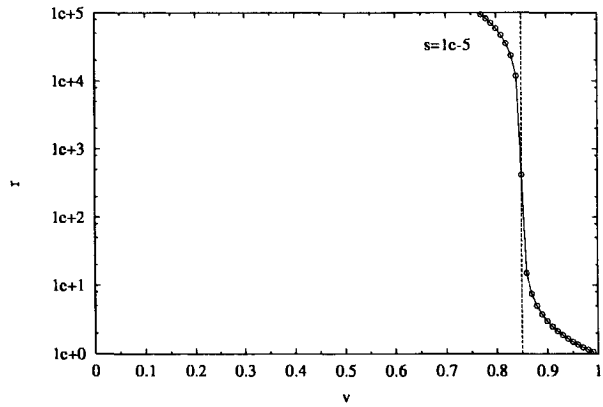

(b)

Figure 3.4: *Simulated compression of a rigid structure filled for 85% with fluid. The horizontal axes refer to the normalized volume, whereas the vertical axes refer to the normalized pressure. (a) Structure with an incompressible fluid. (b) Structure with a nearly incompressible fluid.*

set to zero and only two elements are used, the model will remain flat. As can be seen in Figure 3.4, the pressure becomes negative in case of an incompressible fluid and remains positive in case of a nearly incompressible fluid. These results match with the analytical results as depicted in Figure 3.2. Notice, that the reference volume remains a pyramid with flat faces, which is a consequence of the too coarse model, which consist of only two elements.

The flexible structure consists of a square plate modeled using a fine mesh (see Figure 3.5). As can be seen in Figure 3.6 the pressure becomes negative in case of an incompressible fluid and causes the curvature of the deformed configuration to reverse (see Figure 3.5a). In case of a nearly incompressible fluid the pressure remains positive.

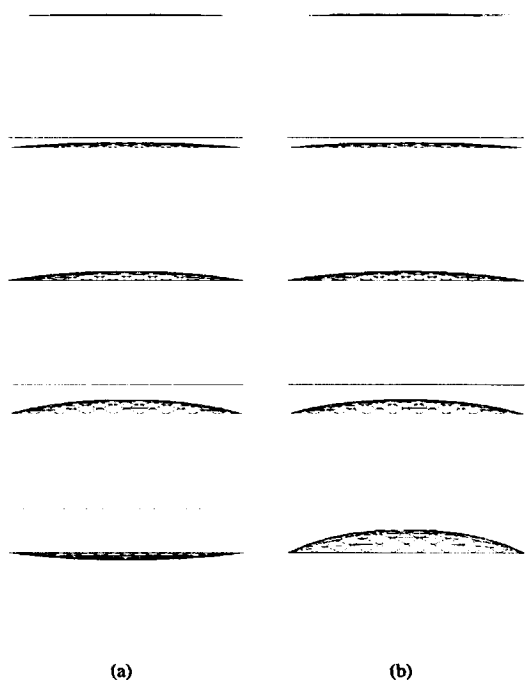

Figure 3.5: *Deformed configurations of a flexible structure filled for 85% with fluid. Two series of subsequent configurations have been depicted. The horizontal lines depict the undeformed configuration. The applied load increases going in downward direction. (a) Deformation of the structure with an incompressible fluid. (b) Deformation of the structure with a nearly incompressible fluid.*

3.5 Application

Two applications for which the pressure influence plays a significant role will be described. The first example is an airspring that has been studied by Berry [7]. The second example is a plastic bottle for edible oil.

An airspring is an air-filled reinforced rubber balloon held fixed between two rigid end plates. As the end plates are moved up and down, the internal volume expands or contracts, providing the additional pressure to support the loads. Nearly all of the load carrying capacity of the airspring is contributed by the enclosed air [7]. The two-bellowed airspring, as used by Berry has been depicted in Figure 3.7. Due to symmetry Berry used an axisymmetric model as depicted in Figure 3.8 , which also depicts the dimensions of the spring. The airspring is made out of rubber reinforced by two layers of polyester cords, which causes the spring to have a very high membrane stiffness and a very low bending stiffness. The results from Berry have been compared with results obtained by the present approach. For this a $\frac{1}{16}$ model of the airspring was modeled using triangular elements [9,72,73]. The model had the dimensions as depicted in Figure 3.8 and isotropic material properties (Young's modules: 3000N/mm^2, Poisson's ratio: 0.35) are used. The airspring is modeled with a thickness of 2 mm. It can be expected that for low internal pressures the load-compression curve will be different as compared to the results of Berry (1996) due to usage of different material properties. However, at higher pressures this effect should decrease.

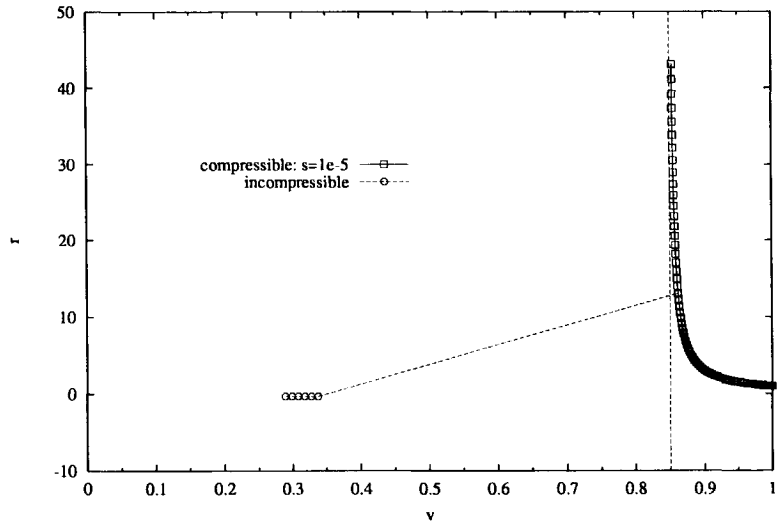

Figure 3.6: *Simulated compression of a flexible structure filled for 85% with fluid. The horizontal axis refers to the normalized volume, whereas the vertical axis refers to the normalized pressure. Two simulations have bee depicted: with (compressible) and without penalty factor (incompressible).*

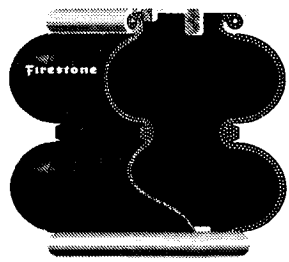

Figure 3.7: *The two-bellowed airspring (By courtesy of Firestone [11]).*

The mesh of the model has been depicted in Figure 3.9, on all sides, except the sides at the top, symmetry conditions have been applied. On the top surface of the airspring displacements in downward direction have been prescribed. The initial internal volume has been set to $1.3257 \times 10^7 \text{mm}^3$, which is conform the actual internal volume of the airspring. Simulations have been carried out for 3 different initial pressures (0.1378, 0.2756 and 0.4134 MPa at 0 mm compression). This is conform the experiments as described by Berry (1996), where the airspring was clamped between two horizontal platen, after which the initial internal pressure was increased to the desired initial internal pressure. The results from simulations and experimental results [7] have been depicted in Figure 3.10. This figure also shows that for small internal pressures, as mentioned before, results differ due to different material properties. This explains why the results for an initial pressure of 0.1378 MPa differ relatively more from Berry's (1996) calculated and experimental results than the results for higher initial pressures.

The second example describes the influence of the internal pressure for a plastic bottle for edible

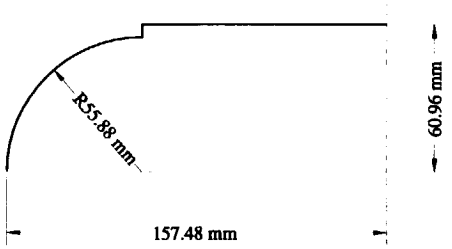

Figure 3.8: *Dimensions of the airspring as used in the model.*

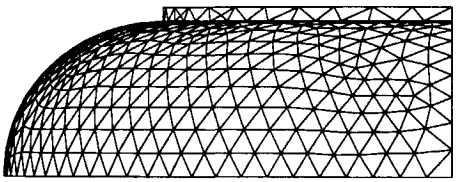

Figure 3.9: *Mesh of the airspring model. The mesh describes* $\frac{1}{16}$ *model of the two bellowed airspring. Along bottom and side edges symmetry conditions have been applied.*

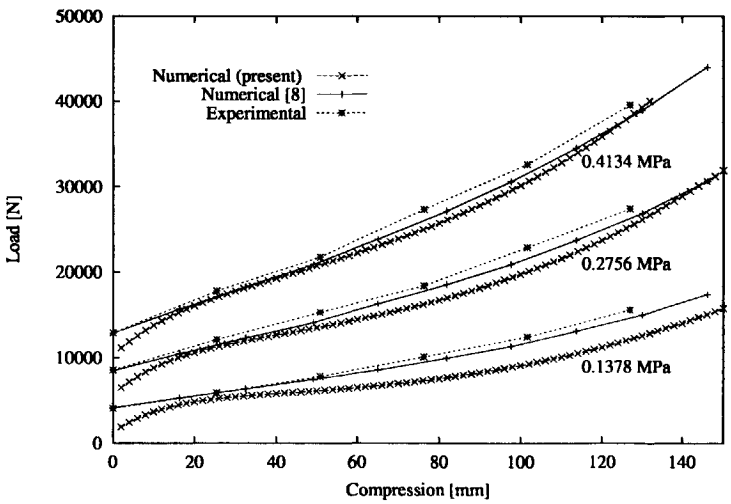

Figure 3.10: *Experimental and simulated results for the airspring example. The horizontal axis refers to the compression of the airspring, the vertical axis gives the required compression force. The pressures 0.1378, 0.2756 and 0.4134 MPa are initial internal pressures at 0 mm compression.*

oil. The bottle as depicted in Figure 3.11 is a 750 ml oPET (oriented PET) stretch-blown bottle for vegetable oil. During compression of the bottle, for example caused by stacking, a significant pressure

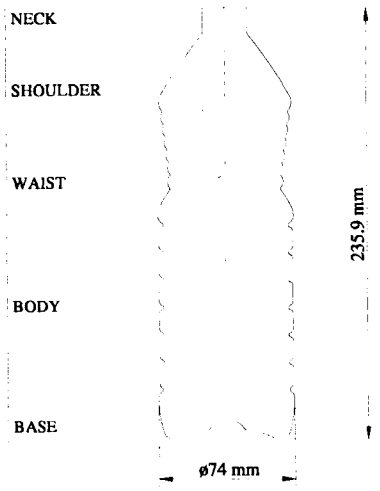

Figure 3.11: *Geometry of the 750 ml round oPET bottle used for packing edible oil.*

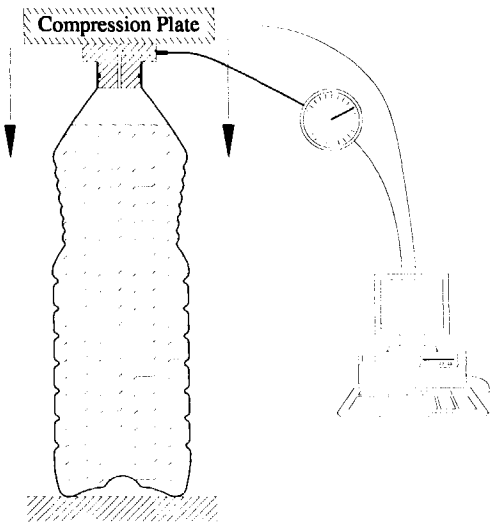

Figure 3.12: *Experimental setup of the pressure and top load measurements.*

increase occurs in the bottle. Several bottles, with different fill levels have been studied experimentally and afterwards simulations have been carried out for validation of the described model. In Figure 3.12 the experimental set up is depicted. During the experiments the bottle was closed with a plug. A small channel inside the plug and a narrow metal tube connected the headspace with the barometer. From several bottles the compression force, the internal (over)pressure and the vertical compression were evaluated and recorded on a computer. In all simulations triangular elements [9, 72, 73], and linear material

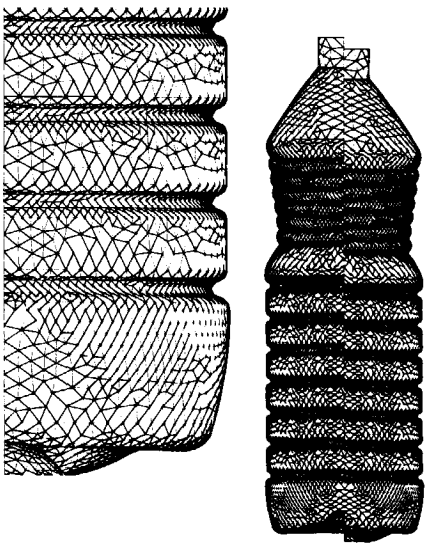

Figure 3.13: *Simulated deformation of a nearly full bottle under top load. This figure depicts a bottle far past its initial buckling. Since the bottle was supported on the outer diameter only (the bottle was standing on a ring), the high internal pressure caused the bottom to buckle outwards. The last is in agreement with experimental results.*

behavior have been used. The finite element model of the bottle is depicted in Figure 3.13. As can be seen in Figure 3.14 the calculated and measured results match well. The fact that the buckling load of the bottle is not adequately described during the simulations can be appointed to the used material properties and the fact that initial imperfections in geometry and wall thickness distribution have not been taken into account [66, 67]. The figure clearly points out that the internal pressure significantly contributes to the strength and stiffness of the structure. The difference between experimental and calculated results at higher internal pressures for a bottle filled for 90% with fluid is caused by solubility effects which have not been taken into account and are further discussed in the next chapter. One might expect that at higher pressures and small gas-fluid ratios, the effect of gas components (in this case oxygen and nitrogen) dissolving in fluid becomes more pronounced.

In current practice the bottle is filled for 96.8% or more with fluid. In this chapter only bottles filled up to 90% have been examined, higher fill levels require inclusion of the solubility effect [71] which is beyond the scope of this chapter.

3.6 Conclusions

Many structures enclose a certain volume. Often this volume is filled with gas whereas in other structures a combination of fluid and gas is present. The gas enclosed by a structure can significantly contribute to the strength and stiffness. The methods to solve the governing equations as described in this chapter take this pressure effect into account even when the initial stiffness matrix is singular and preserve the sparse structure of the system matrix. The complication of a singular modified stiffness matrix ($\mathbf{K}$) has been addressed in Appendix 3.B. In most cases the approach discussed in Section 3.3 will be most efficient. Notice, that only in rare cases the modified system matrix will be singular. The implementation of the solution procedure which is applicable to singular initial stiffness matrices (Appendix 3.B) is

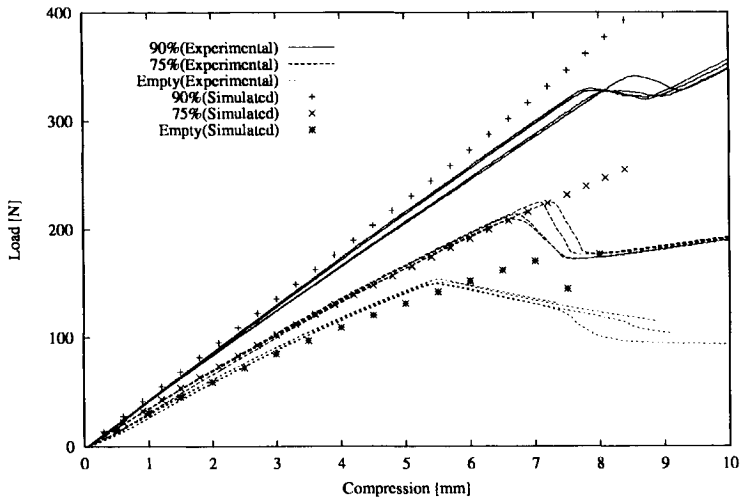

Figure 3.14: *Experimental and numerical results for a bottle filled for 90%, 75% and 0%(empty) with fluid. The compression and the required compression load have been plotted on the horizontal and vertical axis, respectively. Note, that lines have been used for experimental results.*

significantly more involved as compared to the formulation presented in Section 3.3.

Some complications can occur when during a FE analysis the volume change during a linearized step is larger than the remaining gas volume. When the fluid is incompressible this leads to negative internal pressure. Obviously, this situation is physically infeasible. The last can be circumvented by introduction of a fluid compliance. This compliance should be chosen very small in order not to affect the fluid volume in the structure.

The proposed model and its implementation has been verified by two examples and has finally been applied to two practical examples, namely an airspring and a plastic bottle. The calculated results were in good agreement with the experimental results. As for the airspring example adequate information on material data is missing, results indicate discrepancies for low internal pressures. However, as soon as the mechanical behavior is dominated to a significant extent by the internal pressure, numerical and experimental results are in perfect agreement. In case the amount of gas is small as compared to the fluid volume, deviations with experimental results tend to be large. This effect is due to solubility effects which play a crucial role for small gas-fluid ratios. This aspect will be the subject of Chapter 4.

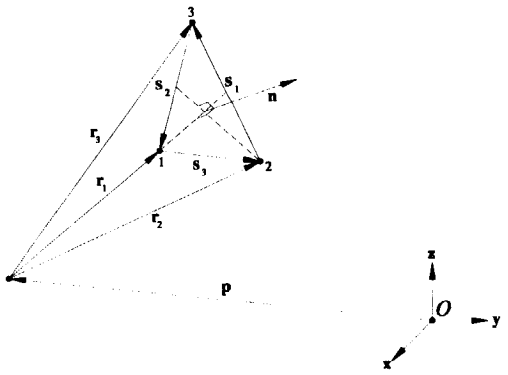

Figure 3.A-1: *Element, reference point and origin.*

Appendix 3.A

Calculation of the enclosed volume

The volume enclosed by the structure can be determined straightforwardly. In Figure 3.A-1 a triangular element [9, 72, 73] has been depicted with a fixed reference point, **p**. The total enclosed volume of a closed structure can be determined by

$$V = \sum_{k=1}^{n} V_k, \tag{3.A-1}$$

where k, n and V_k are the element number, the total number of elements and the contribution of a single element to the reference volume, respectively. The contribution of a single element to the reference volume is defined by the tetraedrical volume which is defined by the reference point, **p**, and the corner nodes of the element. This volume can be calculated using

$$V_k = \frac{1}{6}\mathbf{r}_1 \cdot (\mathbf{r}_2 \times \mathbf{r}_3) , \tag{3.A-2}$$

where $\mathbf{r}_1$, $\mathbf{r}_2$ and $\mathbf{r}_3$ are the position vectors of the corner nodes with respect to the reference point **p**. These vectors span the tetraeder and are depicted in Figure 3.A-1. In every configuration the vectors $\mathbf{r}_i$ are determined by

$$\mathbf{r}_i = \mathbf{x}_i + \hat{\mathbf{u}}_i - \mathbf{p},$$

where $\mathbf{x}_i$ and $\hat{\mathbf{u}}_i$ are the initial corner node location vectors and the nodal displacement vectors, respectively.

First-order derivatives of the volume

From (3.A-2) the first-order variations of the volume can be determined, giving

$$\delta V_k = \frac{1}{6}\delta\mathbf{r}_1 \cdot (\mathbf{r}_2 \times \mathbf{r}_3) + \frac{1}{6}\mathbf{r}_1 \cdot (\delta\mathbf{r}_2 \times \mathbf{r}_3) + \frac{1}{6}\mathbf{r}_1 \cdot (\mathbf{r}_2 \times \delta\mathbf{r}_3) .$$

After rearranging and substitution of $\delta\mathbf{r}_i = \delta\hat{\mathbf{u}}_i$, δV_k reads

$$\delta V_k = \frac{1}{6}\left[\delta\hat{\mathbf{u}}_1^T \delta\hat{\mathbf{u}}_2^T \delta\hat{\mathbf{u}}_3^T\right] \begin{bmatrix} \mathbf{r}_2 \times \mathbf{r}_3 \\ \mathbf{r}_3 \times \mathbf{r}_1 \\ \mathbf{r}_1 \times \mathbf{r}_2 \end{bmatrix} . \tag{3.A-3}$$

Second-order derivatives of the volume

The second-order variations can be obtained by differentiation of the first-order variations. With (3.A-3) the second-order variations of the volume read

$$\delta_1\delta_2 V_k = \frac{1}{6}\left[\delta_1\hat{\mathbf{u}}_1^T\ \delta_1\hat{\mathbf{u}}_2^T\ \delta_1\hat{\mathbf{u}}_3^T\right]\begin{bmatrix}\delta_2(\mathbf{r}_2\times\mathbf{r}_3)\\ \delta_2(\mathbf{r}_3\times\mathbf{r}_1)\\ \delta_2(\mathbf{r}_1\times\mathbf{r}_2)\end{bmatrix}.$$

This can be rewritten as

$$\delta_1\delta_2 V_k = \frac{1}{6}\left[\delta_1\hat{\mathbf{u}}_1^T\ \delta_1\hat{\mathbf{u}}_2^T\ \delta_1\hat{\mathbf{u}}_3^T\right]\Gamma\begin{bmatrix}\delta_2\hat{\mathbf{u}}_1\\ \delta_2\hat{\mathbf{u}}_2\\ \delta_2\hat{\mathbf{u}}_3\end{bmatrix},$$

where Γ is the following matrix

$$\Gamma = \begin{bmatrix}
\cdot & \cdot & \cdot & \cdot & r_3^3 & -r_3^2 & \cdot & -r_2^3 & r_2^2\\
\cdot & \cdot & \cdot & -r_3^3 & \cdot & r_3^1 & r_2^3 & \cdot & -r_2^1\\
\cdot & \cdot & \cdot & r_3^2 & -r_3^1 & \cdot & -r_2^2 & r_2^1 & \cdot\\
\cdot & -r_3^3 & r_3^2 & \cdot & \cdot & \cdot & \cdot & r_1^3 & -r_1^2\\
r_3^3 & \cdot & -r_3^1 & \cdot & \cdot & \cdot & -r_1^3 & \cdot & r_1^1\\
-r_3^2 & r_3^1 & \cdot & \cdot & \cdot & \cdot & r_1^2 & -r_1^1 & \cdot\\
\cdot & r_2^3 & -r_2^2 & \cdot & -r_1^3 & r_1^2 & \cdot & \cdot & \cdot\\
-r_2^3 & \cdot & r_2^1 & r_1^3 & \cdot & -r_1^1 & \cdot & \cdot & \cdot\\
r_2^3 & -r_2^1 & \cdot & -r_1^2 & r_1^1 & \cdot & \cdot & \cdot & \cdot
\end{bmatrix}.$$

Here, r_j^i refers to the i-th component $\mathbf{r}_j$. Note, that Γ is symmetric.

Appendix 3.B

The present appendix discusses two techniques to find the solution of

$$\left[\begin{bmatrix} \mathbf{K}^{cc} & \mathbf{K}^{c0} \\ \mathbf{K}^{0c} & \mathbf{K}^{00} \end{bmatrix} + \kappa \begin{bmatrix} \mathbf{a}^c\mathbf{a}^{cT} & \mathbf{a}^c\mathbf{a}^{0T} \\ \mathbf{a}^0\mathbf{a}^{cT} & \mathbf{a}^0\mathbf{a}^{0T} \end{bmatrix} \right] \begin{bmatrix} \Delta\mathbf{u}^c \\ \Delta\mathbf{u}^0 \end{bmatrix} = \begin{bmatrix} \Delta\mathbf{f}^c \\ \Delta\mathbf{f}^0 \end{bmatrix}.$$

The unknown variables are $\Delta\mathbf{u}^c$ and $\Delta\mathbf{f}^0$, whereas $\Delta\mathbf{u}^0$ and $\Delta\mathbf{f}^c$ are the known variables. Looking at the unknowns, $\Delta\mathbf{u}^c$ only and by trying

$$\Delta\mathbf{u}^c = \mu\mathbf{a}^c + \mathbf{b}^c, \qquad \mathbf{a}^{cT}\mathbf{b}^c = 0, \tag{3.B-1}$$

the following augmented set of equations can be obtained

$$\begin{bmatrix} \mathbf{K}^{cc} & \mathbf{K}^{cc}\mathbf{a}^c + \kappa(\mathbf{a}^{cT}\mathbf{a}^c)\mathbf{a}^c \\ \mathbf{a}^{cT} & 0 \end{bmatrix} \begin{bmatrix} \mathbf{b}^c \\ \mu \end{bmatrix} = \begin{bmatrix} \Delta\mathbf{f}^c - (\mathbf{K}^{c0} + \kappa\mathbf{a}^c\mathbf{a}^{0T})\Delta\mathbf{u}^0 \\ 0 \end{bmatrix}. \tag{3.B-2}$$

The first approach that will be described to solve (3.B-2) will make use of the inverse of the stiffness matrix $\mathbf{K}^{cc}$, while an alternative technique does not and is therefore applicable when $\mathbf{K}^{cc}$ is singular.

Regular stiffness matrix

The first technique assumes a regular stiffness matrix $\mathbf{K}^{cc}$. From (3.B-2) it can be determined that

$$\mathbf{b}^c = \mathbf{K}^{cc^{-1}}\left[\Delta\mathbf{f}^c - (\mathbf{K}^{c0} + \kappa\mathbf{a}^c\mathbf{a}^{0T})\Delta\mathbf{u}^0\right] - \mu\mathbf{a}^c - \mu\kappa(\mathbf{a}^{cT}\mathbf{a}^c)(\mathbf{K}^{cc^{-1}}\mathbf{a}^c). \tag{3.B-3}$$

Pre-multiplication by $\mathbf{a}^{cT}$ gives

$$\mu = \left[\frac{\mathbf{a}^{cT}\mathbf{K}^{cc^{-1}}(\Delta\mathbf{f}^c - (\mathbf{K}^{c0} + \kappa\mathbf{a}^c\mathbf{a}^{0T})\Delta\mathbf{u}^0)}{(\mathbf{a}^{cT}\mathbf{a}^c)(1 + \kappa\,\mathbf{a}^{cT}\mathbf{K}^{cc^{-1}}\mathbf{a}^c)}\right], \tag{3.B-4}$$

where use of $\mathbf{a}^{cT}\mathbf{b}^c = 0$ has been made. Combining (3.B-1), (3.B-3), and (3.B-4) leads to the solution of (3.B-2)

$$\begin{aligned} \Delta\mathbf{u}^c = & -\kappa\left[\frac{\mathbf{a}^{cT}\mathbf{K}^{cc^{-1}}(\Delta\mathbf{f}^c - (\mathbf{K}^{c0} + \kappa\mathbf{a}^c\mathbf{a}^{0T})\Delta\mathbf{u}^0)}{(1 + \kappa\mathbf{a}^{cT}\mathbf{K}^{cc^{-1}}\mathbf{a}^c)}\right]\left(\mathbf{a}^{cT}\mathbf{a}^c\right)\left(\mathbf{K}^{cc^{-1}}\mathbf{a}^c\right) \\ & + \mathbf{K}^{cc^{-1}}\left[\Delta\mathbf{f}^c - (\mathbf{K}^{c0} + \kappa\mathbf{a}^c\mathbf{a}^{0T})\Delta\mathbf{u}^0\right]. \end{aligned}$$

This technique requires only one additional back substitution in order to calculate $\mathbf{K}^{cc^{-1}}\mathbf{a}^c$ and proved very efficient. It is emphasized that the approach works only for a regular stiffness matrix $\mathbf{K}^{cc}$.

Singular stiffness matrix

In case the initial stiffness matrix $\mathbf{K}^{cc}$ is singular the previous technique is not applicable and another approach must be followed to solve (3.B-2). The alternative technique makes (3.B-2) symmetrical by pre-multiplying it with

$$\mathbf{T} = \begin{bmatrix} \mathbf{I} & 0 \\ \mathbf{a}^{cT} & \kappa\mathbf{a}^{cT}\mathbf{a}^c \end{bmatrix},$$

where $\mathbf{I}$ is a unity matrix with the same dimensions as $\mathbf{K}^{cc}$. This results in

$$\begin{bmatrix} \mathbf{K}^{cc} & \mathbf{K}^{cc}\mathbf{a}^c + \kappa(\mathbf{a}^{cT}\mathbf{a}^c)\mathbf{a}^c \\ \left\{\mathbf{K}^{cc}\mathbf{a}^c + \kappa(\mathbf{a}^{cT}\mathbf{a}^c)\mathbf{a}^c\right\}^T & \mathbf{a}^{cT}\mathbf{K}^{cc}\mathbf{a}^c + \kappa(\mathbf{a}^{cT}\mathbf{a}^c)^2 \end{bmatrix} \begin{bmatrix} \mathbf{b}^c \\ \mu \end{bmatrix} = \begin{bmatrix} \Delta\mathbf{f}^c - (\mathbf{K}^{c0} + \kappa\mathbf{a}^c\mathbf{a}^{0T})\mathbf{u}^0 \\ \mathbf{a}^{cT}\left(\Delta\mathbf{f}^c - (\mathbf{K}^{c0} + \kappa\mathbf{a}^c\mathbf{a}^{0T})\mathbf{u}^0\right) \end{bmatrix}. \tag{3.B-5}$$

As can be seen from (3.B-5), the matrix on the l.h.s. is symmetric. In spite of the fact that the stiffness matrix $\mathbf{K}^{cc}$ can be singular, the modified matrix can be regular. The obtained augmented set of equations (3.B-5) can be solved with a direct solver. A more careful inspection of (3.B-5) reveals that only an additional row or column has to be stored, *i.e.* a sparse structure of $\mathbf{K}^{cc}$ will not be destroyed.

Based on: R. van Dijk, F. van Keulen and J.C. Sterk, The Influence of Solubility Effects on the Pressure Increase during Deformation of Closed Thin-Walled Structures, Thin-Walled Structures, 35(1), 25–40, (1999).

Chapter 4

Solubility Effects in Closed Filled Structures

In structures with an internal volume, the enclosed gas can significantly contribute to the strength and stiffness. If this enclosed volume also contains a fluid then an exchange of components between the gas and fluid can take place. This chapter describes these solubility effects and presents a method how to account for the solubility effect in structural analyses. The described method has been studied on a typical packaging problem, namely a closed filled bottle under vertical compression. The numerical studies have been validated by experiments.

4.1 Introduction

Many structures surround a volume which contains both fluid and gas. Typical examples are filled bags, bottles, soft drink cans, *etc.* Deformation of such structures, for example the vertical compression during stacking, causes internal pressure changes which consequently lead to gas dissolving in the fluid or to escaping of gas from the fluid.

The present work originates from the fact it was desirable for Unilever, a large manufacturer of food products, to determine the compression strength of closed filled plastic oil bottles as depicted in Figure 4.1. The compression strength of a bottle is determined by the maximum load the bottle can carry before the occurrence of collapse, for example in a pallet load. During experiments and simulations (which accounted only for pressure effects) significant differences were found between experimental and numerical results for nearly filled bottles. This was indicated to be caused by solubility effects.

Among others [7,10,20,25,29,33,58,78], Berry [7] investigated internal pressure effects and applied his methods to pressurized soft drink cans and an airspring. For these applications fluid-gas interactions have not been addressed. Due to the fact that for small gas-fluid ratios (e.g. 5% gas and 95% fluid) the gas-fluid interactions have a significant influence on the mechanical behavior of the structure, this effect has been described in this chapter.

The present chapter is divided into different parts. Firstly, a theoretical description is given which describes how the contents, gas and fluid, influence on the internal gas pressure. Secondly, it is discussed how the solubility effect has been accounted for. Thirdly, implementational issues are addressed. Thereafter, the described method is verified with experimental results of the bottle filled with water.

4.2 Pressure effects

In Figure 4.2, a typical situation has been depicted. The figure displays a closed structure which contains both gas and fluid. During compression of the bottle the internal pressure will increase and the gas will dissolve in the fluid, consequently leading to a new equilibrium gas pressure. In the sequel it has been

Figure 4.1: *A plastic 750 ml bottle for edible oil.*

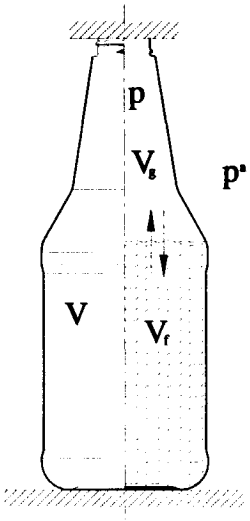

Figure 4.2: *Situation sketch, V, V_g, V_f, p and p^a are the total enclosed volume, the gas volume, the fluid volume, the internal pressure and the ambient pressure, respectively. The arrows visualize the gas exchange due to solubility effects.*

assumed that hydrostatic pressure effects of the liquid are negligible in comparison with the pressure effects of the gas.

The virtual work corresponding to the pressure difference, can be expressed as

$$\delta W_p^{ext} = (p(V_g) - p^a)\,\delta V_g, \tag{4.1}$$

where $p(V_g)$ represents a gas law, giving the total gas pressure as a function of the total gas volume, V_g. When the enclosed volume contains an ideal mixture of gases, then according Dalton's Law of partial

pressures [28, p.36], the total gas pressure can be described as

$$p = \sum_{i=1}^{m} p_i, \qquad i = 1 \dots m, \tag{4.2}$$

where p, p_i and m, are the total internal actual gas pressure, the actual partial internal gas pressure of gas i and the number of gases, respectively. The partial gas pressure is defined as [23]

$$p_i = \frac{n_i}{n} p, \tag{4.3}$$

where n_i and n are the amount of gas i and the total amount of gas, respectively. Note, that $\sum_{i=1}^{m} n_i = n$ [28, p.36], where n is the total amount of gas (in mol). In case of a mixture of perfect gases and making use of (4.3), the gas law can be described as [23, 24]

$$\frac{pV_g}{nT} = \frac{p_i V_g}{n_i T} = \frac{p_i^0 V_g^0}{n_i^0 T^0} = R. \tag{4.4}$$

In the present setting it is more convenient to express the pressure in terms of the total enclosed volume V. In case, the gas is governed by (4.4) and with a constant fluid volume, the pressure is determined by

$$p = \sum_{i=1}^{m} p_i = \sum_{i=1}^{m} \frac{V^0 - V_f}{V - V_f} \frac{n_i}{n_i^0} \frac{T}{T^0} p_i^0. \tag{4.5}$$

After introducing

$$f = \frac{V_f}{V^0}, \qquad v = \frac{V}{V^0}, \qquad \tau = \frac{T}{T^0}, \tag{4.6}$$

where f, v and τ are the initial fluid fraction, the actual volume fraction and the normalized temperature, respectively, (4.5) can be rewritten as

$$p = \sum_{i=1}^{m} p_i = \sum_{i=1}^{m} \frac{n_i}{n_i^0} \frac{1 - f}{v - f} \tau p_i^0. \tag{4.7}$$

The latter results thus in an expression where the internal pressure is given as a function of the internal gasses, the solubility coefficients, the fluid volume and the enclosed volume.

4.3 Solubility effects

For small gas and large fluid volumes in an enclosed structure the gas exchange can have a significant effect on the behavior of the complete structure. According to Henry's law the concentration of a solute gas in a solution is directly proportional to the partial pressure of that gas above the solution [13, 43]. Henry's law is found to be an accurate description of the behavior of gases dissolving in liquids when the concentration and partial pressures are reasonably low [13, 43, 53]. In the sequel it will be assumed that Henry's law is applicable. Further, it needs mentioning that the molar solubility of a gas is temperature dependent: the solubility of a gas decreases for higher temperatures. In the sequel the temperature will be assumed constant: $\tau = 1$, since this is a common manufacturing condition. Following Henry's law for constant temperature, the dissolved amount of gas (in mol) reads

$$D_i = p_i S_i V_f, \tag{4.8}$$

where D_i and S_i are the dissolved amount of gas i (in mol) and the molar solubility of gas i at $T = T^0$, respectively. In the present formulation it has been assumed that the solubility equilibrium is a quasi-static process, in other words the equilibrium occurs instantaneously. This assumption is not verified

in the present thesis but has been derived from experimental work on the compression of closed-filled bottles at different compression speeds.

With (4.8) the amount of gas i becomes

$$n_i = N_i - D_i = N_i - p_i S_i V_f, \tag{4.9}$$

where N_i is the total amount of gas i, *i.e.* both dissolved in the fluid and as gas. Notice, N_i is assumed constant, this means that the structure is a closed system. In other words, gas cannot permeate through the bottle wall and N_i can easily be determined from

$$N_i = n_i^0 + D_i^0, \tag{4.10}$$

where D_i^0 is the initial amount of dissolved gas i in the fluid. $D_i^0/(p_i^0 V_f)$ refers to the initial saturation of the fluid and will in the sequel be denoted by s_i. For a degassed fluid, it holds true $D_i^0 = 0$. In many cases, the filling conditions are ambient and saturation at ambient conditions took place. It can then be assumed that $D_i^0 = p_i^a S_i V_f$, where p_i^a is the partial pressure of gas i at ambient conditions.

Note, that the amount of a certain component in the gas volume now reads, $n_i = n_i^0 + D_i^0 - p_i S_i V_f$ and becomes negative for partial pressures larger than the critical partial pressure, which is defined as

$$p_i^{cr} = \frac{n_i^0 + D_i^0}{S_i V_f}. \tag{4.11}$$

The last is due to the linear relationship between the dissolved amount of gas D_i and the partial pressure p_i as described in (4.8). Therefore, care should be taken not to approach this critical partial pressure numerically. Note that also the gas law as used in this chapter is not valid for very high pressures.

The initial amount of gas i, n_i^0, enclosed by the structure can easily be determined using the gas law, giving

$$n_i^0 = \frac{p_i^0}{TR}(V^0 - V_f). \tag{4.12}$$

When substituting (4.9), (4.10) and (4.12) in (4.7) the partial pressure for $\tau = 1$ becomes

$$p_i = \frac{1-f}{v-f} p_i^0 + \frac{f}{v-f}\left(\frac{D_i^0}{V_f} - p_i S_i\right) TR. \tag{4.13}$$

The equilibrium partial pressure can directly be derived from (4.13)

$$p_i = \frac{1 - f(1 - s_i TR)}{v - f(1 - S_i TR)} p_i^0. \tag{4.14}$$

As mentioned before in (4.11) the critical pressure p_i^{cr} may not be exceeded. Substituting (4.12) in (4.11) gives

$$p_i^{cr} = \frac{1 - f(1 - s_i TR)}{f S_i TR} p_i^0. \tag{4.15}$$

Comparing (4.14) and (4.15) shows that the critical pressure will be exceeded for values $v < f$ thus when the total volume contains only fluid.

Hence, the total internal pressure can now be determined according

$$p = \sum_{i=1}^{m} p_i = \sum_{i=1}^{m} \frac{1 - f(1 - s_i TR)}{v - f(1 - S_i TR)} p_i^0 \qquad \text{and} \qquad v > f, \tag{4.16}$$

and is a function of the enclosed volume only.

As will be shown later also the derivative of the total pressure with respect to the volume will be required, which can be found by differentiation of (4.14),

$$\frac{dp}{dV} = \sum_{i=1}^{m} \frac{dp_i}{dV} = \sum_{i=1}^{m} -\frac{1 - f(1 - s_i TR)}{(v - f(1 - S_i TR))^2} \frac{p_i^0}{V^0}. \tag{4.17}$$

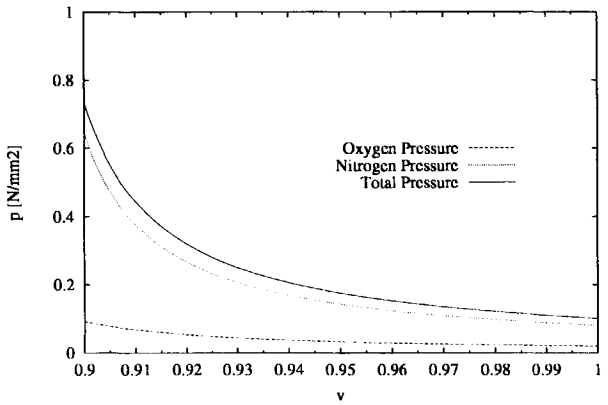

Figure 4.3: *Total, partial oxygen and partial nitrogen pressure for an arbitrary closed structure filled for 90% with fluid, while solubility effects have been taking into account. The figure clearly shows how the total internal pressure depends on the partial pressures. Horizontally, the reference volume v (v = actual volume/initial volume) has been plotted. The vertical axis displays the total as well as the internal partial pressure(s).*

If the solubility can be neglected then expression (4.14) simplifies to

$$p = \sum_{i=1}^{m} \frac{1-f}{v-f} p_i^0 = \frac{1-f}{v-f} p^0, \qquad p^0 = \sum_{i=1}^{m} p_i^0. \tag{4.18}$$

Consequently, the derivative of the pressure becomes

$$\frac{dp}{dV} = -\frac{1-f}{(v-f)^2} \frac{p^0}{V^0}. \tag{4.19}$$

As an example in Figure 4.3 the partial and total pressure(s) have been depicted for an arbitrary closed structure filled for 90% with fluid, using the following assumptions:

- 2 gasses: O_2 and N_2;
- the initial pressure, p_i^0 , of O_2 and N_2 are: 0.02 and 0.08 N/mm^2;
- the solubilities, S_i^0, of O_2 and N_2 are: 1.26×10^{-8} and 6.38×10^{-9} mol/(mm^3 N/mm^2);
- the initial amount of dissolved gas is: $D_i^0 = p_i^a S_i V_f = p_i^0 S_i V_f^0$; this means that it is assumed that the initial internal pressure is ambient and that the fluid was saturated with O_2 and N_2 at ambient conditions;
- the temperature is: 298 K;
- the gas constant is: 8314.4 Nmm/(K mol).

In Figure 4.4, the influence of solubility effects has been depicted using the same assumptions as in Figure 4.3. From Figure 4.4 it can be seen that the solubility has a significant effect on the internal pressure. This figure also shows that for $v < f$, thus when in practice the fluid will be compressed, the internal pressure is not correctly predicted. When the solubility can be neglected, this can occur during a FE calculation, as soon as the volume change caused by a linearized step in the nonlinear

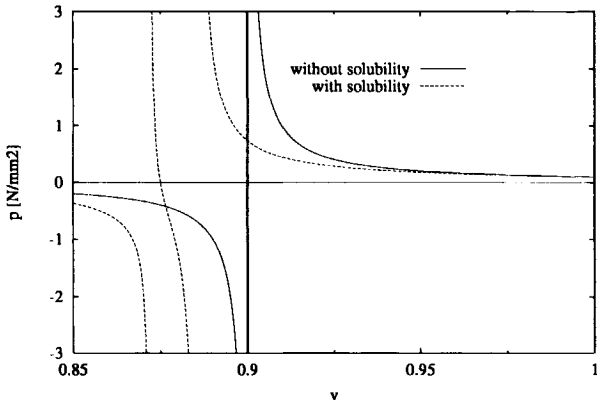

Figure 4.4: *The figure depicts the analytical results for the internal pressure of two different cases (with and without solubility effects) for a structure filled for 90% with fluid ($f = 0.9$). Note, that for both cases the pressure is discontinuous. Along the horizontal axis the reference volume, v, is depicted. The vertical axis displays the* total *internal pressure, p. The figure clearly shows the influence of solubility effects. Note also that for the physically infeasible values $v < f$, thus when the actual volume is less then the fluid volume, the pressure is incorrectly described for cases with and without solubility effects.*

analysis is larger than the current gas volume and consequently, the new gas volume, $v - f$, becomes negative. This will consequently result in a negative pressure. In case the solubility can be neglected this can be circumvented by introducing a penalty factor for the fluid compressibility [71]. In case the solubility cannot be neglected the problem should be solved more rigorously. Since, at the moment of fluid compression, thus $v = f$, all gas is dissolved in the fluid (see also (4.16)), the internal pressure will only be determined by the fluid compression, for example,

$$p = \left(1 - \frac{V_f^*}{V_f}\right) c + p^0, \tag{4.20}$$

where c is the compressibility of the fluid, V_f^* the actual fluid volume and V_f the initial fluid volume. Note, that the here used assumption that all gas will be dissolved at the moment of fluid compression does probably not hold true in practice.

4.4 Finite element approach*

In a general FE setting [6, 79] we often start from the principal of virtual work which reads

$$\delta W^{int} = \delta W^{ext}, \tag{4.21}$$

where δW^{int} and δW^{ext} are the internal and external virtual work, respectively.

Assuming linear elastic material behavior the internal virtual work can be formally described as

$$\delta W^{int} = \delta \boldsymbol{\varepsilon}^T \boldsymbol{\sigma} = \delta \boldsymbol{\varepsilon}^T \mathbf{S} \boldsymbol{\varepsilon}(\mathbf{u})$$

where $\boldsymbol{\varepsilon}, \boldsymbol{\sigma}, \mathbf{u}$ and $\mathbf{S}$ are the generalized deformations, the generalized stresses, the nodal degrees of freedom and a symmetric matrix which depends on the elastic material properties and the precise element

* The reader who read Chapter 3.3 can skip this section.

definitions, respectively. The corresponding rate equations become

$$\left(\mathbf{D}^T\mathbf{S}\mathbf{D} + \mathbf{G}\right)\frac{d\mathbf{u}}{d\lambda} = \frac{d\mathbf{f}}{d\lambda}.$$

The matrix **G** represents the geometric stiffness matrix. The matrix **D** gives the relations between the deformation rates and the nodal velocities. The last term, the load vector **f**, can in the present setting be described by two terms

$$\mathbf{f} = \lambda\mathbf{f}^{\lambda} + \mathbf{f}^{p},$$

where $\lambda\mathbf{f}^{\lambda}$ is an external load vector, independent of **u**, which can be scaled with the load factor λ. The vector $\mathbf{f}^{p}$ is the external load due to the gas which, with the help of (4.1), can be written as

$$\mathbf{f}^{p} = \left(p(V_g) - p^a\right)\frac{\partial V}{\partial \mathbf{u}} \tag{4.22}$$

During a FE analysis the external load will be incremented by changing the factor λ. The corresponding rate equations become

$$\left[\left(\mathbf{D}^T\mathbf{S}\mathbf{D} + \mathbf{G}\right) - \frac{\partial \mathbf{f}^{p}}{\partial \mathbf{u}}\right]\frac{d\mathbf{u}}{d\lambda} = \mathbf{f}^{\lambda}. \tag{4.23}$$

With (4.22) it follows that

$$f^{p}_{i,j} = \frac{dp(V_g)}{dV}V_{,i}V_{,j} + \left(p(V_g) - p^a\right)V_{,ij}, \tag{4.24}$$

where $\cdots_{,i}$ refers to $\frac{\partial \cdots}{\partial u_i}$.

It may be clear, that V is a function of nearly all nodal degrees of freedom due to the use of shell elements. Therefore, the first term in the r.h.s. of (4.24) yields a *non-sparse* contribution to the system matrix. The contribution $f^{p}_{i,j}$ is symmetric and has previously been examined by many investigators [35, 46,47,57,78]. The non-sparse system matrix requires a special method to solve the set of equations using a direct method. Combining (4.23) and (4.24) in such a way that the sparse and non-sparse components are separated leads to

$$[\mathbf{K} + \kappa\mathbf{a}\mathbf{a}^T]\frac{d\mathbf{u}}{d\lambda} = \mathbf{f}^{\lambda}, \tag{4.25}$$

with

$$\mathbf{K} = \mathbf{D}^T\mathbf{S}\mathbf{D} + \mathbf{G} - (p - p^a)\frac{\partial^2 V}{\partial \mathbf{u}\partial \mathbf{u}}$$

$$\kappa = -\frac{dp}{dV}, \qquad \mathbf{a} = \frac{\partial V}{\partial \mathbf{u}}.$$

As can be seen from (4.25), **K** is still sparse, whereas the non-sparse contribution has been described by $\kappa\mathbf{a}\mathbf{a}^T$. A technique to solve (4.25) has been found by trying

$$\frac{d\mathbf{u}}{d\lambda} = \mu\mathbf{a} + \mathbf{b}, \qquad \mathbf{a}\cdot\mathbf{b} = 0.$$

This results in

$$\mathbf{b} = \mathbf{K}^{-1}\mathbf{f}^{\lambda} - \mu\left(\mathbf{a} + \kappa a^2\mathbf{K}^{-1}\mathbf{a}\right)$$

with

$$\mu = \frac{\mathbf{a}^T\mathbf{K}^{-1}\mathbf{f}^{\lambda}}{a^2(1 + \kappa\mathbf{a}^T\mathbf{K}^{-1}\mathbf{a})}, \qquad a^2 = \mathbf{a}^T\mathbf{a}.$$

This way of solving is similar to the Sherman-Morrison formula [1,27,31] where the inverse of a modified matrix is related to the original matrix. Akgün *et.al.* [1] uses the Sherman-Morrison formulas for fast static reanalysis in order to find the response of a structure after modifications by using the original response of the structure. The required computational effort for this is much less than the effort required by a complete analysis. The Sherman-Morrison formulas utilize the property that the solution of a system of linear equations can be updated inexpensively when the matrix is changed by a low-rank increment [1].

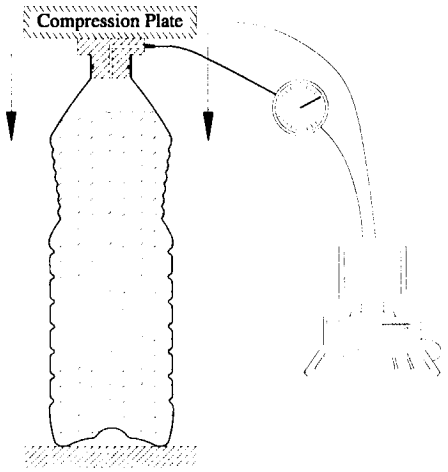

Figure 4.5: *Experimental set-up of the 750 ml round edible oil bottle.*

4.5 Application

The described problem applies to bottles filled with edible oil. During compression of a bottle, for example caused by stacking, the bottle deforms and the internal pressure increases [66,67]. Consequently, the gasses in the 'headspace' of the bottle dissolve in the oil until a new equilibrium pressure has been reached. Several bottles with different fill levels have been tested in an experimental set-up as depicted in Figure 4.5. Five different fill levels were examined: 0% (=empty), 75%, 90%, 95% and 96.8% fluid. In all experiments, the bottle was filled with air-saturated water at room temperature (298 K). In case the bottle would be filled with oil or another liquid then different results can be found due to different solubility rates. Notice, that only few information is available for solubility rates in liquids other than water. During the experiments the compression distance, the reaction force and the internal pressure were evaluated. The experiments were carried out at different compression speeds (10 and 100 mm/min) but no difference in the results was found. In all simulations triangular thin-shell finite elements [9,72,73], and linear material behavior have been used. A quarter of the bottle has been modelled, that is, a quarter of the circumference and the full bottle height using 9814 elements. Symmetry conditions were prescribed along the edges. In Figure 4.6, the mesh as used for the simulations has been depicted. As can be seen in Figure 4.7, numerical results, *without* accounting for solubility effects, and experimental results match for large gas-fluid ratios (empty, 75% and 90% fluid). The sudden loss of load in the experimental curves between 5–8 mm compression is due to a buckling effect. Furthermore, this buckling effect is so fast that the numerical results during and after buckling are not predicted adequate due to several reasons: thermic effects, dynamic effects, non-linear material behavior, contact effects and probably a non-equilibrium with respect to the dissolved amount of gas. The fact that the onset of buckling load of the bottle is not accurately described during the simulations can be appointed to the used material properties and the fact that initial imperfections in geometry and wall-thickness distribution have not been taken into account [25,26]. From Figure 4.7 it can also be concluded that for small gas volumes the experimental and simulated results differ significantly. The last is not unexpected since in the present setting a small gas volume means a small gas-fluid ratio and leads to a higher internal pressure at the same level of compression. Both, a higher internal pressure and a small gas-fluid ratio cause an increase of the dissolving of the gas. The last has been illustrated in Figure 4.8. This figure clearly shows that for small gas-fluid ratios the solubility effect needs to be taken into account and has a large influence on the stiffness of the involved structure.

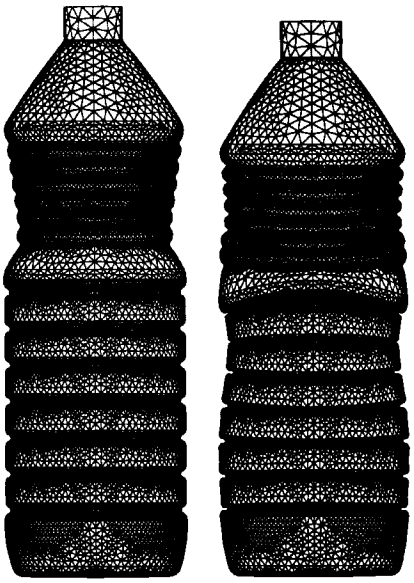

Figure 4.6: *The undeformed (left) and deformed (right) mesh of the bottle using 9814 elements and a quarter model of the bottle.*

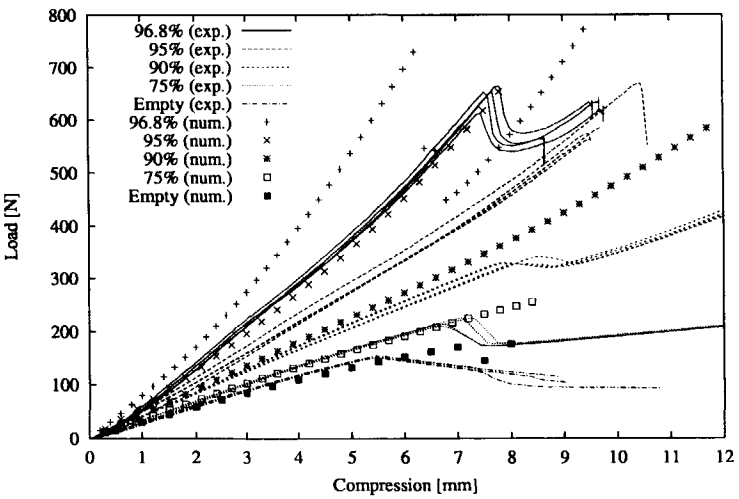

Figure 4.7: *Experimental and numerical results for a closed bottle under vertical compression where* the solubility effect has been neglected *in the simulations. The loss of load for the numerical results for a structure filled for 96.8% with water is due to buckling of the bottom (outwards) of the bottle, during experiments this buckling was encountered occasionally. Note that lines have been used for experimental results.*

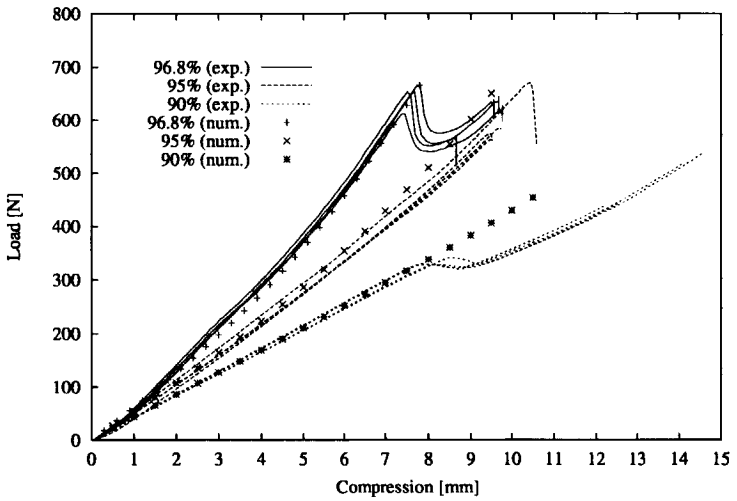

Figure 4.8: *Experimental and numerical results where the solubility effect has been accounted for in the simulations. The loss of load at approximately 650 N for the 96.8% filled bottle is due to buckling. Note that lines have been used for experimental results.*

4.6 Discussion

In structures with an enclosed gas volume the gas can contribute significantly to the strength and stiffness of the structure. If the enclosed volume also contains a fluid then for an increasing internal pressure the gas can dissolve in the fluid and consequently influence on the mechanical behavior of the structure. For large gas-fluid ratios the solubility effects can be neglected, while for small gas-fluid ratios this effect plays a major role and should be included.

The described model to account for solubility effects has been verified by the application to a plastic bottle for edible oil. The calculated results were in good agreement with the experimental results and confirmed that for small gas-fluid ratios the solubility effect should be accounted for during simulations of such structures.

Based on: R. van Dijk, H. de Boer and F. van Keulen, Accurate Design Sensitivities for Closed-Filled Structures; Application to Plastic Bottles, Structural Multidisciplinary Optimization, 27, 239–245, (2001).

Chapter 5

Design Sensitivities

Many efficient structural optimization algorithms require gradient information. Semi-Analytical (SA) design sensitivities are rather popular, as they combine ease of implementation with computational efficiency. For closed-filled structures also the effects of internal pressure changes and solubility of the gas in the fluid may be important. Typical examples for which these aspects are relevant can be found in packaging, e.g. edible-oil bottles. This chapter focuses on design sensitivities for such closed-filled structures. The design sensitivities are based on a refined SA formulation for the structure, whereas the contribution related to its contents is evaluated analytically.

5.1 Introduction

Many structures surround a volume which contains both fluid and gas, i.e. so-called "closed-filled" structures. Typical examples can be found in packaging, e.g. bottles, cans and bags. Since millions of packages are being produced every year, optimization is of great importance as discussed by Van Dijk et al. [67] and in Chapter 2 of this thesis. For effective designs it is important to account for the internal pressure effects. Van Dijk and Van Keulen [68] (see also Chapter 3and 4 of this thesis) discus the modeling of these pneumatic effects which require handling of the complication of a non-sparse tangent operator. The latter originates from the fact that the internal pressure causes a coupling between almost all nodal degrees of freedom. An internal pressure change also leads to a gas-fluid interaction which depends on the solubility of the gas. The relative importance of solubility strongly depends on the gas-fluid ratio. For large gas-fluid ratios, i.e. for a large gas volume and small fluid volume, solubility effects can in general be neglected. However, for small gas-fluid ratios, *e.g.* as found many plastic bottles, this effect has a significant influence and should be taken into account. For longer time periods, permeability and chemical reactions, *e.g.* oxidation of the contents, influence on the internal pressure and should be taken into account. These aspects will be discussed in Chapter 6 and further. The time dependent deformation of the package, *i.e.* relaxation of the package will not be considered in this thesis.

Design and optimization processes may require accurate information on design sensitivities, i.e. information on the derivatives of response functions, such as stresses, strains and displacements, with respect to the independent design variables. Especially for the above mentioned structures, which require non-linear analyses, design sensitivity can be very valuable as they can be retrieved relatively cheaply. In the present work the Refined Semi-Analytical (RSA) approach as described by Van Keulen and De Boer [75] and Van Keulen and De Boer [74], will be adapted for geometrically non-linear analyses of closed-filled structures. Two aspects cause design sensitivity analysis to be more involved. Firstly, the pressure effects cause the tangent operator to be non-sparse, which calls for a special scheme to solve the corresponding set of equations efficiently. Secondly, solubility effects have to be incorporated. In the current chapter the method is demonstrated on the basis of a rectangular plate with a pyramid like control volume, an air-spring and a bottle. The accuracy of the proposed sensitivity analyses will be compared with results obtained using Global Finite Differences (GFD).

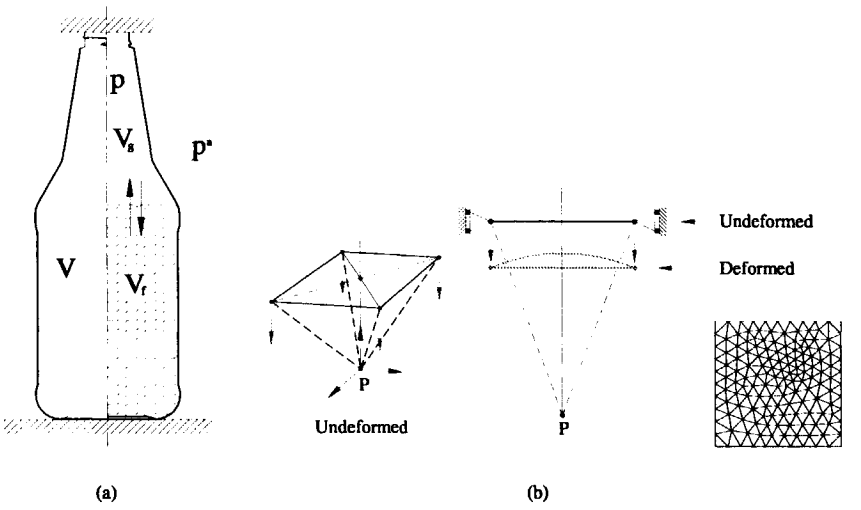

Figure 5.1: *a) Situation sketch, V, V_g, V_f, p and p^a are the total enclosed volume, the gas volume, the fluid volume, the internal pressure and the ambient pressure, respectively. The arrows visualize the gas exchange due to solubility effects. b) Rectangular plate ($2L \times 2L$) which encloses a pyramid shaped reference volume (with top P) and initial enclosed volume V^0. On the right, the finite element mesh of the plate has been depicted.*

5.2 Internal pressure and solubility effects

A typical example of a closed-filled structure is depicted in Figure 5.1a. The virtual work corresponding to the pressure difference, can be expressed as

$$\delta W_p^{ext} = (p - p^a)\delta V_g \tag{5.1}$$

where p is the total internal pressure and p^a denotes the ambient pressure. According to Dalton's Law of partial pressures the total gas pressure p is given by the sum of the partial gas pressures for an ideal mixture of gases [28]. In the present setting $p_i(V^0, V, V_f)$ represents the partial gas pressure as a function of the initial enclosed volume of the structure at ambient pressure (V^0), the actual total volume (V) and the fluid volume (V_f). Thus it has been assumed that the temperature remains constant.

The dissolved amount of gas depends on the partial pressure of the gas above the solution and is defined by Henry's law, described by Dack [13] and Kolthof and Elving [43], which reads $D_i = p_i S_i V_f$, where D_i is the dissolved amount of gas. S_i is the solubility factor of gas i in the fluid. In the present formulation it has been assumed that the solubility equilibrium is a quasi-static process, in other words the equilibrium is assumed to occur instantaneously. The initial saturation of the fluid, thus the saturation before equilibrium, is determined by s_i which is defined as $s_i = D_i^0/(p_i^0 V_f)$, where D_i^0 is the initial amount of dissolved gas and p_i^0 the initial partial pressure. In the work of Kolthof and Elving [43] the above results have been combined with the gas law for an ideal gas, which gives

$$\frac{p_i V_g}{n_i} = \frac{p_i V_g}{n_i^0 + D_i^0 - p_i S_i V_f} = RT \tag{5.2}$$

where n_i and n_i^0 denote the total amount of a certain gas in the gas volume of the structure (V_g) and the initial amount of a certain gas, respectively. The terms R and T denote the universal gas constant and the

temperature, respectively. The initial amount of gas enclosed by the structure can easily be determined using (5.2) and reads $n_i^0 = (p_i^0 V_g^0)/(RT)$. From (5.2), the total internal pressure follows as

$$p = \sum_{i=1}^{m} p_i = \sum_{i=1}^{m} p_i^0 \frac{1 - f(1 - s_i TR)}{v - f(1 - S_i TR)} \tag{5.3}$$

where $f = V_f/V^0$, $v = V/V^0$ and use has been made of $V_g = V - V_f$ and $V_g^0 = V^0 - V_f$. Note that the fluid volume V_f is assumed constant.

5.3 Analysis and design sensitivities

In a general FE setting, we often start from the principal of virtual work, $\delta W^{int} = \delta W^{ext}$, where δW^{int} and δW^{ext} are the internal and external virtual work, respectively. In the present setting the external virtual work contains terms that contribute for the virtual work done by the gas and can be described as

$$\delta W^{ext} = \lambda \mathbf{f}^{ext} \cdot \delta \mathbf{u} + (p - p^a) \frac{\partial V}{\partial \mathbf{u}} \cdot \delta \mathbf{u} \tag{5.4}$$

where the applied load is denoted $\lambda \mathbf{f}^{ext}$. The external load is scaled by a load factor λ. The total load acting on the structure is a function of the nodal degrees of freedom $\mathbf{u}$ and the design variables $\mathbf{s}$. With the principal of virtual work the equation of equilibrium becomes

$$\mathbf{f}^{int} - (p - p^a) \frac{\partial V}{\partial \mathbf{u}} = \lambda \mathbf{f}^{ext}(\mathbf{u}; \mathbf{s}) \tag{5.5}$$

where $\mathbf{f}^{int}$ is the so-called internal force vector, *i.e.* the nodal loads following from the generalized stresses and the discrete equation of equilibrium.

The additional contribution of the internal pressure to the tangent operator reads

$$J_{ij}^p = -p \frac{\partial^2 V}{\partial u_i \partial u_j} - \frac{dp}{dV} \frac{\partial V}{\partial u_i} \frac{\partial V}{\partial u_j}, \qquad i, j = 1 \ldots n \tag{5.6}$$

where $\mathbf{u}$ denotes an array of n nodal degrees of freedom. This additional contribution does not destroy the symmetry of the tangent operator. However, due to the second term in the right-hand side of (5.6) the tangent operator becomes non-sparse. The tangent matrix $\mathbf{J}$ can now be written as

$$\mathbf{J} = \mathbf{K} + \mu \mathbf{a}\mathbf{a}^T \tag{5.7}$$

The first term in the r.h.s. of (5.7) represents the tangent operator without the second term from the r.h.s. of (5.6). The latter is represented by $\mu \mathbf{a}\mathbf{a}^T$, with $\mu = -\frac{dp}{dV}$ and $a_i = \frac{\partial V}{\partial u_i}$. The matrix $\mathbf{K}$ may still have a sparse structure.

Within an incremental-iterative finite element procedure, solutions of $\mathbf{J}\mathbf{x} = \mathbf{y}$ will be required. A solution is now searched in the form of

$$\mathbf{x} = c\mathbf{a} + \mathbf{b}, \qquad \mathbf{a} \cdot \mathbf{b} = 0 \tag{5.8}$$

with c being an unknown scalar and $\mathbf{b}$ an unknown vector. Substitution of (5.8) into $\mathbf{J}\mathbf{x} = \mathbf{y}$ and combination with $\mathbf{a} \cdot \mathbf{b} = 0$, leads to the augmented set of equations

$$\begin{bmatrix} \mathbf{K} & (\mathbf{K}\mathbf{a} + \mu a^2 \mathbf{a}) \\ \mathbf{a}^T & 0 \end{bmatrix} \begin{bmatrix} \mathbf{b} \\ c \end{bmatrix} = \begin{bmatrix} \mathbf{y} \\ 0 \end{bmatrix} \tag{5.9}$$

with $a^2 = \mathbf{a}^T\mathbf{a}$. Note that this augmented set may still have a sparse structure, however an additional row and column have appeared. Provided $\mathbf{K}$ is regular, the solution of this augmented set of equations is given by

$$\mathbf{b} = \mathbf{K}^{-1}\mathbf{y} - c(\mathbf{a} + \mu a^2 \mathbf{K}^{-1}\mathbf{a}) \tag{5.10}$$

with

$$c = \frac{\mathbf{a}^T \mathbf{K}^{-1} \mathbf{y}}{a^2(1 + \mu \mathbf{a}^T \mathbf{K}^{-1} \mathbf{a})} \tag{5.11}$$

If a direct solver is applied, a decomposition of the sparse matrix $\mathbf{K}$ is generally determined. In addition to $\mathbf{K}^{-1}\mathbf{y}$ also $\mathbf{K}^{-1}\mathbf{a}$ must be evaluated, i.e. only an additional back substitution is required. This way of solving turn out to be similar to the Sherman-Morrison formulas, used by Akgün et al. [1], Golub and Loan [27] and Hager [31], where the inverse of a modified matrix is related to the original matrix.

The new term $-(p-p^a)\partial V/\partial \mathbf{u}$ in (5.5), which in the sequel will be denoted by $\mathbf{g}$, will be investigated in more detail. Notice, that $p = p(V^0, V, V_f)$ and $V = V(\mathbf{u}, s)$ where s is the only design variable. In the present setting the attention will be concentrated on a single design variable s for simplicity. Elaboration to more design variables is straightforward. It now follows that

$$\frac{d\mathbf{g}}{ds} = -\frac{dp}{ds}\frac{\partial V}{\partial \mathbf{u}} - (p - p^a)\frac{d}{ds}\frac{\partial V}{\partial \mathbf{u}} \tag{5.12}$$

which can be written as

$$\begin{aligned}\frac{d\mathbf{g}}{ds} = &-\left(\frac{\partial p}{\partial V}\frac{\partial V}{\partial \mathbf{u}}\frac{\partial V}{\partial \mathbf{u}}^T + (p - p^a)\frac{\partial^2 V}{\partial \mathbf{u}^2}\right)\frac{d\mathbf{u}}{ds} \\ &-\left(\frac{\partial p}{\partial V}\frac{\partial V}{\partial s} + \frac{\partial p}{\partial V^0}\frac{dV^0}{ds} + \frac{\partial p}{\partial V_f}\frac{dV_f}{ds}\right)\frac{\partial V}{\partial \mathbf{u}} - (p - p^a)\frac{\partial^2 V}{\partial \mathbf{u}\partial s}\end{aligned} \tag{5.13}$$

Consequently, the differentiation of (5.5) with respect to the design variable gives

$$\mathbf{J}\frac{d\mathbf{u}}{ds} = \lambda\frac{\partial \mathbf{f}^{ext}(\mathbf{u}; s)}{\partial s} - \frac{\partial \mathbf{f}^{int}(\mathbf{u})}{\partial s} + \left(\frac{\partial p}{\partial V}\frac{\partial V}{\partial s} + \frac{\partial p}{\partial V^0}\frac{dV^0}{ds} + \frac{\partial p}{\partial V_f}\frac{dV_f}{ds}\right)\frac{\partial V}{\partial \mathbf{u}} + (p - p^a)\frac{\partial^2 V}{\partial \mathbf{u}\partial s} \tag{5.14}$$

Note, that $\mathbf{J}$ is non-sparse and the resulting set of equations has to be solved as described previously.

The partial derivatives with respect to V^0, V and V_f can be determined on the basis of (5.3), this leads to

$$\frac{\partial p_i}{\partial V^0} = \frac{p_i^0}{V^0}a; \quad \frac{\partial p_i}{\partial V} = -\frac{p_i^0}{V^0}(1 - f(1 - s_i RT))a^2; \quad \frac{\partial p_i}{\partial V_f} = \frac{p_i^0}{V^0}(1 - S_i RT - v(1 - s_i RT))a^2 \tag{5.15}$$

where $a = 1/(v - f(1 - S_i RT))$.

Typically, the term dV_f/ds, which indicates the containing fluid volume, is defined by the designer. Three general situations can be distinguished

1. a constant fluid volume : $dV_f/ds = 0$;
2. a constant gas volume, with $V^0 = V_f + V_g^0$ this gives : $dV_g^0/ds = 0$ and $dV^0/ds = dV_f/ds$;
3. a constant fill-'level' : $V_f = fV^0$ and $dV_f/ds = f(dV^0/ds)$.

The partial derivatives $\partial V/\partial s$ and $\partial^2 V/(\partial \mathbf{u}\partial s)$ are calculated using analytical expressions for V as function of $\mathbf{u}$ and the nodal locations $\mathbf{X}$. For a single element these derivatives can easily be computed using

$$\frac{\partial V^e}{\partial s} = \frac{\partial V^e}{\partial \mathbf{X}^e}\frac{d\mathbf{X}^e}{ds}, \qquad \frac{\partial^2 V^e}{\partial \mathbf{u}\partial s} = \frac{\partial^2 V^e}{\partial \mathbf{u}\partial \mathbf{X}^e}\frac{d\mathbf{X}^e}{ds}, \tag{5.16}$$

where $d\mathbf{X}^e/ds$ refers to the design velocity field at element level. The latter has been approximated using a finite difference scheme.

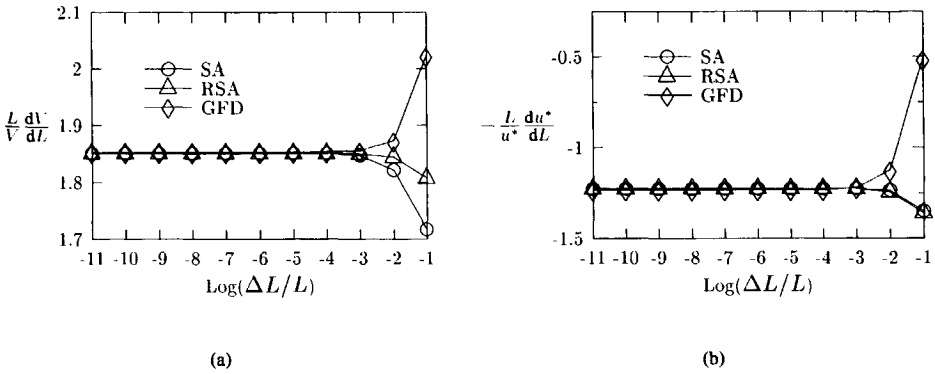

Figure 5.2: *a) Influence of perturbation on design sensitivities with the internal volume as response variable. b) Influence of perturbation on design sensitivities for the relative displacement in the middle of the plate denoted by* u^*.

5.4 Examples

The described method has been applied to two examples. The first example is a rectangular flexible plate (dimensions: $2L \times 2L$ and $L = 10$) with a thickness h ($h = 0.2$). The structure was modelled with a Young's modules of 3400 N/mm^2 and a Poisson's ratio of 0.35. The rectangular plate encloses a pyramid shaped reference volume as depicted in Figure 5.1b and was filled for 75% with fluid. Solubility effects have not been taken into account in this example. A displacement in downward direction is prescribed along the simply supported boundary until the internal volume reaches 90% of the initial volume. This was followed by sensitivity analyses with L being the design variable. The results thereof, using logarithmic design sensitivities, have been depicted in Figure 5.2. The curves labelled SA refer to a standard semi-analytical formulation [75], whereas RSA refers to the refined semi-analytical formulation [75]. GFD indicates results obtained by global finite differences. Figure 5.2 clearly demonstrates that the RSA gives the best results for the entire range of design perturbations. For small design perturbations no significant difference between the methods can be observed. Note that in Figure 5.2b the relative displacement is depicted. The relative displacement u^* is the vertical bulging in the middle of the plate.

The second example is an air-spring like structure from which the axial-symmetric geometry is depicted in Figure 5.3a. The air-spring is filled for 75% with water which was saturated under ambient conditions. Non-linear analyses were carried out where the air-spring was compressed for 20 mm. In Figure 5.4 the result of these analyses are depicted and clearly demonstrate the influence of solubility for smaller enclosed gas volumes and thus higher internal pressures. At the end of the non-linear analyses sensitivity analyses were carried out with the height H of the air-spring as design variable. The design variable H only affects the cylindrical part of the air-spring, thus the radius $R = 55.88$ as depicted in Figure 5.3a remains constant. In Figure 5.5 the response of the volume is plotted for perturbations ranging from 10^{-2} to 10^{-10} for an air-spring with and without solubility effects. The volume change for a structure without solubility effects has a larger influence on the internal pressure than for a structure with solubility effects. The latter might explain the larger discrepancy between the the GFD and SA/RSA methods for the structure without solubility effects at large perturbations.

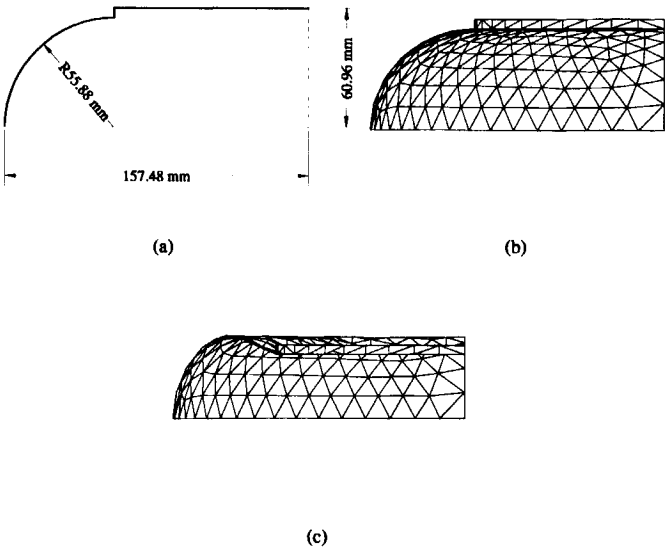

Figure 5.3: *a) Axial-symmetric geometry of the air-spring. b) Undeformed mesh. c) Deformed mesh of a quart air-spring model*

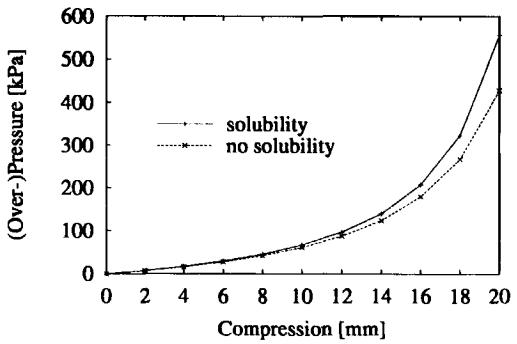

Figure 5.4: *Results of non-linear analyses, vertically the internal pressure and horizontally the compression have been plotted.*

5.5 Application

A typical example of a closed-filled structure is a plastic bottle for edible oil as depicted in Figure 5.6a. In most cases these bottles are filled for 96.8%, or more, with oil. During storage and transportation they are subjected to compression which has a significant influence on the internal pressure. After manufacturing of plastic bottles their geometry might change slightly, *e.g.* due to shrinkage of the bottle after manufacturing. It is therefore of interest to see how certain geometric details, which exhibit these changes, influence on the compression strength of the bottle.

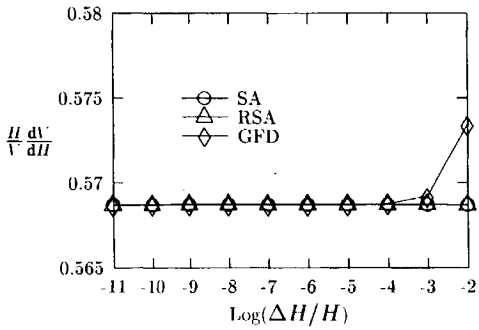

(a)

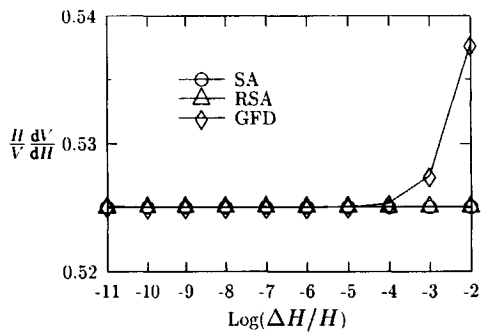

(b)

Figure 5.5: *a) Influence of perturbation on design sensitivities with solubility effects. b) Influence of perturbation on design sensitivities without solubility effects.*

Deformation induced pressure changes lead to gas dissolving in or escaping from the fluid. These effects have been depicted in Figure 5.6b, where the compression up to 6 mm of a for 96.8% water-filled bottle, has been depicted. At a larger compression the structure will collapse. The undeformed and deformed mesh of the structure are depicted in Figure 5.7. The maximum compression of an empty bottle is 156.8 N [67]. The load-displacement relation for a closed-bottle is here mainly determined by the internal pressure. It is therefore of interest to examine how certain parameters of the bottle influence on this pressure. Three design variables of the bottle have been investigated, namely: the wall-thickness, h, the height H and the height I, as depicted in Figure 5.8. For all variables the RSA, SA and GFD solutions have been determined, all taken into account solubility effects. The sensitivities were determined at 6 mm compression for bottles with a constant fluid volume and with a relative perturbation of 10^{-6}. As described in Table 5.1 , RSA, SA and GFD give similar results. Both the height H and height I significantly influence the internal gas-volume and thus the internal pressure and compression strength.

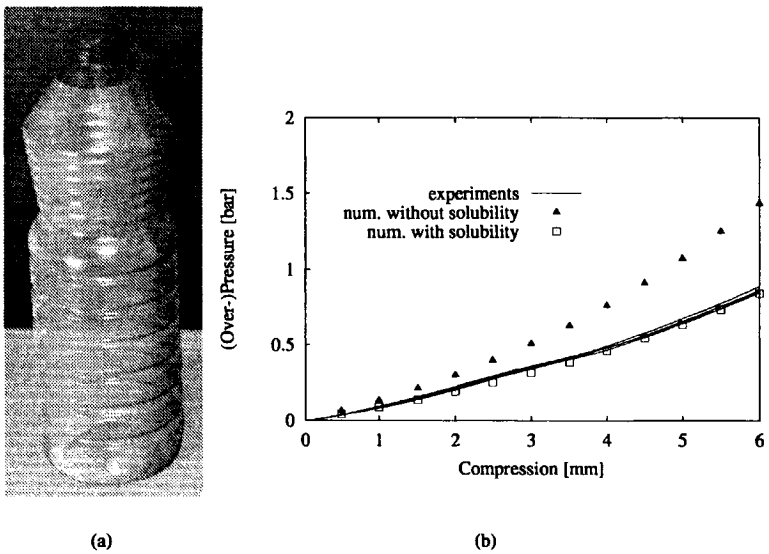

Figure 5.6: *a) Bottle for edible oil. b) The influence of pressure and solubility effects for the compression of closed-filled bottles.*

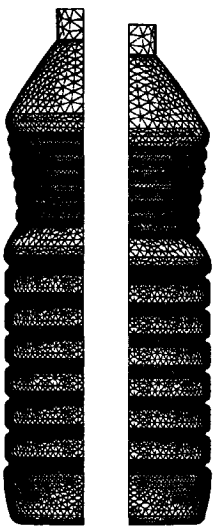

Figure 5.7: *Undeformed (left) and deformed (right) structure at a described displacement of 6 mm.*

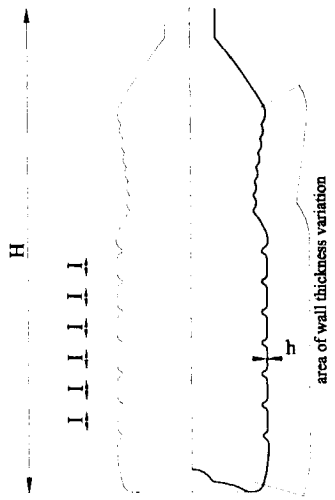

Figure 5.8: *Investigated parameters: the total height H, the height between two circumferential ribs l and the wall thickness h, which is variable for the indicated area only.*

	RSA	SA	GFD
$\frac{H}{p}\frac{dp}{dH}$	-1.688	-1.688	-1.687
$\frac{h}{p}\frac{dp}{dh}$	0.06833	0.06833	0.06833
$\frac{l}{p}\frac{dp}{dl}$	-3.409	-3.409	-3.407

Table 5.1: *Logarithmic design sensitivities for a water-filled bottle with solubility effects at a compression of 6 mm.*

5.6 Results and conclusions

The internal pressure for an ideal gas in closed-filled structures can be described adequately by a combination of Henry's law and the general gas law. This makes it also possible to determine dP/dV analytically. Following this, the tangent operator can be modified for the internal pressure changes leading to a non-sparse system matrix. The proposed method for solving the non-sparse set of equations proved very effective in combination with a direct solver.

Pressure and volume effects are easily determined analytically and therefore do not spoil the accuracy of the sensitivity analysis. The examples and application as studied here clearly demonstrate that solubility effects may have a significant influence on the structural behavior for small gas-fluid ratios.

For large perturbations the SA and RSA method give better results than the GFD method.

Based on: R. van Dijk and F. van Keulen, Simulation of Closed-Filled Structures; Permeability, Solubility and Chemical Reactions, Proceedings of the European Conference on Computational Mechanics (ECCM'99), August 31 – September 3, 1999, Munich, Germany.

Chapter 6

Permeability, Solubility and Chemical Reactions

Oxidation of the contents of closed-filled packages significantly influences on the internal pressure and can lead to unacceptably deformed packages and rancidity of the contents. A model is proposed to describe the behavior of the structure due to internal pressure changes which are caused by oxidation, solubility and permeability effects. This model is partially based on experimental results which have been described. Finally, the mechanical behavior of closed-filled structures has been simulated and it is shown that the structure cannot be simplified to either a non-resistant structure or a rigid structure, thus it is necessary to take the deformation of the structure due to internal pressure changes into account.

6.1 Introduction

Many thin-walled structures surround a volume which contains both fluid and gas. Typical examples can be found in packaging, e.g bottles, pouches, cans, bags, among others. Since millions of packages are being produced annually optimal use of packaging material is of major importance. The function of the package is not solely keeping a product together during transportation and storage. Especially, in the case of food-packaging the package also has a function to protect the product from oxidation. Since almost all food products are sensitive to oxygen, contact between oxygen and the product should be avoided or minimized.

Oxidation occurs due to two reasons. Firstly, the contents reacts with the enclosed oxygen gas in the package. Secondly, permeation of oxygen through the wall of the structure will be followed by a chemical reaction with the contents. A side effect of the oxidation is its influence on the internal pressure and therefore on the strength and stiffness of the structure. Internal pressure changes also cause a dissolving or a fugacity of gases into and/or out of the contents, respectively. Simulation of the pressure, oxidation, permeability and solubility effects can lead to a better shelf life estimation and to improvement of package designs.

Internal pressure changes of closed-filled structures can cause a substantial deformation of the structure [7] and sometimes lead to a complete disappearing of the enclosed gas volume. An internal pressure change also leads to gas-fluid interaction which depends on the solubility of the gas. For increasing pressures the gas will start to dissolve in the fluid, while a decreasing internal pressure might lead to a fugacity of gas from the fluid (depending on the fluid conditions). The relative importance of solubility effects depends on the gas-fluid ratio. For large gas-fluid ratios, i.e. for a large gas volume and small fluid volume, solubility effects can often be neglected. However, for small gas-fluid ratios this effect has a significant influence and should be taken into account. These small gas-fluid ratios typically occur in food-packaging.

The effects of permeability on the behavior and contents of the structure have been examined in [22, 41, 45, 48–51]. The effect of oxidation on the internal pressure change for flexible and rigid packages

has been described by Talasila and Cameron [61]. Talasila and Cameron distinguished only two kinds of structures, rigid and non-resistant; where for the non-resistant structure any pressure change is completely translated in a volume change. Most structures have a certain resistance against pressure changes and can not accurately be described by one of these models. The complexity is therefore to determine the relation between pressure and volume of the structure [67] and to combine this with the permeation, solubility and oxidation effects.

In this chapter the influence of permeation and oxidation has been modelled with an explicit integration scheme. Oxidation and solubility effects have been included using models from literature [34,42,61].

Finally, the proposed method will be applied to a plastic bottle for edible-oil. The described bottle is a typical example of a closed-filled structure with an oxygen sensitive content. Due to oxidation of the oil the internal pressure decreases and causes an in-stream of oxygen through the thin wall of the package. Furthermore, depending on the initial conditions the internal pressure change causes gas to escape from the contents. Experimental work with respect to the deformation of the bottle will be used to obtain numerical results with respect to predictions in the long term behavior of the package.

6.2 Assumptions

The following has been assumed:

- $\sum_{i=1}^{m} n_i = n$ [28], where n is the total amount of gas (in mol);
- it is assumed that the package, the gas and the product always have an equal temperature and the structure is closed at filling temperature;
- it is assumed that, after filling and closing of the package, the temperature of the contents and the structure are equal to ambient temperature; this condition is referred to as the ***initial*** condition of the structure;
- no oxidation and permeation take place during filling and cooling to ambient temperature;
- the temperature after filling is constant and equal to ambient temperature;
- both the gases and the contents do not react chemically with the structure.

6.3 Governing equations

This section introduces models, for the description of solubility, permeability and oxidation effects and structural behavior of closed-filled structures.

6.3.1 Gas law

In Figure 6.1, a typical situation has been depicted. The figure displays a closed structure which contains both gas and fluid. When the enclosed volume contains an ideal mixture of gases, then according to Dalton's Law of Partial Pressures [28], the total gas pressure can be described as

$$p = \sum_{i=1}^{m} p_i, \qquad i = 1 \ldots m. \tag{6.1}$$

The partial gas pressure is determined by [23]

$$p_i = \frac{n_i}{n} p. \tag{6.2}$$

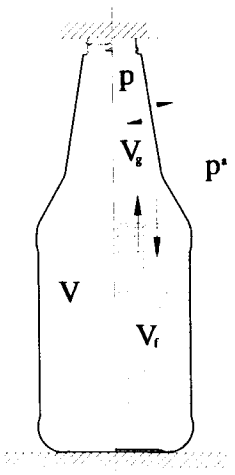

Figure 6.1: *Situation sketch, V, V_g, V_f, p and p^a are the total enclosed volume, the gas volume, the fluid volume, the internal pressure and the ambient pressure, respectively. The arrows visualize the gas streams due to solubility and permeability effects.*

In case of a mixture of ideal gases and making use of (6.2), the gas law can be described as [23, 24]

$$\frac{pV_g}{nT} = \frac{p_i V_g}{n_i T} = R. \tag{6.3}$$

For calculation of the internal pressure at any time after filling it is necessary to determine the gas volume in the structure after filling. Generally, the gas volume is defined by

$$V_g = V^a((T - T^a)\lambda + 1)^3 - V_f((T - T^a)\gamma + 1) + f_V^g, \tag{6.4}$$

where γ is the volumetric expansion coefficient of the contained product and λ is the linear expansion coefficient of the enclosing structure. The initial enclosed volume at ambient temperature and the actual temperature are denoted by V^a and T, respectively. The function f_V^g describes the volume change of the package due to internal pressure changes. This function is assumed to be temperature independent. In the sequel it will be assumed that the temperature after filling is constant and equal to ambient temperature, (6.4) can therefore be described as

$$V_g = V^a - V_f + f_V, \tag{6.5}$$

where f_V describes the volume change of the package due to internal pressure changes at ambient temperature. Substituting (6.5) in (6.3) gives

$$\frac{p_i\,(V^a - V_f + f_V)}{n_i T^a} = R. \tag{6.6}$$

For flexible-rigid structures the gas volume changes when the internal pressure changes. In that case f_V can be expressed in terms of the internal pressure. However, if the structure collapses the function should be expressed in terms of the amount of gas since after buckling the internal pressure will remain approximately constant, as will be shown later.

6.3.2 Solubility effects

For small gas and large fluid volumes in a closed structure the dissolving of the gas in the fluid should be taken into account. According to Henry's law the concentration of a solute gas in a solution is proportional to the partial pressure of that gas above the solution [13, 43]. Henry's law is found to be an

accurate description of the behavior of gases dissolving in liquids when the concentration and partial pressures are reasonably low [13, 43, 53]. For this study it has been assumed that Henry's law is applicable. Furthermore, it needs mentioning that the molar solubility of a gas is temperature dependent, to be more precise the solubility of a gas decreases for higher temperatures. Following Henry's law for constant temperature, the dissolved amount of gas (in mol) in equilibrium condition reads

$$D_i = p_i S_i V_f. \tag{6.7}$$

In the present formulation it has been assumed that the solubility equilibrium is a quasi-static process, in other words the equilibrium occurs instantaneously. With (6.7) the amount of gas i at ambient temperature becomes

$$n_i = N_i - D_i = N_i - p_i S_i V_f, \tag{6.8}$$

where N_i is the total amount of gas i, i.e. dissolved in the fluid and as gas. N_i is not constant, as the structure is not a closed system. In other words, gas may permeate through the bottle wall and the gas may react chemically with the fluid. The determination of N_i follows from

$$N_i = n_i^f + D_i^f + \eta_i, \tag{6.9}$$

where η_i is the change of a gas component in time (and thus time dependent) and is governed by the permeability and chemical reactions. D_i^f and n_i^f are the dissolved amount of component i at filling conditions and the amount of gas i at filling conditions, respectively. The function η_i is defined by

$$\eta_i = \Psi_i - \Phi_i, \tag{6.10}$$

where Ψ_i and Φ_i are the permeated amount of gas i into the structure and reacted amount of gas i with the contents, respectively. Both Ψ_i and Φ_i are time dependent. Initially (during and immediately after filling), $\eta_i(0) = 0$, $\Psi_i(0) = 0$ and $\Phi_i(0) = 0$, since we assume there is no oxidation and permeation during filling.

Mostly, the contents is stored for a certain time at ambient conditions. In rare occasions the contents is heated prior to filling in order to speed up the filling process. The initial dissolved amount of component i, D_i^f, can now be determined according $D_i^f = p_i^a S_i V_f$, where it is assumed that the product is saturated at ambient temperature and ambient pressure. It is further assumed that the contents is not heated prior to filling. The initial amount of gas i, n_i^f, enclosed by the structure can easily be determined using (6.3), giving

$$n_i^f = \frac{p_i^f}{T^f R} V_g^f. \tag{6.11}$$

The gas volume at filling conditions, V_g^f, is determined by (6.4) with $V_g = V_g^f, T = T^f$ and $f_V^g = 0$.

In order to determine the partial pressure while accounting for solubility effects, (6.8) has been substituted in (6.6) resulting in the general gas law,

$$\frac{p_i \left(V^a - V_f + f_V\right)}{(N_i - p_i S_i V_f) T^a} = R. \tag{6.12}$$

As mentioned earlier, during and immediately after filling Ψ_i and Φ_i are assumed zero. If the function f_V is known then the pressure after filling can be determined. The conditions just after filling will be referred to as the *initial* conditions and will be denoted by the superscript ^{0}, e.g. p_i^0 refers to the initial partial pressure (thus just after filling) of component i at ambient temperature. Now, together with (6.9), (6.12) can be written as

$$\frac{p_i^0 \left(V^a - V_f + f_V(p^0)\right)}{(n_i^f + D_i^f - p_i^0 S_i V_f) T^a} = R. \tag{6.13}$$

Combining (6.12) for two gas components gives a relation between the actual partial pressures which reads

$$p_j = \frac{p_i N_j}{N_i - p_i S_i V_f + p_i S_j V_f}. \tag{6.14}$$

Note, that complications might arise when the term $N_i - p_i S_i V_f$ of (6.12) becomes zero. This can happen when all the gas i has been dissolved, thus when $n_i^f + D_i^f + \eta_i - p_i S_i V_f = 0$. Or, more likely, when all the gas i has reacted with the contents and the newly permeated amount of gas i immediately reacts with the contents, thus when $N_i = 0$. Care should therefore be taken that (6.12) will only be used when $N_i - p_i S_i V_f > 0$; for $N_i - p_i S_i V_f \leq 0$ the partial pressure p_i will be set to zero.

6.3.3 Behavior of the structure

Up to now it has been assumed that the function f_V is unknown. However, in practice it is possible to make a clear distinction between certain structures, which are:

1. rigid structures, for example glass structures. For these kind of structures deformation induced by internal pressure changes can be neglected.
2. non-resistant structures, for example plastic bags. These kind of structures will hardly resist to any internal pressure changes. Therefore the internal pressure remains approximately equal to the ambient pressure.
3. flexible structures, for example plastic bottles. These kind of structures will deform due to internal pressure changes but will give a substantial resistance to the pressure change.

The degree of flexibility, rigid/non-resistant/flexible, is determined by the function f_V. For a rigid structure this function is zero. In practice most structures are of the third kind. Note that the function f_V can be non-linear and time dependent, e.g. due to stress relaxation.

From (6.12) it can be seen that the partial pressure is not easily derived when f_V is non-linear and defined by the total internal pressure. In Chapter 2 experiments on plastic bottles indicate a linear relation between the internal pressure and the volume change of the structure while after buckling the internal pressure remained approximately constant. Therefore in the present setting and for internal pressures higher than the critical pressure, thus before buckling, a linear function for f_V will be examined. Hence,

$$f_V(p) = \alpha(p - p^a) = \alpha \left[\left(\sum_{i=1}^{m} p_i \right) - p^a \right], \qquad \text{if} \qquad p \geq p^{cr}, \tag{6.15}$$

where p^{cr} is the critical pressure of the structure, *i.e.* the pressure at which buckling/collapse of the structure occurs. The amount of gas present in the structure at the moment of collapse is denoted by n^{cr}. The gas volume as described in (6.5) now becomes $V_g = V^a - V_f + \alpha(p - p^a)$, where α is a newly introduced coefficient which refers to the volume-pressure compliance of the package. It may be clear that for a rigid pack α is zero and for a non-resistant pack α is infinite. As will be shown in Section 6.6, the pressure remains approximately constant and equal to p^{cr}, after collapse. This means that any change in the amount of gas after buckling will immediately result in a volume change of the structure. Therefore after buckling, $p = p^{cr}$ and for constant temperature (6.15) can be written as

$$f_V(n) = \frac{TR}{p^{cr}} n - V^a + V_f, \qquad \text{if } n \leq n^{cr}. \tag{6.16}$$

The gas volume in the structure after buckling as defined in (6.5) hereby becomes $V_g = V^a - V_f + f_V(n) = \frac{TR}{p^{cr}} n$. Together with (6.15), (6.12) can now be written as

$$\begin{aligned} &\frac{p_i\left(V^a - V_f + \alpha\left[\left(\sum_{k=1}^{m} p_k\right) - p^a\right]\right)}{(N_i - p_i S_i V_f)T^a} = R, \quad \text{if } p \geq p^{cr}, \\ &\frac{p_i\left(\frac{TR}{p^{cr}} \sum_{k=1}^{m} n_k\right)}{(N_i - p_i S_i V_f)T^a} = R, \qquad \text{if } n \leq n^{cr}. \end{aligned} \tag{6.17}$$

The first equation, thus when $p \geq p^{cr}$, should be used before buckling. After buckling the internal pressure remains by approximation constant and equal to p^{cr}. Therefore after buckling the internal volume can be determined on the hand of n while n^{cr} is the amount of gas at the moment of buckling. The equilibrium pressures can now be determined from (6.17).

6.3.4 Permeability effects and chemical reactions

From a cost perspective many structures are being optimised which leads to products with as less material as possible. For closed-filled structures this can results in constructions with very small wall thicknesses. Especially for such structures permeability becomes a potentially important factor. The present section describes permeation of gas through the wall of the structure. As mentioned before, it has been assumed that the equilibrium pressure in the structure will be reached instantaneously, in other words the solubility process is a quasi-static process.

Actually, permeation is the process of diffusion of gas from the ambient environment into the wall of the structure followed by diffusion from the wall into the gas volume and contents of the package. The diffusion from the wall into the contents is a much slower process, due to a solid-fluid interaction than diffusion into the gas volume. The diffusion from the wall into the fluid has therefore been assumed negligible.

Substituting (6.9) and (6.10) in (6.8) gives the amount of a certain gas in the structure at a constant ambient temperature at time t, consequently

$$n_i = n_i^f + D_i^f + \Psi_i - \Phi_i - p_i S_i V_f. \tag{6.18}$$

Rate equations follow by differentiation of (6.18), which gives,

$$\frac{dn_i}{dt} = \frac{d\Psi_i}{dt} - \frac{d\Phi_i}{dt} - S_i V_f \frac{dp_i}{dt}.$$

This can also be written as [61]

$$\frac{dn_i}{dt} = \frac{P_i A}{h}(p_i^a - p_i) - r_i(p_i)V_f - S_i V_f \frac{dp_i}{dt}, \tag{6.19}$$

where the first term in the r.h.s. refers to the permeability and the second term in the r.h.s refers to the oxidation of the fluid. The permeability is determined by the surface exposed to permeability A, the thickness of the structure h, and the permeability coefficient P_i. The chemical reaction is here determined by the reaction speed $r_i(p_i)$, which depends on the partial pressure, and the volume V_f of the contents. Note that for the present application as discussed in Section 6.6 only the oxygen, which causes oxidation, reacts with the contents. Definition of the reaction is carried out similar to the work of Herlitze *et.al.* [34], Penzkofer [50] and Talasila [61]. Herlitze and Penzkofer used a polynomial function which gives the oxidation speed as an approximate function of the partial oxygen pressure. Kiritsakis [42, p.108] mentions a progressive oxidation for olive oil. He describes the oxidation process in three phases: initiation, propagation and termination. The duration of the initiation phase depends on the saturation and the presence or absence of antioxidants. In the present setting the oil is assumed to be in the propagation phase and only the linear term of the polynomial as given by Penzkofer [50] and Herlitze *et.al.* [34] has been accounted for. As will be discussed in Section 6.6, oxidation data of ketchup will be used during the simulations due to the absence of accurate oxidation date of vegetable oil. Experiments as carried out by Herlitze *et.al* [34]showed a linear dependence between the oxidation speed and the partial oxygen pressure for ketchup. The oxidation speed is hereby thus defined as

$$r_i(p_i) = \varpi_i p_i, \tag{6.20}$$

where ϖ_i determines the oxidation factor and i refers to the oxygen gas.

As will be shown in Section 6.6, for values of $p = p^{cr}$ it can be assumed that $(dp/dt)_{p=p^{cr}} = 0$. The term dp_i/dt for $p > p^{cr}$, *i.e.* an internal pressure which does not lead to buckling, can be obtained by differentiation of (6.3) for a constant ambient temperature, which gives

$$\frac{dn_i}{dt} = \frac{V_g}{T^a R}\frac{dp_i}{dt} + \frac{p_i}{T^a R}\frac{dV_g}{dt}. \tag{6.21}$$

Note that, $dp/dt = 0$ for a non-resistant structure and $dV_g/dt = 0$ for a rigid structure. If the function V_g can be described according to (6.5), then the derivative dV_g/dt is fully determined by df_V/dt. Assuming a constant ambient pressure and constant ambient temperature the derivative of f_V with respect to time reads,

$$\frac{df_V}{dt} = \begin{cases} \alpha\frac{dp}{dt}, & \text{if } p > p^{cr} \text{ (before buckling)}, \\ \frac{T^a R}{p^{cr}}\frac{dn}{dt}, & \text{if } n \leq n^{cr} \text{ (after buckling)}. \end{cases} \tag{6.22}$$

Combining (6.19) and (6.21) gives the general equation for the pressure change

$$\frac{V_g}{T^a R}\frac{dp_i}{dt} + \frac{p_i}{T^a R}\frac{dV_g}{dt} = \frac{P_i A}{h}(p_i^a - p_i) - r_i(p_i)V_f - S_i V_f \frac{dp_i}{dt}. \tag{6.23}$$

With (6.22) and using $V_g = V^a - V_f + f_V$, (6.23) becomes

$$\begin{aligned} &\tfrac{V_g}{T^a R}\tfrac{dp_i}{dt} + \alpha\tfrac{p_i}{T^a R}\tfrac{dp}{dt} = C_i - S_i V_f \tfrac{dp_i}{dt}, && \text{if } p > p^{cr}, \\ &\tfrac{n}{p^{cr}}\tfrac{dp_i}{dt} + \tfrac{p_i}{p_{cr}}\tfrac{dn}{dt} = C_i - S_i V_f \tfrac{dp_i}{dt}, && \text{if } n \leq n^{cr}, \end{aligned} \tag{6.24}$$

where $C_i = P_i A(p_i^a - p_i)/h - r_i(p_i)V_f$.

For 'non-buckling' pressures $p > p^{cr}$ the terms dp_i/dt and dn_i/dt can be derived from (6.24). In order to determine these terms after buckling occurred, *i.e.* when $p = p^{cr}$, use should be made of $\sum_{i=1}^{m}\frac{dp_i}{dt} = 0$ and differentiation of (6.2). As can be seen from foregoing results the problem simplifies as soon either the permeability ($P_i = 0$) or the solubility ($S_i = 0$) can be neglected.

6.4 Special cases

Three special cases will be distinguished:

- negligible solubility effects;
- negligible permeability effects;
- negligible solubility and permeability effects.

The first two cases have been mentioned briefly at the end of the previous section and do not lead to a significant simplification of the problem. However, if solubility and permeability can be neglected then this leads to a significant simplification.

If both the solubility and permeability can be neglected ($S_i = 0, D_i^f = 0$ and $P_i = 0$) and gas i is still present then the amount of gas in the structure is defined by (6.8), (6.9) and (6.10) and becomes

$$n_i = N_i = n_i^f + \eta_i = n_i^f - \int_0^t r_i(p_i)V_f dt. \tag{6.25}$$

Herewith, (6.17) simplifies to

$$\begin{aligned} &\tfrac{p_i\left(V^a - V_f + \alpha\left[\left(\sum_{k=1}^{m} p_k\right) - p^a\right]\right)}{n_i T^a} = R, && \text{if } p \geq p^{cr}, \\ &\tfrac{p_i \frac{TR}{p^{cr}} \sum_{k=1}^{m} n_k}{n_i T^a} = R, && \text{if } n \leq n^{cr}. \end{aligned} \tag{6.26}$$

Before buckling ($p \geq p^{cr}$), summation of (6.26) gives

$$p(V^a - V_f + \alpha(p - p^a)) = nT^aR, \qquad \text{if } p \geq p^{cr}.$$

The total pressure can easily be determined and is given by

$$p = \frac{-(V^a - V_f - \alpha p^a) + \sqrt{(V^a - V_f - \alpha p^a)^2 + 4\alpha TRn}}{2\alpha}, \qquad \text{if } p \geq p^{cr}.$$

The partial pressure follows by substitution of the total pressure in (6.26). Differentiation of the above equation or (6.24) with respect to time leads to

$$\frac{dp}{dt} = \frac{-V_f T^a R \sum_{k=1}^{m} r_i(p_i)}{V^a - V_f + 2\alpha p - \alpha p^a}, \qquad \text{if } p > p^{cr}.$$

After buckling ($n \leq n^{cr}$), summation of (6.26) confirms that the critical pressure remains constant.

6.5 Simulation

Simulation of the development of the package behavior as a function of time should indicate if permeation is relevant and in which extend oxidation should be accounted for. This information will in Chapter 8 be used to define the constraints for the package during optimization.

After determination of dp_i/dt and dn_i/dt from (6.24) a first order estimate for the new internal pressure and amount of gas can be found by,

$$p_i(t + \Delta t) \approx p_i(t) + \frac{dp_i}{dt}\Delta t, \tag{6.27}$$

and

$$n_i(t + \Delta t) \approx n_i(t) + \frac{dn_i}{dt}\Delta t. \tag{6.28}$$

In such way an incremental solution for the pressure change can be obtained. The total amount of component i that reacted can be approximated using

$$\Phi_i(t + \Delta t) \approx \Phi_i(t) + r_i(p_i)\Delta t. \tag{6.29}$$

Note that $r_i(p_i)\Delta t$ can not exceed the enclosed gas amount plus the during the step permeated amount into the structure of component i.

The total amount of the component that permeated through the wall of the structure can be determined according to

$$\Psi_i(t + \Delta t) \approx \Psi_i(t) + \frac{P_i A}{h}(p_i^a - p_i(t))\Delta t. \tag{6.30}$$

The above calculated values are first order approximations to the real solution and will therefore drift away from the exact solution and the gas equilibrium as described in (6.12). It is therefore necessary to select the time increments sufficiently small.

6.6 Application

The atmosphere normally contains approximately 20% oxygen and 80% nitrogen. It is therefore in many cases sufficient to simplify the problem to these 2 gases. Cases where more then 2 gases are involved are products containing or producing CO_2 (in certain cases CO_2 is created during oxidation), *e.g.* carbonated lemonades. The latter cases will not be discussed in this thesis. However, the described model is also applicable for those products.

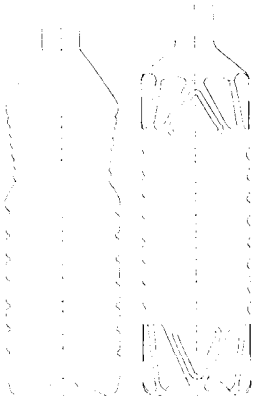

(a) (b)

Figure 6.2: *(a)Round and (b)square bottle for edible oil.*

	α [m^3/kPa]	p^{cr} [kPa]
Round	$6.7 \cdot 10^{-10}$	77.50
Square	$21.781 \cdot 10^{-10}$	93.75

Table 6.1: *Experimental coefficient determining the appropriate pressure-volume relation and critical pressure for the round and square bottle tested under an ambient pressure of 100 kPa.*

The following application involves a situation where only 2 gases are involved, namely, a bottle filled with edible oil. The bottle is filled and respectively closed at ambient temperature. Hereafter, the gases O_2 and N_2 , start to permeate through the wall of the structure and the oxygen will start to react with the oil, in other words the oil starts to oxidize. The oxygen does not react with the structure and during its reaction with the contents no gases are being created. Due to oxidation of the oil an internal underpressure is created. It is further assumed that the nitrogen gas does not react with the contents nor with the structure.

The influence of an internal vacuum on the behavior of plastic bottles has thoroughly been discussed in Chapter 2. In that chapter, round and square plastic bottles for edible oil, as depicted in Figure 6.2 have been studied. The bottles were subjected to an internal vacuum and the behavior of the structure was observed. In Figure 6.3 the bottles are depicted in a post buckling configuration , thus the internal pressure is smaller than the critical pressure p^{cr}. Figure 6.4 indicates that after buckling the pressure remains approximately constant. From Figure 6.4 the critical pressure p^{cr} and and the pressure compliance α for both packages can be determined and are listed in Table 6.1. In the present work only the round bottle will be studied since the paneling problem is easily circumvented for square bottles as discussed in Chapter 2. The deformation of the round bottle due to internal pressure changes can be described by (6.15) and (6.16).

The simulations which will be discussed examine the influence of oxidation, permeation and solubility effects on the pressure changes in the package. Rigid and flexible structures have been compared. In this study it has been assumed that the oxidation speed is determined by the function

$$r_{O_2}(p_{O_2}) = 1.125 \cdot 10^{-5}\, p_{O_2},$$

which gives the oxidation speed in [mol m $^{-1}$ N^{-1} day $^{-1}$] . This function has been determined from experimental work on ketchup [34]. Since no accurate date has been found for vegetable oil the latter

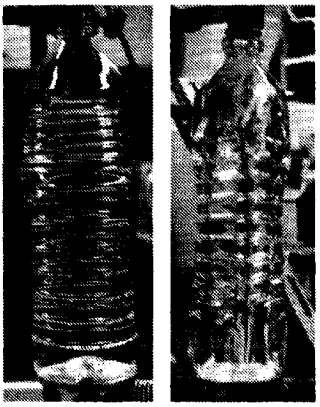

(a) (b)

Figure 6.3: *(a)Round and (b)square deformed bottle during vacuum resistance testing.*

T	293	K
p^a	100	kPa
V_f	$7.5 \cdot 10^{-4}$	m^3
V_g	2	%
h	$2.4 \cdot 10^{-4}$	m
A	0.003	m^2
p^{cr}	77.5	kPa
α	$6.7 \cdot 10^{-10}$	$m^3\ kPa^{-1}$
P_{O_2}	$3.53 \cdot 10^{-13}$	mol m day^{-1} N^{-1}
P_{N_2}	$6.15 \cdot 10^{-14}$	mol m day^{-1} N^{-1}
S_{O_2}	$5.06250 \cdot 10^{-5}$	mol m^{-1} N^{-1}
S_{N_2}	$2.73214 \cdot 10^{-5}$	mol m^{-1} N^{-1}

Table 6.2: *Values as used during the simulation. The volume-pressure compliance and the internal buckling pressure are respectively denoted by α and p^{cr}.*

is considered to give a reasonable indication of the importance of the oxidation process. It is further assumed that filling and closing took place at ambient conditions. At the start of the simulation the oil is saturated. Other coefficients necessary for the simulations are mentioned in Table 6.2. The simulations were carried out with a time increment of 0.01 day while a period of 90 days has been examined. Figure 6.5 depicts the results for a flexible non-buckled and a rigid configuration of the round bottle. This figure clearly shows that solubility effects play a significant role. Furthermore, For a time period of 90 days and different buckling pressures p^{cr} the pressure as a function of time is plotted in Figure 6.6, while the amount of O_2 and N_2 are plotted in Figure 6.7. The last two figures clearly indicate that permeability does not significantly influence the quality of the contents, the gas volume and/or the behavior of the structure in due time. It also shows that any new incoming oxygen reacts completely in the next time step. It is therefore possible to neglect permeability since it will not influence the optimization of the whole structure as will be described in Chapter 8. Note that for smaller wall thicknesses this effect might become important and cannot be neglected. Figure 6.7a shows that almost all oxygen reacts within 25-30 days, depending on the structure. Oxidation causes rancidity of the oil, it should therefore be avoided or

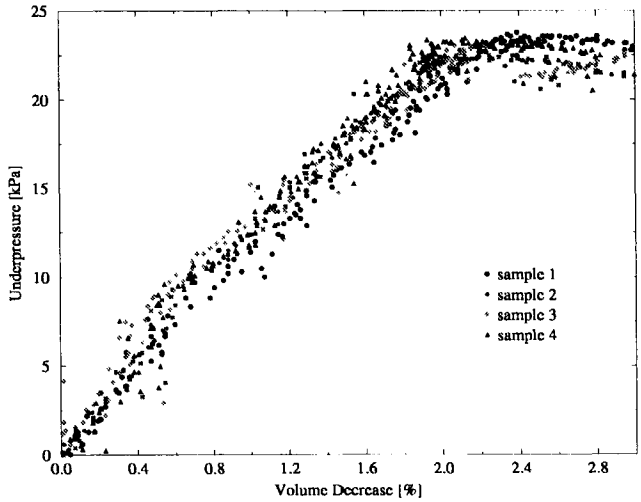

(a)

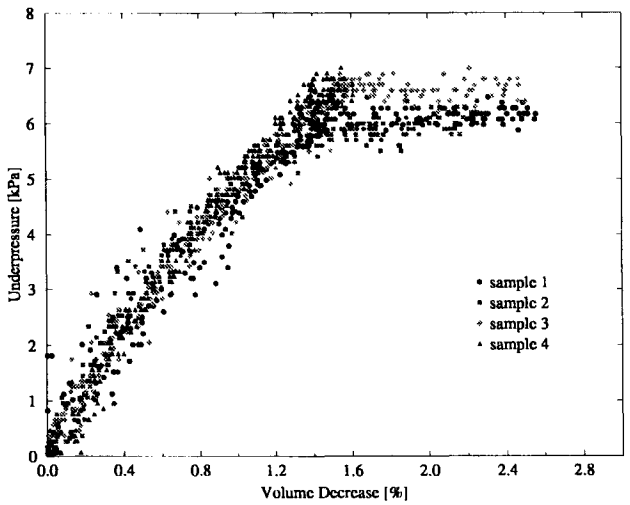

(b)

Figure 6.4: *Experimental results for the round and square bottle during vacuum resistance testing. The vertical axis depicts the internal under-pressure,* i.e. $p^a - p$, *while the horizontal axis depicts the percentage of volume decrease of the structure. The figure clearly shows that the behavior of the structure till buckling is almost linear. It also demonstrates that the internal pressure remains approximately constant after buckling.*

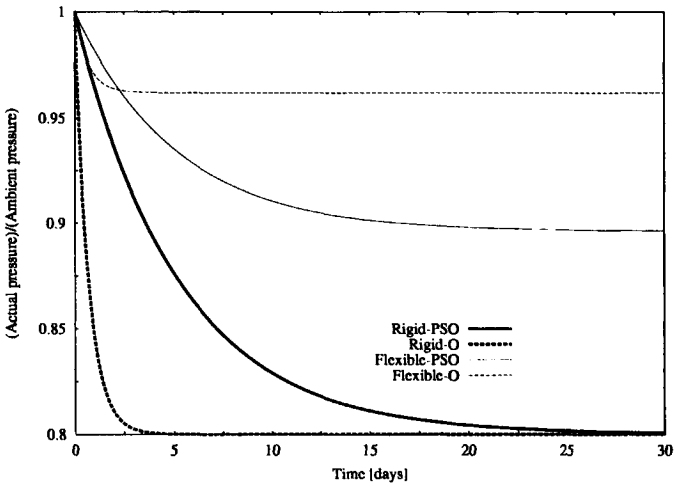

Figure 6.5: *Result of simulations for flexible and rigid bottles. The index P,S and O, which stand respectively for permeability, solubility and oxidation, indicate which effects were taken into account. The flexible bottle had a buckling pressure of 77.5 kPa which was enough to resist buckling.*

minimized. The presented results illustrate that the latter can be done by reducing the amount of initial oxygen. This can be carried out by degassing of the oil prior to filling and to fill the package under an absence of oxygen gas, *e.g.* blanketing the oil with nitrogen. Finally, care must be taken that the headspace of the bottle is as small as possible in order to take care that any accidental incoming amount of oxygen is as small as possible.

Generally, in countries where the paneling problem occurs, the shelf-life of the product should be guaranteed up to 1 year. For defining the constraints for the package at the end of its shelf-life it is thus possible to assume that all oxygen gas reacted and that the behavior of the structure is only determined by the nitrogen gas. Use of the latter will be made in Chapter 8 during optimization of the bottle.

6.7 Conclusions

The present work shows that the mechanical behavior of the structure and the internal pressure as caused by oxidation have a significant influence on each other. It has also been illustrated in Figure 6.5 that solubility effects have a large influence on the internal pressure and should therefore be taken into account. Permeability effects in contrary have only a minor influence on the behavior of the package and on the contents. The latter can be neglected in the present setting.

The oxidation model as used in the present chapter was derived from models suggested by Herlitze *et.al.* [34] and Penzkofer [50]. The accuracy of the model as used here might be discussed. However refining hereof will most likely not lead to different conclusions since all oxygen gas reacts in a period much shorter than the shelf life. The latter has also been confirmed experimentally by Evans [21] who describes a complete disappearing of all oxygen within three weeks. If the shelf-life of a package is constrained to a maximum of three weeks or less than use can be made hereof since the required critical buckling pressure p^{cr} can be higher. The latter implies a potential possibility to reduce the bottle weight and thus the material costs, for this a more accurate description of the oxidation might be required.

The described model has not been used to examine why in due time (one year) all enclosed gas volume can disappear. The results as described in this chapter indicate that this is not caused by permeability. An explanation may be found in the time dependent behavior of the structure and a complete

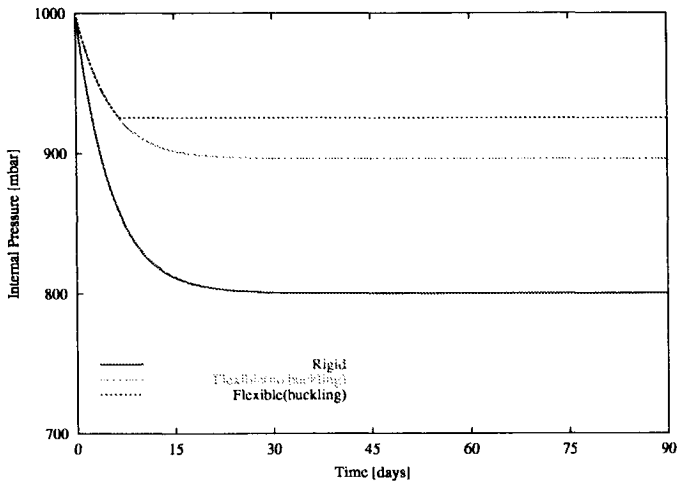

(a)

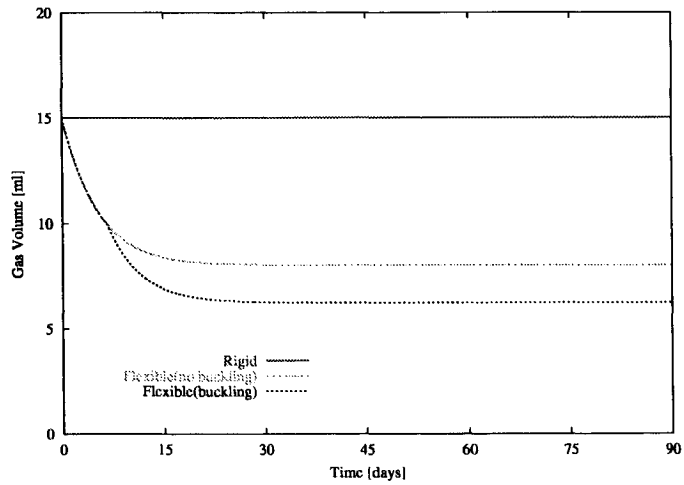

(b)

Figure 6.6: *(a) The internal pressure as a function of time for three different bottles: rigid, $p^{cr} = 77.5$ kPa (no buckling) and $p^{cr} = 92.5$ kPa (buckling), respectively. (b) The gas volume as a function of time.*

dissolving of all nitrogen into the contents.

The described results are based on a linearized behavior of the package with respect to internal volume and internal pressure. The latter does not have to be so, in such cases the model can be elaborated easily to more accurate behavior of the structure which can be determined with finite element analysis. The latter will be described in more detail in Chapter 7.

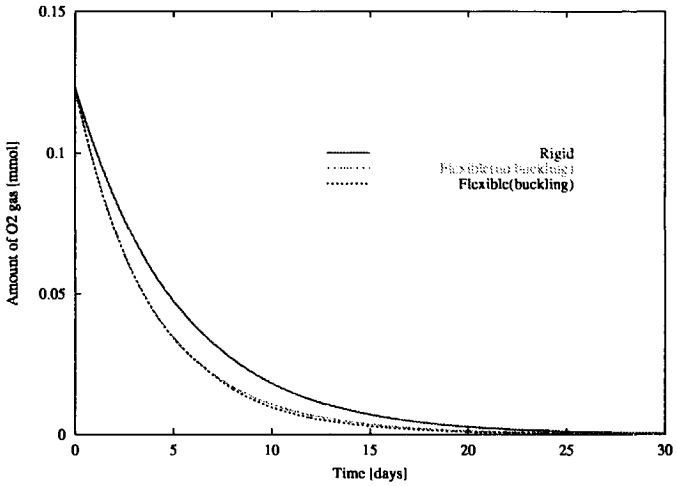

(a)

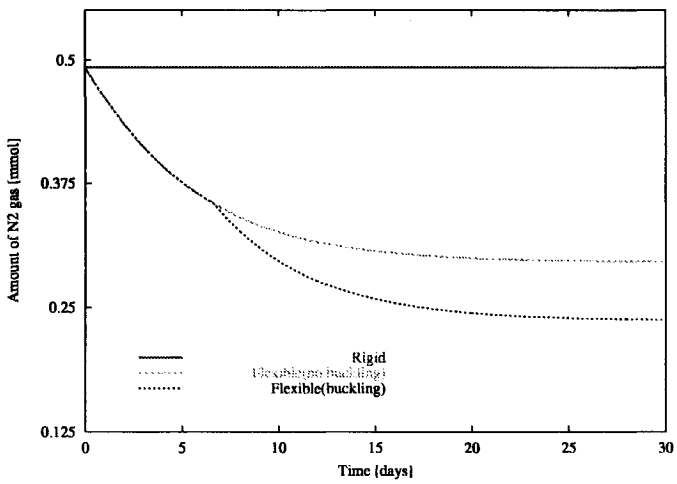

(b)

Figure 6.7: *The amount of O_2 and N_2 as a function of time for the three bottles as mentioned in Figure 6.6.*

It has not been examined how humidity and vapour pressures influence on the results. These effects are expected not to have a significant influence for the edible oil example. However, the model can also be used for detergents or chemicals. Especially for volatile liquids the effects of vapour pressure might be important.

Based on: R. van Dijk and F. van Keulen, Deformation of Closed-Filled Packages due to Oxidation, Permeation and Solubility Effects, Proceedings for the IASS-IACM conference, 4–7 June, 2000, Chania, Greece.

Chapter 7

Deformation of Closed-Filled Packages

Oxidation of the contents of closed-filled packages significantly influences on the internal pressure and in due time leads to unacceptably deformed packages and a reduced quality of the contents. Obviously, these complications should be avoided or minimized. Simulation of the package taken into account mechanics, oxidation, permeation and solubility can be used to estimate the relative importance of each of these aspects. A model which takes into account these effects hereby making use of a simplified behavior of the package has been described in Chapter 6. The present chapter will elaborate hereon and will make use of a more accurate volume-pressure relation for the package. The latter gives more accurate results for the internal pressure as a function of time. The simplified behavior of the package can be exploited during optimization as will be discussed in more detail in Chapter 8.

7.1 Introduction

One of the functions of packaging is preservation of the contents. In most cases the contents oxidizes and in due time becomes rancid [60]. The process of oxidation is very complex and influenced by many factors such as pollution of the contents, pollution of the packaging material, presence of additives *etc.*. During oxidation the enclosed oxygen gas will be consumed. Consequently, this influences on the enclosed gas-volume and/or the internal pressure. In the present work the relative importance of the processes as described above will be estimated. This will be done on the basis of a numerical model.

In practice, three types of packaging can be distinguished. The first type of packages are the so-called non-deformable or rigid packages, *e.g.* glass bottles and metal cans. For these packages the gas volume, and thus also the total volume, remains as a good approximation constant. For the second type of packages, the so-called non-resistant packages [41], *e.g.* bags and pouches, the internal pressure remains equal to ambient. The third type are the flexible packages. The majority of the packages are among this type, from which a typical example is depicted in Figure 7.1. For the first two types of packaging the behavior of the package and its influence on the oxidation-parameters can easily be predicted and was previously studied by Talasila [61]. For the flexible packages internal pressure changes may induce a substantial deformation, eventually resulting into buckling of the package. The latter gives the consumer the impression that the contents is affected and gives the package a reduced appearance. A complete uptake of the initial gas volume can be observed for bottles containing edible oil after one year of storage. A model which takes into account the solubility of gas in the fluid, the permeability of gas through the wall of the package, and the mechanical behavior of the package has previously been described in Chapter 6. In Chapter 6 the behavior of the flexible packages has been approximated by a model with a linear volume-pressure relation before buckling and a constant internal pressure after buckling. In the current chapter the volume-pressure relation is not necessarily linear and obtained either through experiments or through Finite Element Analyses (FEA). The latter leads to a more accurate description of the remaining volume and pressure as a function of time.

The model for oxidation is based on models as found in literature [34, 42, 61]. In these models

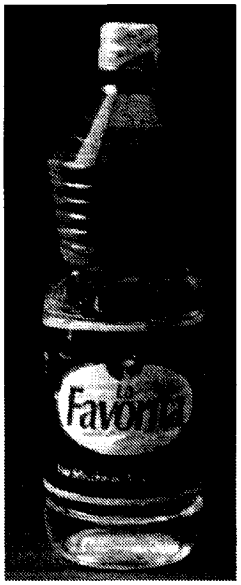

Figure 7.1: *A plastic bottle for edible oil. The oxidation caused a substantial deformation of the package.*

the oxidation is assumed to depend solely on the partial oxygen pressure. Solubility effects have been incorporated using Henry's law while assuming that the solubility equilibrium occurs instantaneously. For the prediction of the internal pressure, volume , *etc.* an explicit time integration scheme is used. In the present setting only the oxygen and nitrogen gas have been accounted for.

The main purpose of this chapter is to identify the relevance of the physical processes involved and to examine whether during optimization use can be made of the more simplified approach as discussed in Chapter 6. The latter will be discussed in more detail in Chapter 8.

In chronological order this chapter describes the problem, the governing equations, the behavior of the package, the determination of the oxidation induced deformation and conclusions.

7.2 Problem description and assumptions

The processes involved in this problem are visualized in Figure 7.2 and can be distinguished as follows. Firstly, the internal gas pressure is defined by the sum of the internal partial gas pressures [24], *i.e.* $p = \sum p_i$. In this thesis ideal gases will be assumed, the gas law therefore reads

$$\frac{p_i V_g}{n_i T} = R, \tag{7.1}$$

where n_i, T and R are the amount of a certain gas in the gas volume V_g, the temperature and the gas constant, respectively. Secondly, for a constant temperature dissolving of gas can be described by Henry's law [13, 37, 38, 43, 45] which reads,

$$D_i = p_i S_i V_f, \tag{7.2}$$

where S_i and V_f are the solubility coefficient and the fluid volume, respectively. In Figure 7.2 the dissolving/fugating is indicated by D. Thirdly, the contents of the package oxidizes, indicated by Φ. Furthermore, due to the absence of equilibrium between internal and external partial gas pressures, gas

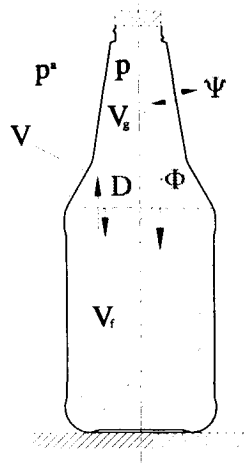

Figure 7.2: *Situation sketch, V, V_g, V_f, p and p^a are the total enclosed volume, the gas volume, the fluid volume, the internal pressure and the ambient pressure, respectively. The arrows visualize the gas streams due to solubility D, permeability Ψ and oxidation Φ effects.*

will permeate through the wall of the package which is indicated by Ψ. Due to internal pressure changes the package will deform. On its turn, the deformation of the package influences the physical processes mentioned above.

As the present study is intended for identifying the relative importance of different physical processes, the following assumptions have been made:

- package, gas and contents always have a temperature equal to ambient;
- no oxidation and permeation take place during filling of the package;
- both, the gases and the contents, do not react chemically with the package;
- the enclosed air initially contains 20% oxygen and 80% nitrogen;
- the oxidation process does not create residual gases.

These assumptions originate from common practice with respect to bottling edible oil and significantly reduce the complexity of the problem. Note that it is straightforward to create a model without the above assumptions.

7.3 Governing equations

The following balance equation can be formulated for each component i,

$$n_i = N_i^0 - D_i + \Psi_i - \Phi_i. \tag{7.3}$$

The total initial amount of a certain component, dissolved and as gas, is denoted by N_i^0. The current dissolved amount of a gas is given by D_i. The permeated and reacted amount of a certain component are given by Ψ_i and Φ_i, respectively. It should be noted that the reacted amount of a certain component in

the present setting only refers to the oxygen gas. It is assumed that the nitrogen gas does not react with the package nor with the contents.

The solubility rate is given by differentiation of Henry's law which leads to

$$\frac{dD_i}{dt} = S_i V_f \frac{dp_i}{dt}, \tag{7.4}$$

where S_i and V_f are the solubility coefficient for a constant temperature and the fluid volume, respectively.

The rate of permeation reads [61],

$$\frac{d\Psi_i}{dt} = \frac{P_i A}{h}(p_i^a - p_i), \tag{7.5}$$

where P_i, A, h and p_i^a are the permeability coefficient, the area of permeation, the wall thickness and the ambient partial gas pressure, respectively. Note that permeability as well as solubility is temperature dependent [49].

The same model as in Chapter 6 has been used for the oxidation. Chapter 6 uses the following function for the reaction, here oxidation, rate

$$\frac{d\Phi_i}{dt} = r_i(p_i)V_f, \tag{7.6}$$

where $r_i(p_i)$ is the reaction speed per unit volume and defined as $r_i(p_i) = \varpi_i p_i$, i refers to the oxygen gas. Here ϖ_i is a constant reaction speed per unit contents-volume and per unit partial pressure. This model is based on the models as proposed by Herlitze *et al.* [34] and Penzkofer [50]. A justification for this model is given in Section 6.3.4.

The complete oxidation process is very complicated and influenced by many factors, *e.g.*, temperature [26], light, presence of traces of metal, humidity [51], oil quality, additives *etc.* which will not be further discussed in this thesis. In Chapter 6 it has been described that the oxidation takes mainly place during the first three weeks. During these weeks all initially present oxygen reacts with the contents. Hereafter the oxidation speed is governed by permeation of oxygen through the wall of the structure. Since the period of interest is usually longer than three weeks an more accurate description of the oxidation process will be omitted. If the shelf-life is however constraint to a maximum of three weeks or less than the oxidation model should be refined.

Differentiation of (7.3) and substitution of (7.4), gives the governing rate equations,

$$\frac{V_g}{T^a R}\frac{dp_i}{dt} + \frac{p_i}{T^a R}\frac{dV_g}{dt} = \frac{d\Psi_i}{dt} - \frac{d\Phi_i}{dt} - S_i V_f \frac{dp_i}{dt} \tag{7.7}$$

where the left-hand side is obtained by differentiation of the gas law (7.1) for constant temperature.

7.4 Deformation of the structure

Before we can make use of (7.7) the deformation of the structure should be available. In practice it is possible to distinct three kind of structures:

1. *Rigid structures*, for example glass structures. For these kind of structures deformation induced by internal pressure changes can be neglected.

2. *Non-resistant structures*, for example plastic bags. These kind of structures will hardly resist to any internal pressure changes. Therefore the internal pressure remains approximately equal to the ambient pressure.

3. *Flexible structures*, for example plastic bottles. These kind of structures will deform due to internal pressure changes but will give a substantial resistance to pressure change.

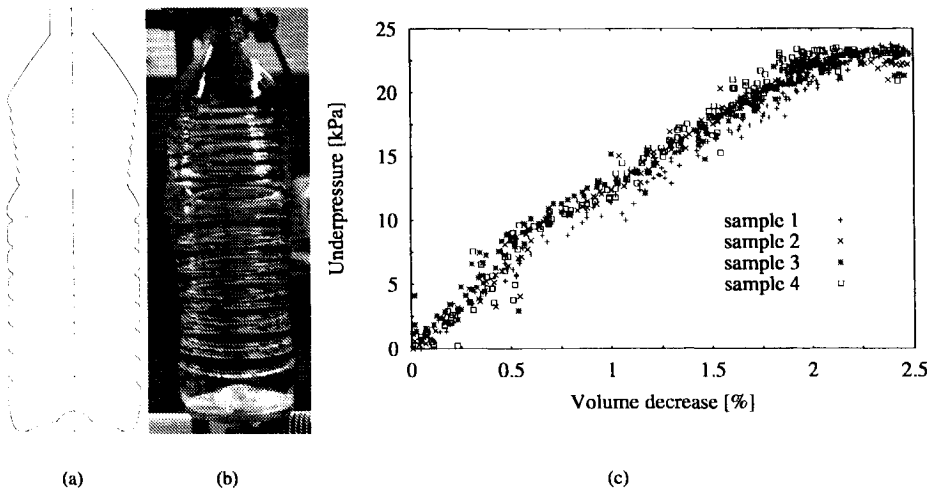

Figure 7.3: *(a) Sketch of the analysed bottle. (b) Post buckling deformation in experimental setup. (c) Experimental pressure-volume relation of the package.*

In Chapter 2 it has been described that the packages considered here (see Figure 7.1) have an approximate linear pressure-volume relationship until buckling of the package. While after buckling the internal pressure remains constant. The latter is illustrated for a 750 ml round bottle for edible oil in Figure 7.3 and Figure 7.4. Before buckling the gas volume can be approximated with $V_g = V_g^0 + \alpha(p - p^a)$ where α is a so-called volume-pressure compliance for the package. After buckling the gas volume in the package can be approximated by $V_g = (nTR)/p^{cr}$, where p^{cr} is the internal pressure at which buckling occurs. This approximate piece-wise linear behavior of the structure makes solving of (7.7) easy, since V_g and its derivative dV_g/dt are now available. However, the experimentally found results as depicted in Figure 7.3 can also be approximated by a non-linear function. The latter is depicted in Figure 7.4 where a 10-th order polynomial function has been used. After fitting of this function the term dV_g/dt is again easily obtained. In the next sections it will be investigated if simplification to a piece-wise linear approach is justified.

There might be situations where there are no samples available due to the fact that the package is still in its development stage. In such cases the behavior of the structure can be simulated with Finite Element Analysis (FEA). An example hereof is depicted in Figure 7.5, here a bottle with a Young's modulus of 5700 Nmm^{-2} and a Poisson's ratio of 0.35 has been modeled with triangular elements [73]. This structure has previously been discussed in the previous chapters. The overall wall thickness, which was modeled uniformly, is in contradiction with practice where the wall thickness varies significantly. Geometric imperfections have also not been taken into account in the Finite Element model. It is therefore that there is a certain discrepancy between the experimental and the simulated results.

7.5 Determination of the oxidation induced deformation

After determination of dp_i/dt and dn_i/dt for each of the gases from (7.1), (7.7) and the relationship between volume and pressure following from the structure an estimate for the new internal pressure and amount of gas can be found by,

$$p_i(t + \Delta t) \approx p_i(t) + \frac{dp_i}{dt}\Delta t, \tag{7.8}$$

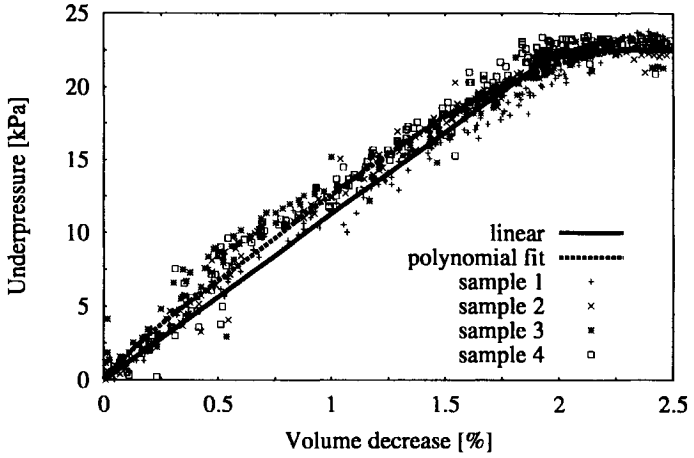

Figure 7.4: *Experimental results, linear and 10-th order polynomial fitted results.*

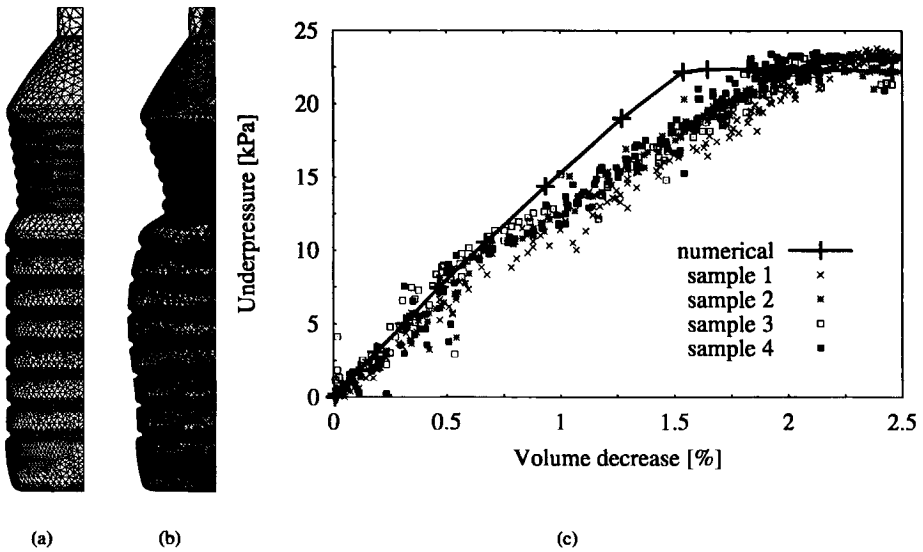

Figure 7.5: *(a) Undeformed configuration of the bottle with six ribs. (b) Deformed configuration of the bottle with six ribs. (c) Experimental and numerical pressure-volume relationships.*

and

$$n_i(t + \Delta t) \approx n_i(t) + \frac{dn_i}{dt}\Delta t, \tag{7.9}$$

respectively. In such way an incremental solution for the pressure change has been obtained. The total amount of component i that reacted can be approximated using

$$\Phi_i(t + \Delta t) \approx \Phi_i(t) + \varpi_i p_i V_f \Delta t. \tag{7.10}$$

Note that $\varpi_i p_i V_f \Delta t$ can not exceed the enclosed gas amount plus the amount of component i that permeates into the structure. The total amount of the component that permeated through the wall of the structure can be estimated on the basis of

$$\Psi_i(t + \Delta t) \approx \Psi_i(t) + \frac{P_i A}{h}(p_i^a - p_i(t))\Delta t. \tag{7.11}$$

The above equations describe the explicit integration scheme as used in the present setting. In order to avoid drifting from the exact solution it is necessary to select the time increments sufficiently small.

7.6 Results

The significance of the effects involved has been evaluated on the hand of an example. This example is a plastic bottle for edible oil as currently used by Unilever and is depicted in Figure 7.5. The data as used in the simulations are equal to the data as used in Chapter 6, see Table 6.2. The oxidation speed is defined as $r_{O_2}(p_{O_2}) = 1.125 \cdot 10^{-5} p_{O_2}$ similar to Chapter 6.

A common measure for oil quality is the PerOxide Value (POV) [38], where 1 POV equals the conversion of 16 mg O_2 per kg of oil into hydroperoxides. The PerOxide Value (POV) is an indication for the amount of oxygen in the structure per unit weight (of the contents). Therefore the POV is a measure for the amount of dissolved and reacted oxygen [38] and thus the rancidity of the oil.

In the Figures 7.6, 7.7 and 7.8 the results of the simulations are depicted. From these figures it can be concluded that within a period of approximately 21 days all initially present oxygen reacts with the oil, the latter is experimentally confirmed by Evans [21]. Hereafter, newly permeated oxygen which entered the structure reacts immediately with the oil. Thus, after all initial oxygen has reacted, the mechanical behavior of the structure is fully determined by the remaining nitrogen gas and a constant stream of oxygen permeating into the structure which consequently leads to a constant,but small, increase of POV since the partial pressure-difference for oxygen equals $p_{O_2}^a$. These figures also show that the permeability effect is very small and can be neglected. This conclusion is based on the constant pressure and gas volume after all initial oxygen reacted. The latter has also been concluded in Chapter 6.

The Figures 7.6 and 7.7 show a difference in predicted underpressure and volume change depending on the behavior of the structure. For an accurate determination of the remaining gas volume and pressure the non-linearity of the pressure-volume behavior of the package should be accounted for. However, if it is desired to optimize the involved package then for each design a complete non-linear calculation should be carried out. The latter can cause the optimization to become very expensive. During an optimization the piece wise linear volume-pressure relation can be used as an approximation. At the end of the optimization a check should then be performed if a non-linear volume-pressure relation determined with FEA on the optimal bottle design will not violate the applied constraints.

Simplifying the behavior of the bottle to either a non-resistant structure or a rigid structure can lead to wrong results. For example, we have a plastic bottle which buckles at an internal pressure of 82.5 kPa. If we assume that the bottle behaves like a rigid structure then the internal pressure after consumption of all oxygen will be 80.0 kPa. In reality a pressure of 80.0 kPa will cause the real bottle to buckle. However, the structure has a certain flexibility and therefore the internal pressure might not exceed the critical pressure depending on the volume-pressure compliance α.

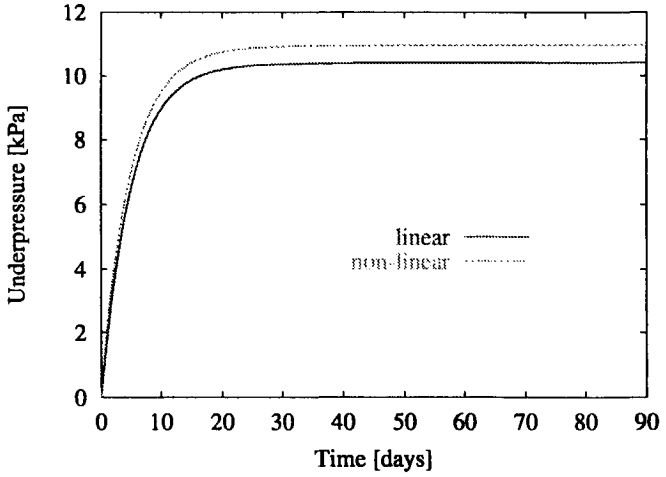

Figure 7.6: *Underpressure as a function of time.*

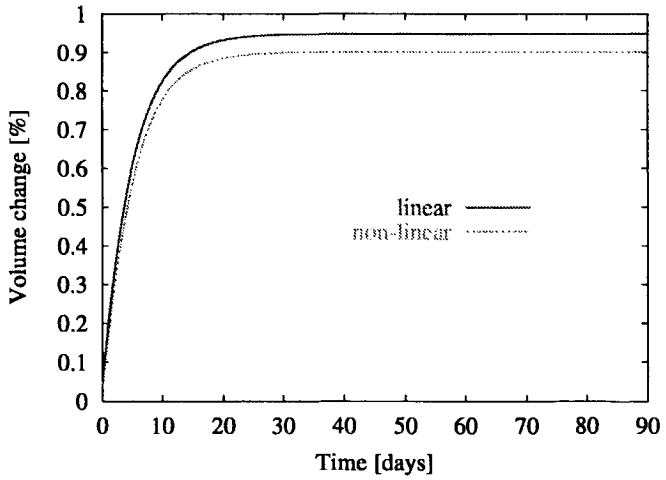

Figure 7.7: *Volume change as a function of time.*

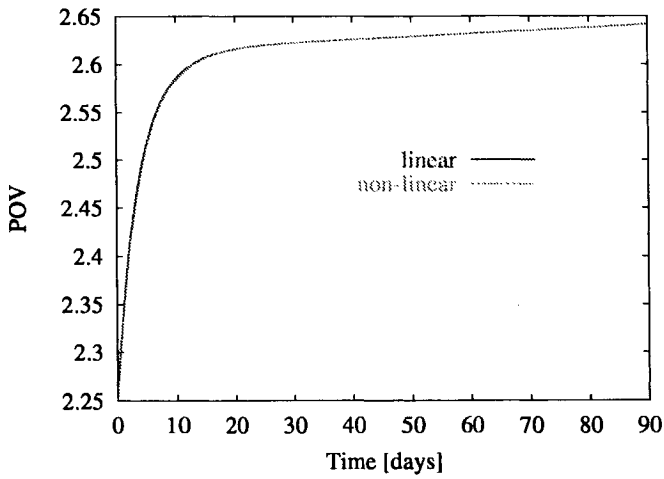

Figure 7.8: *Peroxide value [38] through time. The linear and non-linear results completely coincide.*

7.7 Conclusions

The following conclusions can be formulated for the flexible package in the present setting:

- After all oxygen reacted, any new incoming oxygen immediately reacts with the contents;
- After all oxygen reacted, the mechanical behavior of the package is fully determined by the nitrogen;
- Permeability effects can be neglected. Note, that a significant reduction of the wall thickness might lead to a different conclusion;
- The POV value of the contents at the end of the shelf life can be predicted using the initial amount of oxygen present added with the amount of oxygen permeated during the shelf life while assuming a zero oxygen pressure after closing;
- If the focus is on the mechanical behavior only, *i.e.* the product's shelf life and the oxidation is not a point of interest, then the above conclusions justify simplification of the model by neglecting permeability;
- A non-linearity in the volume-pressure relation of the package has a significant influence on the prediction of internal pressure and volume. Taking this non-linearity into account can lead to a very expensive optimization problem. Therefore, it is beneficial to make use of a piece-wise linear volume-pressure relation during optimization. Fine-tuning of the design concept can then be done using a non-linear volume-pressure relation.

Based on: R. van Dijk and F. van Keulen, Optimization of Food Packaging; Explorative study to the optimal bottle design, Proceedings of the European Congress on Computational Methods in Applied Science and Engineering (ECCOMAS'2000), 11–14 September, 2000, Barcelona, Spain.

Chapter 8

Bottle Optimization

Many packages are being produced and disposed every year. It is therefore of great importance to minimize the material required for these packages from a cost as well as an environmental perspective. Not only is packaging loaded *e.g.*, during stacking, transportation, handling, *etc.* also the contents can cause mechanical loadings. The latter are especially important when packaging foods. Due to oxidation of the contents, here edible-oil, an internal under-pressure is created which might lead to buckling of the package. Therefore, optimization of packages with respect to, for example, weight calls for an integrated approach which takes behavior of the contents as well as the mechanical behavior of the package into account. This chapter describes the optimization of a plastic bottle for edible oil making use of the different optimization techniques. Prior to optimization the importance of solubility, permeability and oxidation have been discussed. Moreover it has been indicated how these processes can be accounted for during the optimization.

8.1 Introduction

Since millions of packages of fast moving consumer goods are sold and disposed of every year, optimization hereof can lead to significant material savings and thus less environmental loading. Optimization of packages requires an approach which takes not only the mechanical aspects but also chemical and physical processes into account. In this chapter the optimization process of a plastic bottle for edible oil, as depicted in Figure 8.1, is described.

Due to oxidation the internal oxygen gas is consumed which causes an under-pressure. This under-pressure can exceed the vacuum resistance, *i.e.* the under-pressure at which buckling occurs. The latter can in due time lead to a significantly deformed package as discussed in Chapter 2. On its turn this deformation influences the internal pressure, the dissolved amount of gas and the oxidation speed. Note that the oxidation speed depends on the partial oxygen pressure [70]. For the consumer buckling of the package is an indication that the contents has been affected. Any deformation of the package should therefore not be visible to the consumer.

Models to describe the oxidation process have been developed by Talasila [61], Kiritsakis [42] and Herlitze [34]. Talasila [61] coupled the oxidation process to the mechanical behavior of the structure for rigid and non-resistant packaging *e.g.* plastic bags, pouches *etc.*.

The pressure induced deformation of the package is influenced by the design of the bottle. Optimization of the design of the package should therefore take the oxidation process into account. Here, use will be made of a simplified oxidation model [69, 70], Finite Element Analyses (FEA) and the Multipoint Approximation Method (MAM) [76]. This chapter explores better designs, here defined as lighter designs, for a plastic bottle for edible oil. Totally three optimization problems will be discussed. All these optimization problems have the same objective function, which is the weight of the package and which is to be minimized. The optimization problems differ only in constraint formulation. In the sequel these different optimization problems are denoted as different constraint situations. This approach is chosen to illustrate the influence of the constraint formulations on the obtainable results in material savings.

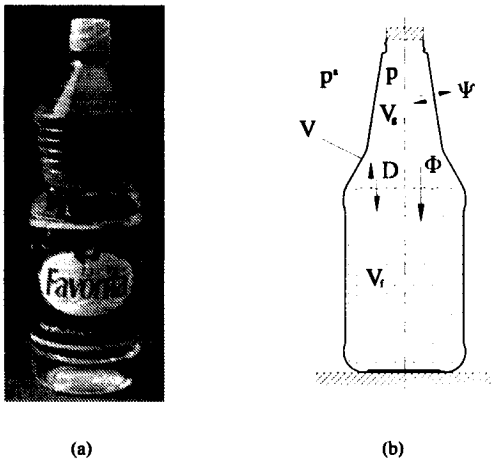

Figure 8.1: *(a) Bottle deformed due to under-pressure as caused by oxidation of the contents. (b) Situation sketch. V, V_g, V_f, p and p^a are the total enclosed volume, the gas volume, the fluid volume, the internal pressure and the ambient pressure, respectively. The arrows visualize the gas flows due to solubility and permeability effects.*

The first constraint situation prevents buckling of the package according the adapted model and assumes that there are no other physical processes involved than the ones described here. However, in practice situations occurred where all initial gas volume disappeared resulting in a buckled package. The current model does not explain this effect which is most likely caused by non-linear material behavior [69]. This problem can however be circumvented by applying a constraint which enforces that the volumetric deformation of the package before buckling is as large as the initial gas volume, or larger. The latter is done in the second constraint situation. While the third constraint situation requires the optimal package to omit both the first and second constraint situation. Each constraint situation leads to a different optimum. It depends on manufacturing requirements which constraint situation will be adapted.

Structural optimization techniques have earlier been applied in packaging by Hamada [32] who tried to optimize the thermoforming process. Bhakuni [8] used structural optimization techniques in order to optimize aluminium beverage can bottoms.

In chronological order this chapter describes: the problem and adopted assumptions, simulations of the whole bottle with FEA, simplification of the problem to a smaller FE model, design sensitivities [14, 75] and the Multipoint-Approximation technique, results and finally the conclusions.

8.2 Problem description and assumptions

The relevant physical and chemical processes acting in the package have been depicted in Figure 8.1b. Here the permeability, solubility and oxidation effects are denoted by Ψ, D and Φ. Assumptions which have been used in the present setting are:

- package, gas and contents always have a constant ambient temperature;
- no oxidation occurs during filling of the package;
- permeation effects can be neglected; Earlier work carried out by the author [69, 70] illustrated that these effects can indeed be neglected in the present setting;

- both the gases and the contents do not react chemically with the package;
- initially, the enclosed air contains 20% oxygen and 80% nitrogen;
- initially the contents is saturated under air (20% oxygen and 80% nitrogen) at ambient pressure;
- the oxidation process does not create residual gases;
- the packed fluid is and remains homogeneous.

Vacuum resistance is only one of the requirements for the involved package. In current practice there also exist specifications for the empty vertical compression strength of a bottle as discussed in Chapter 2. Including this specification as a constraint for the optimization problem will most likely result in a design with only few material-savings gained. Chapter 3 showed that the compression strength of the here used closed-filled bottle is significantly higher than the compression strength of the empty bottle. To guarantee no failure during vertical compression it is thus required to apply a good closure. If such a closure is applied then the bottle does not have to be constrained for this compression and consequently does not restrict further weight reduction.

In conclusion, in the present setting the bottle will be optimized with respect to its weight and under the condition that no buckling will occur due to internal pressure changes. In practice, the latter implies three different constraint situations as described above. Depending on the manufacturing requirements the desired constraint situation should be applied.

8.3 Model description

The model for the behavior of the package as a function of time includes mechanical, solubility and oxidation effects. The effect of permeation has been neglected based on the results obtained in Chapter 6. Consequently, now two stable situations can be distinguished. The first situation is an equilibrium between the gas, the dissolved amount of gas and the deformation of the package before any oxidation took place, thus at $t = 0$ where t is the time in days. In the sequel this will be referred to as the pre-oxidation or first equilibrium. It is assumed that this equilibrium occurs instantaneously after capping. Here, the pre-oxidation equilibrium does not lead to internal pressure changes or mechanical deformation due to the imposed assumptions as mentioned in the introduction above. The second stable situation occurs when all oxygen reacted. This situation will be referred to as the post-oxidation or second equilibrium. In both situations the package can be either in its buckled or none buckled configuration depending on the initial conditions. In many cases a complete uptake of all oxygen can be expected within three weeks after closure [21, 70]. Only the post-oxidation equilibrium is of interest.

There is no post-oxidation equilibrium for packages where the time dependent mechanical behavior of the package is taken into account. This time dependent material behavior directly influences the internal pressure.

The internal gas pressure is determined by the sum of the internal partial gas pressures [24], *i.e.*, $p = \sum p_i$. In this thesis ideal gases have been assumed, the gas law therefore reads

$$\frac{p_i V_g}{n_i T} = R, \tag{8.1}$$

where p_i, n_i, T and R are the partial gas pressure, the current amount of a certain gas in the gas volume V_g, the temperature and the gas constant, respectively. For a constant temperature the gas dissolves in the fluid according to Henry's law [13, 37, 38, 43, 45] which reads,

$$D_i = p_i S_i V_f, \tag{8.2}$$

where D_i, S_i and V_f are the dissolved amount of gas i, the solubility coefficient for gas i at a constant temperature and the fluid volume, respectively.

The following general balance equation can now be formulated,

$$n_i = N_i^0 - D_i - \Phi_i, \tag{8.3}$$

where the total initial amount of a certain component, *i.e.* dissolved and in gas form, is denoted by N_i^0. The reacted amount of a certain component is given by Φ_i. Substitution of (8.1) and (8.2) into (8.3) gives for the current problem,

$$\begin{array}{rcl} n_{O_2} = N_{O_2}^0 - D_{O_2} - \Phi_{O_2} & = & \frac{p_{O_2}^a V_g^0}{RT} + (p_{O_2}^a - p_{O_2}) S_{O_2} V_f - \Phi_{O_2} \\ n_{N_2} = N_{N_2}^0 - D_{N_2} & = & \frac{p_{N_2}^a V_g^0}{RT} + (p_{N_2}^a - p_{N_2}) S_{N_2} V_f, \end{array} \tag{8.4}$$

where V_g^0, Φ_{O_2} and p_i^a are the initial gas volume, the reacted amount of oxygen and the ambient partial pressure of gas i.

In some cases a drop of liquid nitrogen is added to the contents just before closing of the package. This is done to obtain an initial over-pressure in the package to prevent buckling. For this situation (8.4) must be modified. As such additions ($\ll$0.5% of the gas volume) are very small, the influence hereof on the contents volume can be neglected. Adding a small amount of nitrogen is cost increasing and therefore not preferred and not further examined in the present setting. In rare cases the oil is nitrogen blanketed [40], also then (8.4) should be modified.

Here $\Phi_{O_2} = 0$ and $\sum p_i = p_{N_2} + p_{O_2} = p$ for the pre-oxidation equilibrium, while for the post-oxidation equilibrium $n_{O_2} = 0$ and $\sum p_i = p_{N_2} = p$. In order to determine the gas pressures and the gas volume for equilibrium of interest, the behavior of the structure with respect to the internal pressure is required. Basically, three types of packages can be distinguished:

1. ***rigid packages***, for example glass bottles. For these kind of structures deformation induced by internal pressure changes can be neglected.

2. ***non-resistant packages***, for example plastic bags. These kind of structures will hardly resist to any internal pressure changes. Therefore the internal pressure remains approximately equal to the ambient pressure.

3. ***flexible packages***, for example plastic bottles. These kind of structures will deform due to pressure changes but will give a substantial resistance to the pressure change.

It is obvious that in the present setting we are dealing with flexible packages since non-resistant and rigid packages do not exhibit buckling.

The relation between the internal pressure and the enclosed volume has previously been described in Chapter 2, where an experimental setup which revealed the volume-pressure relation has been described. In Chapter 6 a linear volume-pressure relation has been used before buckling while after buckling the internal pressure remains constant. This model is illustrated in Figure 8.2 for the bottle for 750 ml of edible oil as considered here. The same model is also adopted here. The volume-pressure compliance is the derivative of the linear volume-pressure relation as depicted in Figure 8.2 and is denoted by α (in ml kPa^{-1}). In Table 8.1 the functions for the internal gas volume for the post-oxidation equilibrium, which is the only equilibrium of interest here, have been listed. In practice a buckled package is not desired. In the sequel the buckled post-oxidation equilibrium is therefore not addressed further. Substitution of (8.2) and the balance equations (8.4) in (8.1), gives an expression for the post-oxidation equilibrium pressure p^{equi} **before** buckling which reads

$$p^{equi} = p_{N_2} = \frac{-q + \sqrt{q^2 + 4\alpha(RTp_{N_2}^a S_{N_2} V_f + p_{N_2}^a V_g^0)}}{2\alpha}, \tag{8.5}$$

with $q = V_g^0 - \alpha p^a + RTS_{N_2} V_f$. In Figure 8.3 the equilibrium pressure has been plotted as a function of α for a bottle with 15 ml gas and 750 ml edible-oil. After buckling the gas pressure is equal to p^{cr} and

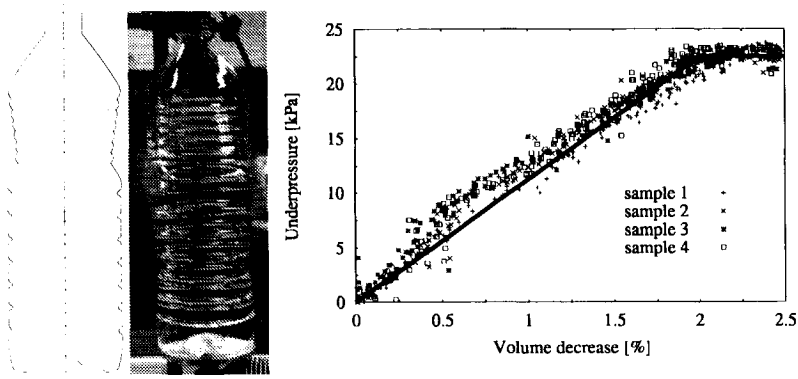

Figure 8.2: *(a) Sketch of the analysed bottle. (b) Post buckling deformation in experimental setup. (c) Experimental pressure-volume relation of the package.*

	General form	Post oxidation equilibrium
Before buckling	$V_g = V_g^0 + \alpha\Delta p$	$V_g = V_g^0 + \alpha(p_{N_2} - p^a)$
After buckling	$V_g = nTR/p^{cr}$	$V_g = n_{N_2}TR/p^{cr}$

Table 8.1: *Volume as a function of the internal pressure. The internal pressure at which buckling occurs is denoted by p^{cr}. Note that after buckling the pressure is approximated by a constant pressure $p = p^{cr}$. The coefficient α is the volume-pressure compliance of the linearized volume-pressure relation and here defined in ml kPa^{-1}.*

fully determined by the nitrogen. Figure 8.3 clearly illustrates that for a rigid bottle ($\alpha = 0$) the internal equilibrium pressure is 80.0 kPa while for a non-resistant bottle ($\alpha = \infty$) the internal pressures is equal to ambient. Figure 8.3 also shows that for larger values of α the required vacuum resistance, which is defined as $= p^a - p^{cr}$, reduces. An optimal bottle design should at least have a critical internal pressure p^{cr} equal to the equilibrium pressure p^{equi} to prevent buckling.

As discussed earlier, cases have been found were all gas volume has been consumed. The latter can be prevented by taking care that the volumetric deformation before buckling is at least as large as the initial gas volume, *i.e.* $\alpha(p^a - p^{cr}) \geq V_g^0$. The latter will be discussed further in Section 8.5.

8.4 Current bottle design

Before optimization of the bottle as depicted in Figure 8.4 the current bottle design will be evaluated with Finite Element Analyses (FEA). If simulations and experiments are in reasonable agreement then FEA can be used for optimization of the bottle. In Figure 8.5a the results of a linearized buckling analysis of a quart-bottle model with an overall wall thickness of 0.24 mm has been depicted. Note that, before buckling the bottle remains axial-symmetric. Experimentally the buckling pressure p^{cr} of this bottle is 77.5 kPa while numerically a buckling load of 78.9 kPa was found. Since the used FE model

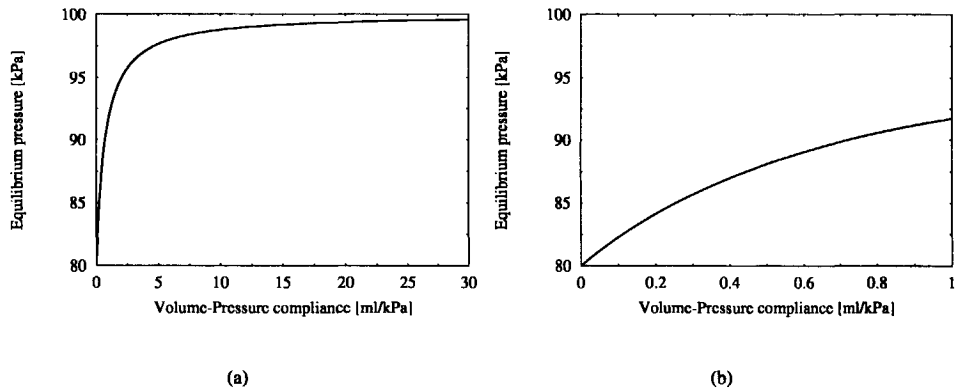

Figure 8.3: *(a) The internal post-oxidation equilibrium pressure as a function of the volume-pressure compliance α. (b) Detail of Figure 8.3a.*

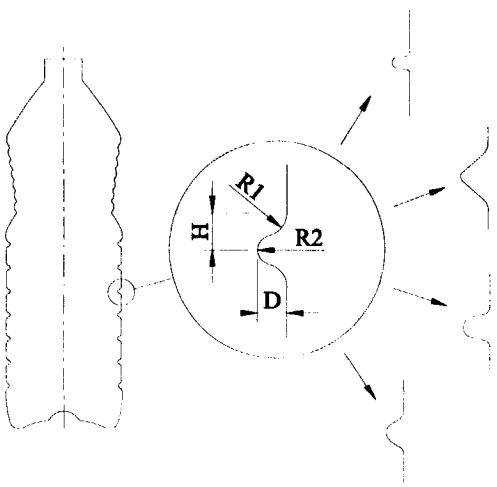

Figure 8.4: *Optimization of the ribs of the bottle. The design variables are the rib depth (D), two-rib radii ($R1$, $R2$) and the height of the rib (H). On the right hand side several possible rib configurations have been depicted. The parametric model is made such that only depicted and similar rib variants are allowed.*

gives reasonable results it will be used for optimization. Note however, that the mesh is rather coarse as depicted in Figure 8.5b.

In Table 8.2 the results of FEA are listed for the current bottle design. From this table it is also possible to conclude that the current bottle design is not able to compensate for the initial gas volume of 15 ml. The current design is however able to resist the post oxidation equilibrium pressure. One of the easiest ways of optimization is a reduction of the wall thickness. The same design has been evaluated with a wall thickness of 0.16 mm. In Table 8.2 the results hereof have been listed. From this it can be concluded that this bottle is also able to resist the post-oxidation equilibrium pressure. Similar to the

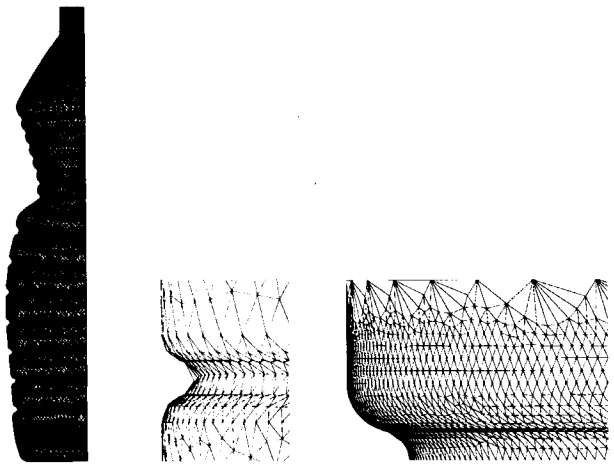

Figure 8.5: *(a) Buckling mode of a quart bottle-model with an internal vacuum. Before buckling the bottle remains axial-symmetric. (b) Detail of a single rib. (c) Detailed FE model of the current rib shape. This model is closed at the top by a rigid plate while along the bottle edge symmetry conditions have been applied.*

Wall thickness [mm]	Post-oxidation equilibrium press. [kPa]	p^{cr} [kPa]	α [ml kPa^{-1}]	Volume change at p^{cr} [ml]
0.24	87.8	78.9	0.476	10
0.16	92.3	91.0	1.128	10

Table 8.2: *Current bottle design with a wall thickness of 0.24 mm compared with the same design with a wall thickness of 0.16 mm.*

current design this bottle is also not able to compensate for the initial gas volume. Reducing the wall thickness of the current design to 0.16 mm can be carried out without loss of performance. The latter leads to a weight saving of 23%.

As mentioned earlier there are also cases where the total initial gas volume has been consumed, which might have been caused by time dependent behavior of the package. The latter is not investigated in more detail in the present setting. In the remaining of this chapter it will be explored if the design of the bottle can be modified such that the bottle is able to resist the post oxidation equilibrium pressure and able to compensate for the initial gas volume while still achieving significant material savings.

8.5 Optimization

As described in the previous section reducing the wall thickness of the bottle leads to significant material savings, while maintaining a similar performance. It has also been mentioned that the constraint can be formulated in two ways. The first way of defining the constraint is requiring that the volume change before buckling is at least as large as the initial gas volume. The latter is called the volume-constraining-method and will always prevent buckling since the containing fluid is nearly incompressible. The second way of constraining requires that the package should resist the post-oxidation equilibrium pressure. Here,

Design var.	Current value [mm]	Lower boundary [mm]	Upper boundary [mm]	Log. design sensitivity	Optimal (MAM) [mm]
H	3.1856	1	6	-3.4×10^{-2}	3
$R1$	2	0.2	2.5	9.6×10^{-3}	0.5
$R2$	1.25	0.2	2.5	-1.6×10^{-2}	2.5
D	2.5	0.7	4.5	3.3×10^{-1}	4.5

Table 8.3: *Possible values of the design variables and the logarithmic design sensitivities,* $\frac{H}{V}\frac{dV}{dH}$, $\frac{R1}{V}\frac{dV}{dR1}$, $\frac{R2}{V}\frac{dV}{dR2}$, $\frac{D}{V}\frac{dV}{dD}$, *respectively, for the current value of the design variables. V denotes the volume enclosed by a* $\frac{1}{8}$ *closed rib segment. The design sensitivities have been obtained using the Global Finite Difference method.*

this is called the pressure-constraining method. Both constraints can be applied, however deciding which constraints should be applied is left to the manufacturer. In the present setting all three methods will be discussed. Both packages, the current design and the reduced wall thickness bottle do not satisfy the volume constraint. As described previously, this constraint prevents paneling even if all gas volume disappears.

Optimization of the whole bottle in the current configuration would require a very fine mesh in order to describe the geometry accurately. The latter will result in high computational costs. From experiments and FEA it was found that the bottle behaves axial-symmetrically until buckling occurs. Moreover, most deformation takes place in the ribbed area of the bottle. Therefore, it is possible to imagine that it makes sense to create a FE sub-model which examines a single rib of the bottle. This new sub-model is depicted in Figure 8.5c and is a $\frac{1}{8}$ rib segment which is closed at the top by a rigid plate. Along the symmetry edges symmetry conditions have been applied. The FE model of this rib segment is small in comparison with the model of the quart bottle and therefore more suitable for optimization. Note that this approach is only of interest for the volume constraint since it is expected that the volumetric deformation of a single rib is somehow related to the volumetric deformation of a complete bottle; while the buckling pressure off a single rib can not be extrapolated to the buckling pressure of a complete bottle. In order to compensate for the initial gas volume the volume change of the bottle should be large enough. For a single rib this means that the volume change of this rib should be as large as possible since we do not know how to extrapolate the results of the single rib to the complete bottle. If this optimization is carried out for a single rib then afterwards it should be verified if the optimum rib design compensates for the whole initial gas volume when applied in the bottle. In case the package should also meet the pressure-constraint then also the buckling pressure of the bottle with the optimal rib shape should be checked. The described approached of examining a single rib will most likely not lead to an optimal solution for the bottle. However, any improved design can be considered as an iteration to the optimal design.

It is now of interest to find a combination of the design variables as depicted in Figure 8.4 for which the volume change of the $\frac{1}{8}$-rib segment is largest given a prescribed external pressure. Design sensitivities [75] have been used to get a first indication which of the design variables have a significant influence on the volumetric deformation of the single rib. The results hereof are listed in Table 8.3. This table already indicates that the depth of a rib has a significant influence on the volumetric deformation. Hereafter, the Multi-point Approximation Method (MAM) [76] has been used to find an optimal combination of the design variables. The optimal rib design as found by the MAM is depicted in Figure 8.6a. In Table 8.3 the optimal values of the design variables for the rib-segment have been listed. In Table 8.4 the volume pressure compliance α for the rib segments have been compared. It is clear that the volume change of the optimal rib is significantly better. Finally, it has been investigated if the optimal rib shape as determined by MAM for a certain constant wall thickness changes for different values of this wall thickness. The latter turned out not to be the case.

The optimal rib shape can now be applied in a quart-bottle model for final evaluation. The latter has been done for several wall thicknesses as listed in Table 8.5. The weight of the rib was not taken into account during optimization of a single rib. The latter also allowed generation of ribs which will result

Current	Optimal
$\alpha_{\frac{1}{8}\ rib}$ [ml kPa^{-1}]	$\alpha_{\frac{1}{8}\ rib}$ [ml kPa ^{1}]
6.2×10^{-3}	2.5×10^{-2}

Table 8.4: *Comparison of the current volume-pressure compliance of the rib segment and the optimized variant.*

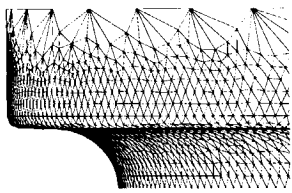

(a)

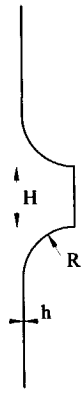

(b)

Figure 8.6: *(a) Obtained optimum rib shape. (b) Alternative rib shape which is aesthetically more attractive. This rib shape is expected to have a similar performance to the rib shape as depicted in Figure 8.6a.*

Wall thickness [mm]	α [ml kPa^{-1}]	Weight savings [%]
0.24	1.748	-8.9
0.22	2.144	-2.3
0.20	2.680	4.4
0.18	3.424	11
0.16	4.500	18

Table 8.5: *Weight savings for different values of the wall thickness.*

in a larger total bottle weight, *i.e.* negative weight savings. This is the case for the optimal rib shape with a wall thickness equal to the current bottle design (0.24 mm). In spite of the fact that an optimal rib is applied it should not be applied in the bottle with this wall thickness. In Figure 8.7 the results of buckling analyses for bottles with an optimal rib shape but different wall thickness have been depicted. From this figure it can be concluded that all these bottles are able to resist the post-oxidation equilibrium pressure. Together with Table 8.5 it can be concluded that weight savings up to 18% are feasible while satisfying both the volume and the pressure constraint. It can also be concluded that this 'optimal' bottle is able to compensate for 32 ml initial gas volume while only 15 ml is required. The latter implies that this 'optimal' bottle is over-dimensioned and that further optimization might lead to a weight reduction larger than 18%.

Note that the weight saving while satisfying both constraints is less than the weight saving of 23% which was obtained by just reducing the wall thickness of the current design to 0.16 mm based only on the pressure constraint.

The optimum rib shape as depicted in Figure 8.6a has a significantly simpler geometry than the current rib geometry. The optimum as depicted here is however not too attractive from an aesthetic point of view due to its pronounced appearance. It does however give a clear insight to the type of ribbing

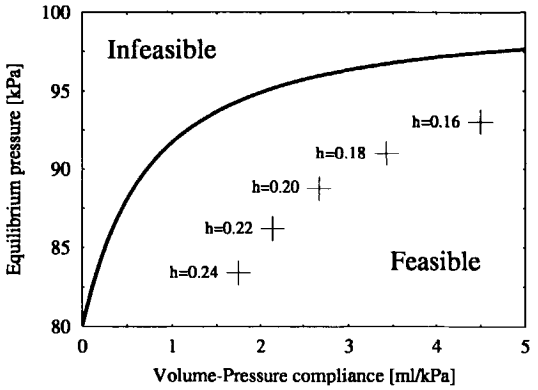

Figure 8.7: *Predicted post-oxidation equilibrium pressure, the feasible,* i.e. *no buckling will occur, and the infeasible areas,* i.e. *buckling will occur, have been indicated. The points refer to results obtained from calculations with different wall thicknesses h for a bottle with the optimal rib shape.*

Applied constraint	α [ml kPa^{-1}]	ΔV^{max} [ml]	p^{cr} [kPa]	p^{equi} [kPa]	Design var. h; R; H [mm]	Weight savings [%]
Volume	1.9	15	92.0	94.8	0.16;4.00;1.14	30
Pressure	2.9	11	96.1	96.2	0.10;2.12;0.42	46
Vol. and press.	2.3	15	93.3	95.4	0.15;3.89;1.33	27

Table 8.6: *Obtained optima depending on the constraint(s). The maximal volume change is indicated by* ΔV^{max}

required. A rib shape which is more commonly accepted is depicted in Figure 8.6b. This rib shape will be examined for the optimization of the here involved bottle. The geometry of this rib is defined by three parameters, the wall thickness h, the rib-radius R (a quart circle) and the height H. This rib geometry is easier defined than the current ribs and therefore also more robust for mesh-generation during optimization.

During the optimization the wall thickness h could vary between 0.1 mm and 0.3 mm, the height H between 0.2 mm and 5 mm and the radius R between 0.2 and 4 mm. The analytical interval volume of the bottle was kept constant during optimization. On the bottle a pressure loading has been prescribed. For each bottle design a linear calculation and an eigenvalue buckling analysis were carried out. From the linear calculation the volume pressure compliance α can be determined. The eigenvalue analysis gives the buckling pressure p^{cr} of the bottle. Consequently, the post-oxidation equilibrium pressure for a non buckled package can be determined by substitution of α in [8.5]. Multiplying α by $p^{a} - p^{cr}$ gives the maximal volume change before buckling. In Table 8.6 the results of three optimization runs, each with different constraints, are given. All optimization runs led to weight savings which outrange the previously found weight savings. Figure 8.8 illustrates the different optimum rib shapes. For completeness the volume pressure compliance α as determined by a linear FE analysis is verified with a non-linear FE analysis. The result hereof is depicted in Figure 8.9 for a bottle with a wall thickness $h = 0.16$ mm, a radius $R = 4$ mm and a height $H = 1.14$ mm (see also Figure 8.6b). From this figure it can be determined that the initial volume-pressure compliance $\alpha = 2.00$ ml kPa^{-1} while the linear analysis let to $\alpha = 1.94$ ml kPa^{-1}. The latter is considered satisfactory. Furthermore, this figure illustrates that the buckling pressure as determined with the eigenvalue analysis matches the buckling pressure as found in non-linear analysis. Finally, this figure shows that due the non-linearity in the volume-pressure relation

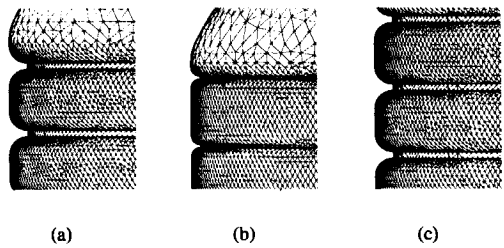

Figure 8.8: *Results of MAM optimization on a quart bottle model. (a) Optimal rib shape for a bottle with only a volume constraint. (b) Optimal rib shape for a bottle with only a pressure constraint. (c) Optimal rib shape for a bottle with a volume and a pressure constraint.*

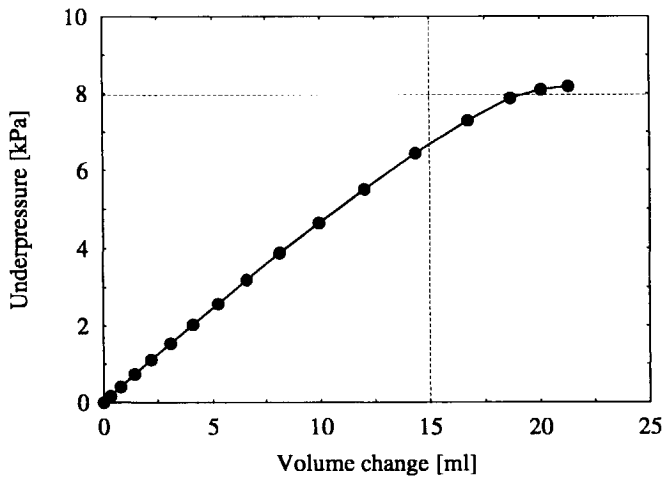

Figure 8.9: *Volume-pressure relation of a bottle ($h = 0.16$ mm, $R = 4$ mm and $H = 1.14$ mm) determined by a non-linear FE analysis. The horizontal line indicates the eigenvalue buckling underpressure of the same bottle. The vertical line indicates the predicted linearized volume change based on $\alpha(p^a - p^{cr})$. This figure clearly indicates, by means of a non-linear calculation, that this bottle is able to 'absorb' more than the predicted linearized volume change.*

the bottle is able to compensate for more than 15 ml of volume change, which is the predicted amount of volume absorption based on $\alpha(p^a - p^{cr})$. The latter indicates that an optimization which uses the non-linear volume-pressure relation might still lead to further weight reduction.

8.6 Conclusions

The following conclusions can be formulated:

- an optimal bottle should at least be able to resist the post-oxidation equilibrium pressure;
- ideally, the volumetric deformation of the bottle due to under-pressure before buckling occurs should be as large as the initial gas volume;
- during optimization of the described package simplified models for oxidation of the contents and behavior of the structure can be used;
- material savings up to 23% can be obtained by reducing the wall thickness of the current bottle without loosing performance;
- material savings up to 18% can be obtained while also satisfying the requirement that the complete initial gas volume should be compensated for; these savings are not optimal and determined by optimization of a single rib;
- optimization of the structure through optimizing a single rib of the bottle gains understanding in the direction of the optimal bottle geometry but does not lead to an optimal bottle;
- optimization of the whole bottle can lead to material savings up to 46%;
- the linearized predicted volume change is smaller than the volume change as predicted in non-linear analysis;
- taking into account the non-linearity in the volume-pressure relation might in the present setting lead to even further weight savings;
- the above mentioned potential material savings are based on geometrically perfect structures; imperfections might influence hereon (due to the linearized approach as used here this effect is expected to have only a small influence);
- the above mentioned material savings assume that the filled compression strength of the bottle is sufficient. This compression strength is also assumed to outrange the empty compression strength significantly.

Based on: R. van Dijk and F. van Keulen, Optimization of plastic packaging, Proceedings of the First ASMO UK/ISSMO Conference on Engineering Design Optimization, July 8–9, 1999, Ilkley, UK.

Appendix A
Optimization of Plastic Packaging

Mass reduction of plastic packaging requires advanced design approaches. Mass reduction of plastic packaging in most cases influences on the mechanical behavior of the structure. This mechanical behavior involves, top load performance, impact resistance, *etc.*. This chapter describes the optimization of a round tub (which can contain 500 gr. product) using design sensitivity analysis in combination with multi-point approximation methods. For verification of the simulated results several experiments were carried out. Design sensitivity analysis has been used to identify the most influential design variables at low computational costs. Further optimization of the tub with respect to top load performance and material usage led to an alternative design for which the initial top load was maintained but at a mass reduction of approximately 23%.

Introduction

Mass reduction of plastic packaging requires advanced design approaches. One of such an approach is automated optimization. Optimization is concerned with achieving the best outcome of a given objective while satisfying certain restrictions [30].

The present study investigates the potential mass, and here especially costs, savings that can be obtained by optimization of a tub for 500 gr. product. Like in most industrial settings the formulation of the optimization problem is complex. One of the reasons is the fact that the required quality has not previously been defined and/or quantified. Other reasons involve capriciousness of the design appreciation and other not easily definable human factors of the customer and marketeer. Furthermore, if an optimization problem was previously defined then external influences, *e.g.* governmental regulations, that were not included in the problem description might currently have a significant influence. The latter might make re-optimization necessary.

Any changes in the design of an existing configuration will most likely result in additional costs for implementation. In many industrial applications the objective is therefore defined by expenditure and income. For the present application this means that any modifications to the tub should result in cost savings that outrange the investments for the involved modifications and implementation.

Contrary, to the easiness of defining the objective is defining the constraints of the problem. In many cases the constraints are based on common practice, which is based on current and previous experience with the product, here a tub. In the present application the tub will be optimized with respect to its mass. The only constraint is the critical top load, which should not decrease. The selection of the critical top load as constraint is based on common practice and driven by the ease of its quantification and experimental verification. The selected minimum value of the critical top load is thus equal to the current critical top load which functions satisfactory. However, a thorough investigation of the actually required top load based on, *e.g.*, its loading and handling conditions has not been carried out and might offer even more savings.

In the present study it is not investigated if a modification of the package has a negative influence on other aspects which were not yet taken into account during the optimization, *e.g.* impact resistance, handling conditions, marketing aspects, *etc.*. The latter, however, do determine whether the proposed

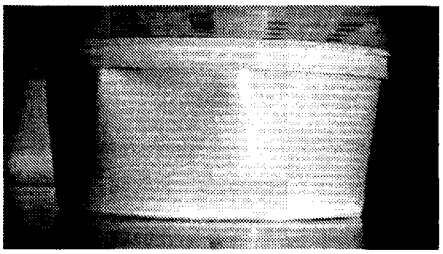

Figure A-1: *Deformation of the tub during top load testing.*

design changes can actually be implemented in order to realize cost savings. The complexity in taking these additional aspects into account is the difficulty to measure or quantify certain aspects or due the heuristic and unpredictable behavior of people. The results of the present study should therefore be interpreted carefully.

After having defined objective and constraints, the design variables should be identified. Since, only small geometric changes are allowed this did not give rise to serious problems. If, however, marketing aspects would also be part of the constraints and large geometric changes would be allowed, then the problem becomes almost immediately uncontrollable.

This chapter tries, in a systematic way, using optimization techniques, to verify and quantify a potential option to reduce the costs of the tub without loss of quality. Structural optimization techniques are not yet common tools in industry, where still most design decisions are based on experience. Therefore, the effectiveness of some of these techniques will be demonstrated carefully.

In chronological order the chapter describes: experimentally obtained results, (parametric) design of the tub, sensitivity analyses, optimization, multi-point approximation method and conclusions.

Experimental results

The experiments that were conducted on the tub involved top load and wall distribution measurements. The results from both experiments will be presented briefly. For the experiments only a limited amount of samples was available. The thermo-formed tubs are made out of PP (Poly-Propylene, density 0.92 gr ml^{-1}). The mass of the tub is 13.0 gr.

Top load testing

Several tubs have been tested on a Zwick 1445 compression tester. During top load testing the tub was compressed between two horizontal platen with a speed of 100 mm min^{-1}. The deformed shape of a compressed tub has been depicted in Figure A-1. The critical top load is defined as the maximum load that can be applied on the empty tub. During top load testing care was taken that enclosed gas could escape in order to prevent an internal over-pressure. The deformed, buckled, shape of the tub is symmetric with respect to two perpendicular planes of symmetry. These planes of symmetry intersect at the axes of axial symmetry of the undeformed configuration. The top load has been evaluated for tubs without lid. Three tubs were subjected to top load testing which resulted in top loads of 263, 265 and 272 N.

Wall thickness distribution

From all tubs that were subjected to top load testing the wall thickness distribution prior to testing was analyzed. The wall thickness distribution measurements will not be further discussed. The measurements led to the conclusion that the wall thickness can be considered axial-symmetric. Only slight variations

Location	X-coord.	Y-coord.
A	63.5	60.7
B	62.25549	64
C	60.35098	64
D	$\tilde{X}_D$	$\tilde{Y}_D$
E	$\tilde{X}_E$	Y_E
F	X_F	12.20188
G	49.63115	0
H	26.3	0
I	22.8359	2
J	0	2

Table A-1: *Coordinates of the points A until J. Independent variables have been denoted by a tilde. Remaining variables are either constant or dependent design variables.*

(up to 10%) were found at a few places. Thickness variations in the rim of the tub have been neglected since no significant deformations occur in this area during compression.

For manufacturing purposes a certain minimum wall thickness for the rim of the tub is desired. The thickness of the base, *i.e.* segment E-F-G-H as depicted in Figure A-2, is variable but constant for the whole segment. It will be validated that by reducing this thickness significant material savings can be obtained in combination with small geometric modifications. The initial value of this variable wall thickness is 0.4 mm. Since it of no interest to use more material for the tub this should also be the upper boundary of the wall thickness as soon as other geometric changes have no significant influence on the mass. However, this chapter investigates a slightly wider range. The lower boundary for the wall thickness is taken as 0.2 mm due to manufacturing constraints. The wall thickness in the areas A-E and H-I is 0.5 mm, in the area I-J the wall thickness is 0.6 mm. These assumptions are in line with experimentally found values. However, if the mass of the tub is calculated on the basis of the experimentally derived wall thickness distribution, the mass is slightly over-predicted, being 13.46 gr. calculated while 13 gr. experimentally. The latter can be explained by a bias in wall-thickness measurements for the areas, A-E and H-I. This bias has been neglected based on the absence of significant deformation in these areas and because these areas are kept constant during optimization.

Parametric model of the tub

Optimization requires certain possibilities to change the structure. The present section describes the parametric model of the tub and indentifies the areas where geometric or thickness modifications can be applied. In Figure A-2 the model of the tub is depicted. In Table A-1 and A-2 the geometry of the tub has been described on the hand of the locations as indicated in Figure A-2. The variables overlined by a tilde are the primary design variables. The other variables are dependent and can be derived from these primary design variables. The dependency between the design variables is described in Table A-3. The initial values are given in Table A-4.

Simulations

Because of symmetry in deformed as well as undeformed configuration only a quarter model of the tub was modeled using Finite Elements [6]. Note, that this implies that also a modified design is assumed to behave symmetrically. This assumption should be checked afterwards.

The quarter tub was modeled using triangular shell elements [9, 72, 73]. The material has been assumed isotropic with a Young's modulus of 1000 MPa (based on experiments) and a Poisson's ratio of 0.35. Along the inner top circumference of the tub a load in vertical direction was prescribed. The

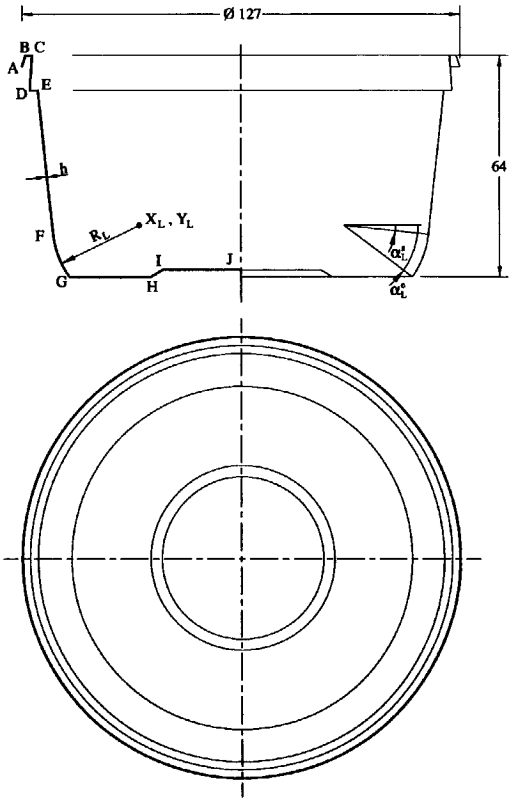

Figure A-2: *Parametric model of the tub.*

Location	Symbol
Bottom radius, centre point, x-coord.	X_L
Bottom radius, centre point, y-coord.	Y_L
Bottom radius, start angle	α_L^s
Bottom radius, end angle	α_L^e
Bottom radius	$\tilde{R}_L$
Thickness	$\tilde{h}$

Table A-2: *Coordinates of the bottom radius and value of the wall thickness. From all the listed variables only the thickness $\tilde{h}$ and the radius $\tilde{R}_L$ are primary design variables.*

displacements in horizontal direction were prescribed for the inner top circumference. Symmetry conditions were applied to the edges of symmetry. The critical top load has been determined with a linearized buckling analysis.

The simulation using a quarter model of the tub resulted in a critical top load of 272 N while the average experimental critical top load is 267 N which is a difference of 2%. Further investigation to which factors cause this difference have not been conducted. The results of these simulations have been used as a basis for sensitivity analyses.

$$
\begin{aligned}
Y_{CD} &= Y_C - \tilde{Y}_D = 64 - \tilde{Y}_D \\
&[= 10] \\
Y_{EF} &= \tilde{Y}_D - 12.20188 \\
&[= 41.79812] \\
X_L &= X_F - \cos(\arctan((\tilde{X}_E - X_F)/Y_{EF})) \\
&[= 29.49379] \\
\alpha_L^s &= (3\pi)/2 + \arccos(Y_L/\tilde{R}_L) \\
&[= 5.648898] \\
\alpha_L^e &= 2\pi - \arctan((X_E - X_F)/Y_{EF}) \\
&[= 6.178466] \\
X_G &= X_L + R_L \sin(\alpha_L^s - (3\pi)/2) \\
&[= 49.63115]
\end{aligned}
$$

Table A-3: *The dependencies of the design variables. The value between square brackets indicate the initial value.*

Primary des. variable	Initial value [mm]
$\tilde{X}_D$	= 61.05
$\tilde{Y}_D$	= 54
$\tilde{X}_E$	= 58.75
$\tilde{R}_L$	= 25
$\tilde{h}$	= 0.4

Table A-4: *The initial values of the design variables.*

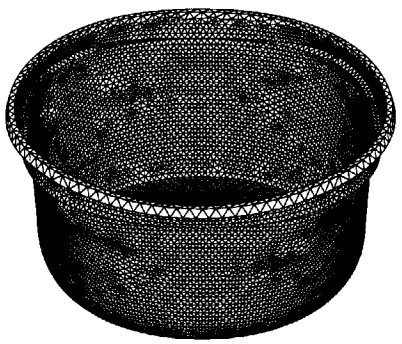

Figure A-3: *Buckling mode of the initial tub. Note that only a quarter of the tub was modeled.*

Sensitivity analysis

For completeness a description of the calculation of design sensitivities in a finite element context is given. This description is based on the semi-analytical method and gives industrial readers a brief overview of the basic idea. In this chapter the refined semi-analytical [74, 75] method has been used for the tub. Details of the refined semi-analytical method have been omitted in this chapter.

As shown in the previous section the finite element method can be very useful in analyzing or predicting the behavior of a structure. During a general linearized pre-buckling finite element calculation we solve the equation [74]

$$\mathbf{Ku} = \mathbf{f}, \tag{A-1}$$

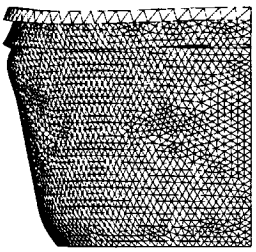

Figure A-4: *Buckling mode of the initial tub.*

where $\mathbf{K}$, $\mathbf{u}$ and $\mathbf{f}$ are the stiffness matrix, the nodal degrees of freedom and the load vector, respectively. In order to determine the linearized buckling load which in the previous section was denoted by the top load of the structure, we have to solve the eigenvalue problem

$$(\mathbf{K} + \lambda\mathbf{G})\,\mathbf{v} = \mathbf{0}, \tag{A-2}$$

where $\mathbf{G}$, $\mathbf{v}$ and λ denote the geometrical stiffness matrix, the buckling mode and the factor to scale the applied load. Differentiation of (A-2) with respect to a design variable ι gives

$$(\mathbf{K} + \lambda\mathbf{G})\,\mathbf{v}' + (\mathbf{K}' + \lambda\mathbf{G}')\,\mathbf{v} + \lambda'\mathbf{G}\mathbf{v} = \mathbf{0}, \tag{A-3}$$

where a prime refers to differentiation with respect to ι. If the focus is on the design sensitivities for the load factor λ rather than for $\mathbf{v}$, then (A-3) can be more conveniently expressed as

$$\lambda' = -\frac{\mathbf{v}^T\mathbf{K}'\mathbf{v} + \lambda\mathbf{v}^T\mathbf{G}'\mathbf{v}}{\mathbf{v}^T\mathbf{G}\mathbf{v}}. \tag{A-4}$$

One can say that the design sensitivities indicate the sensitivity of the structure to a certain change of the design. During the computation of the design sensitivities the original design, *e.g.* the geometry, of the structure will be slightly distorted by perturbing the corresponding design variable and all its dependencies. The design sensitivity that follows, analyzes the structures sensitivity with respect to small changes of this variable. Thus, a high value of a design sensitivity implies that the corresponding variable has a significant influence on the performance of the structure, whereas a very small value implies that the corresponding design variable has no significant influence.

In the present chapter the design sensitivities for the primary design variables of the involved tub have been calculated and are presented in Table A-5 and Table A-6. The design sensitivity has also been indicated in a logarithmic manner in both tables. The logarithmic sensitivity indicates how the design variable influences on the performance, a logarithmic design sensitivity of 2 means a quadratic dependence between the design variable and the response function, *e.g.* mass. A linear dependence is thus indicated by a design sensitivity 1. Note that the design sensitivity is a reflection of a local situation, *i.e.* if a design is changed the design sensitivities may also change.

The range in which the first 3 variables, $\tilde{X}_D$, $\tilde{Y}_D$ and $\tilde{X}_E$, can be varied is in the order of approximately ± 2 mm. The variable $\tilde{R}_L$ can be changed with ± 10 mm and the wall thickness $\tilde{h}$ can be varied within the range of 0.2 mm to 0.475 mm. The ranges in which these variables can change are listed in percentages in the tables. Combination of the logarithmic design sensitivities and the relative changes of the design variables allows to provide a rough estimate of the potential influence of a particular design variable. For that purpose, suppose we have a response function f and a design variable ι. Their nominal values are given by f_0 and ι_0, respectively. The maximum relative change in the response function of f, caused by a change of s can now be estimated using

$$\frac{\Delta f}{f_0} \approx \frac{\iota_0}{f_0}\frac{df}{d\iota}\frac{\Delta\iota}{\iota_0} = \frac{d_l f}{d_l \iota}\Delta\zeta,$$

Design var.	$\frac{dF^c}{dt}$	$\frac{d_l F^c}{d_l t}$	$\Delta\zeta$ [%]	$\frac{\Delta F^c}{F_0^c}$ [%]
$\tilde{X}_D$	-15.8	-14.1	±3	±42
$\tilde{Y}_D$	2.6	2.1	±3	±6
$\tilde{X}_E$	29.2	25.2	±3	±76
$\tilde{R}_L$	0.28	0.10	±40	±4
$\tilde{h}$	204.6	1.2	-50,+70	-60,+84

Table A-5: *Design sensitivities, dF^c/dt, of the initial tub configuration for the buckling load. The critical top load and logarithmic design sensitivity are indicated by F^c and $\frac{d_l F^c}{d_l t}$, respectively. The percentage change of the design variable and the corresponding percentage change in buckling load is denoted by $\Delta\zeta$ and $\frac{\Delta F^c}{F_0^c}$, respectively.*

Design var.	$\frac{dM}{dt}$	$\frac{d_l M}{d_l t}$	$\Delta\zeta$ [%]	$\frac{\Delta M}{M_0}$ [%]
$\tilde{X}_D$	55.3	0.92	±3	±3
$\tilde{Y}_D$	-11.3	-0.17	±3	±1
$\tilde{X}_E$	19.8	0.32	±3	±1
$\tilde{R}_L$	3.3	0.023	±40	±1
$\tilde{h}$	6217	0.68	-50,+70	-34,+48

Table A-6: *Design sensitivities of the initial tub configuration for the mass of the structure. The mass has been indicated by M. Design sensitivities and logarithmic design sensitivities have been indicated by $\frac{dM}{dt}$ and by $\frac{d_l M}{d_l t}$, respectively.*

with $\Delta\zeta = \Delta t/t_0$. The estimates for the percentual change of the critical top load and the mass are given in Table A-5 and A-6, respectively.

With this information it can now be concluded that the variables $\tilde{X}_D$, $\tilde{X}_E$ and the wall thickness $\tilde{h}$ have the most significant influence on the critical top load of the tub.

In Table A-6 the sensitivity for the mass of the tub is listed. The last column clearly indicates that a potential mass reduction can only be achieved by a reduction of the wall thickness $\tilde{h}$. The influence on tub mass of other design variables can be neglected.

The value $\tilde{X}_E$-$\tilde{X}_D$ defines the rim depth which in the sequel will be denoted by $\tilde{r}$. During sensitivity analyses the influence of $\tilde{X}_E$ and $\tilde{X}_D$ on the critical top load was simulated separately. Therefore a high sensitivity for both of these coordinates reconfirms the importance of the rim depth. In the sequel the problem is simplified to 2 dimensions which are the rim depth and the wall thickness. The rim depth is from now on defined as $\tilde{r}$=61.05-$\tilde{X}_E$, thus $\tilde{X}_D$ remains constant. In the sequel overlining of the primary design variables by a tilde will be omitted.

Optimization problem

In the previous section we found that the top load of the tub depends to a large extent on the wall thickness and the rim depth. Furthermore, it was concluded that a mass change of the tub is mainly determined by a change in wall thickness and that changes of other design variables have a negligible influence on the mass. It is thus obvious to examine these two variables further and to try to find an optimal combination of these two variables.

Between industrialists and scientist there is a different perception about the meaning of optimization. Many industrialist name the rational process, *e.g.* systematic, experience wise or either trial and error, which leads to an improved design, optimization. For scientists working in structural optimization, optimization means a systematic plan that leads to a maximum of efficiency. This chapter describes a

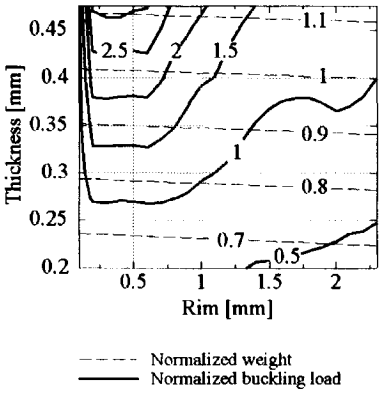

Figure A-5: *Evaluation of the design space for the design variables corresponding to the rim depth and wall thickness distribution. The mass and buckling load have been normalized with their initial values. The optimum is given by a rim of 0.7 mm and a thickness of 0.275 mm.*

systematic as well as a more straightforward method to find the optimum combination for the mentioned variables.

First, the optimization problem will be formulated. In case it is desirable to minimize the mass of the tub without loss in top load performance then the optimization problem can be defined as

$$\begin{aligned} &\textbf{minimize} \quad M(h,r) \\ &\textbf{such that} \quad F^c(h,r) \geq F^c(h=0.4, r=2.3), \end{aligned} \tag{A-5}$$

where $F^c(h,r)$ is the top load performance of the tub and $M(h,r)$ the mass of the tub. The initial values of h and r are 0.4 mm and 2.3 mm, respectively, and result in a mass of 13.46 gr. and a critical top load of 272 N.

The more straightforward method of finding the optimum solution for the combination of both variables is scanning the design space. Since the current problem is a two dimensional problem this scanning does not impose significant problems and gives a clear and complete picture of the problem. The optimization problem as described in (A-5) has been evaluated for $r = 0.1, 0.2, \ldots, 2.3$ and $h = 0.2, 0.225, \ldots, 0.475$, which thus required 276 computations. It is obvious that this is not an efficient way to find to solve the mentioned optimization problem. It is however a reliable method and gives a clear understanding about the influence of the variables on the mass and critical top load performance of the tub. The results hereof have been depicted in Figure A-5 where the buckling load has been normalized according $F^c(h,r)/F^c(0.4;2.3)$, and should be equal or larger than 1. The mass has been normalized as $M(h,r)/M(0.4;2.3)$. From this figure also the optimum can be derived at $r = 0.7$ and $h = 0.275$, corresponding to a buckling load of 284 N and a mass of 10.4 gr. The material savings belonging to this wall thickness reduction and geometry change are approximately 23%. Due to the stepwise approach as used during the scanning of the design space the buckling load is slightly above its constraint value of 272 N. Creating a finer grid, or using additional optimization techniques as discussed in the next section could solve this. Figure A-5 clearly indicates an increasing top load performance for increasing wall thickness and decreasing rim depth. The reduction of wall thickness and rim depth do influence the buckling mode of the structure. The buckling mode belonging to a reduced rim depth is depicted in Figure A-6. Figure A-5 also shows that a complete removal of the rim is not satisfactory since it reduces the buckling load significantly. Note, that the validity of the used shell theory is a point of discussion near the optimum solution. Since here, rim depth divided by wall thickness is approximately 1. It is assumed that erosion of the optimum [62] does not influence on the obtained optimum. However, rigorous checks have to be made.

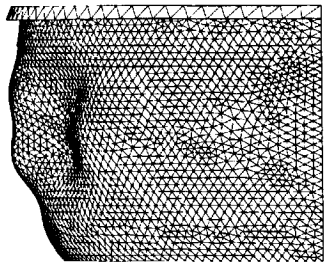

Figure A-6: *Buckling mode of the tub with reduced wall thickness and rim depth.*

It should however be mentioned that the rim of the tub cannot simply be reduced since it also gives the tub a de-stacking capability, *i.e.* thus when the rim depth will be reduced the de-stacking facility should be taken over by other design features in the tub, *e.g.* de-stacking notches in the bottom. For completeness the reader is once more reminded that top load is only one requirement and that is has not been examined if de-stacking force, impact resistance, shelf life *etc.* have been affected by the new geometry.

Multi-point approximations

As described in the previous section, scanning of the design space required 276 function evaluations. Most likely the optimum within the design space could also have been found using significantly less function evaluations. The reliability of the solution is however smaller since it is not known if the obtained solution is a local optimum and how the top load depends on the design variables for not evaluated design variable values. Thus from an industrial point of view it is unsatisfactory to implement the design changes solely based on the results of an automated optimization using for example the Multi-point Approximation Method (MAM) [76]. The costs of mapping the design space for the described problem stand in no relation to the costs that might evolve from law suits with respect to product reliability and should therefore always be considered. The latter might change as soon as more variables are involved and a fine scanning of the design space becomes very expensive or even impossible.

As mentioned, one of the automated optimization techniques is MAM. The latter replaces the actual optimization problem by a sequence of approximate ones, each having a limited range of applicability. Therefore, it carries out in each iteration function evaluations at several points in the space of design variables. Based on these function values, mid-range approximations are constructed, that are defined as relatively simple functions of the design variables and a vector of tuning parameters to be found using a weighted least-squares method. Standard mathematical programming routines solve the optimization problem given in terms of these approximations and intermediate move limits easily. This solution, a so called sub-optimum point, is used as a starting point for the next iteration step until convergence is found. Based on a number of indicators [76], for example quality of the approximations, new intermediate move limits are defined or the process is terminated. The mathematical programming problem to be solved in each iteration is computational inexpensive as it is formulated in terms of relatively simple approximation functions. The advantage of MAM is threefold. Firstly, the mathematical programming to be solved in each iteration is computational inexpensive as it is formulated in term of relatively simple approximation functions. Secondly, the method can be used whether or not design sensitivities are available. Finally, the MAM is relatively insensitive to (numerical) noise in response evaluations since noise can be averaged out using a weighted least squares method to determine the approximate functions. For more information about the present MAM, the reader is referred to [63, 76].

For the MAM applied to the tub the rim depth r ranged from 0.1 mm to 5.05 mm and the initial move

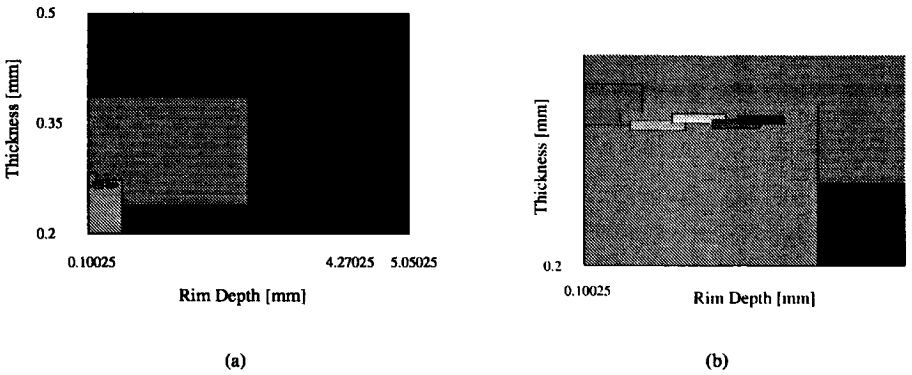

Figure A-7: *Regions were the design variables have been evaluated during the MAM. Due to the fact that the problem is only 2 dimensional, visualization for all design variables is possible. a) Movement of subregions in the design space. b) Movement of subregions in the design space during the last iterations. Magnified view of Figure A-7a.*

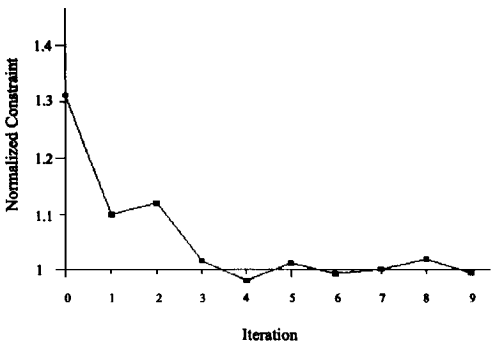

Figure A-8: *History of the normalized buckling constraint.*

limits were 0.1 mm and 4.27 mm. The wall thickness h ranged from 0.2 mm to 0.5 mm and the initial move limits were 0.35 mm and 0.5 mm. The solution converged within 9 iterations. After four iterations the optimum was already indicated, as depicted in Figure A-8 and Figure A-9. The remaining iterations had no further significant influence on the obtained mass savings. The converged optimum configuration for the tub was found at a rim depth of 0.45 mm and at a wall thickness 0.267 mm. The mass of the tub for the optimal solution is M(0.267;0.45)=10.4 gr. which is similar to the optimum found graphically in the previous section were a mapping of the design space was carried out.

Discussion

Many packages are being produced and disposed of every year. It is therefore of great importance to minimize the material required for these packages from a cost as well as environmental perspective. Current computational techniques give the possibility to analyze a structure prior to manufacturing. This

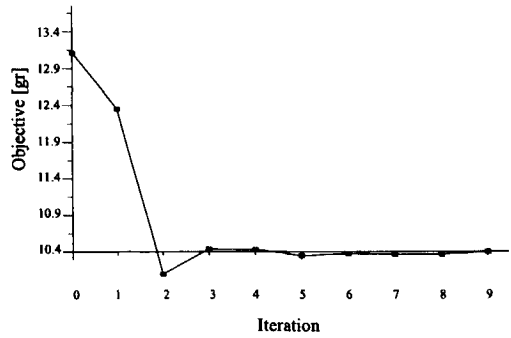

Figure A-9: *History of the objective function.*

also gives the opportunity to optimize the structure prior to manufacturing. During such an optimization study there will be a number of requirements, *e.g.*, costs of manufacturing, material costs, governmental regulations (environmental tax), performance during manufacturing, performance at the customer, *etc.*. The costs involved in packaging can be very large due to very large volumes. When a new design is proposed it is therefore required that the cost savings generated by a new concept outrange the required investments necessary for implementation. Very important is also the reliability of the new design. If in a later stage it is proved that the new design functions unsatisfactory or caused collateral damage then this might result in large damage claims and a damaged consumer image. The latter should be taken into account for each optimization study that is carried out.

In this chapter a round tub for 500 gr. margarine has been optimized with respect to its costs and top load performance (required during stacking of the tub). Firstly, some experimental work was carried out on actual tubs. Secondly, the experiments were simulated and design sensitivity analyses were carried out. The design sensitivity analyses indicated that the two variables rim depth and wall thickness have a significant influence on the critical top load and mass of the tub, respectively.

These two variables were then further examined by two methods. The first method scans the design space of the two variables while a second optimization method, MAM, uses a more efficient approach. This resulted in a design change of the tub such that the mass of the tub reduced by 23%. Note, that this reduction of mass can only be implemented if other aspects are not influenced by the geometry changes.

Discussion

A package is subject to different simultaneous load cases during its way to the consumer. These load cases have a mechanical (deformation), physical (solubility and permeability) and chemical (oxidation) nature. Here, these processes have been discussed for a particular plastic bottle. For the involved bottle two main mechanical load cases have been examined: compression strength and vacuum resistance. The compression strength of the involved package is required for stacking and transportation while vacuum resistance is required to prevent paneling of bottles. Paneling is created by a combination of gases dissolving into the fluid and by oxidation of the contents.

On a first impression these two load cases seem conflicting. However, here compression strength and vacuum resistance can be examined independently. The latter is due to the fact that here the filled compression strength is more than large enough to prevent failure during stacking. The large filled compression strength is caused by a possibility to build up internal gas pressure during vertical compression and does not depend on the wall thickness of the bottle. This possibility is created by the harmonica like deformation of the bottle. The paneling prevention of the bottle benefits in two ways from the harmonica shape. Firstly, such geometries have a high vacuum resistance and secondly such geometries can compensated for under-pressure creation by volumetric deformation. Consequently, replacing the empty compression strength requirements with requirements with respect to the bottle closure opens opportunities towards significant material savings.

The physical processes involved are dissolving of gases into the fluid and permeation of gases through the bottle wall. The solubility effects have a large influence on the internal pressure during paneling as well as during compression of filled bottles. Permeability effects, however, can be neglected in the present setting. The latter might change if material properties will significantly change or for packages with a much smaller wall thickness, *e.g.* films and pouches. The most dominant chemical process involved is oxidation of the contents. Generally, all initial present oxygen is consumed far before expiring of the shelf life. Therefore, during most of its life time the behavior of the package is only determined by the nitrogen gas and the mechanical behavior of the structure. The situation after disappearing of all oxygen is static, since time dependencies in the mechanical behavior have not been taken into account. Consequently, the mechanical behavior of the structure has been simplified to a piece-wise linear volume pressure relation by introducing the volume-pressure compliance which indicates the amount of volume change for a certain pressure change. The latter created the opportunity to predict the volumetric deformation and the equilibrium pressure easily.

The previous mentioned simplifications let to a well-defined optimization problem where the objective function is the weight of the package. Like for most practical optimization problems the constraint definition is not unique. In the present thesis different constraint formulations have been evaluated each leading to a different objective value after optimization. For the optimization use has been made of the Multipoint Approximation Method. This resulted in significant weight savings and clearly illustrates the strength of optimization techniques. Additionally, any new design change can be followed by a new optimization run which automatically updates design details to prevent excessive material usage.

The optimization as described in this thesis is not limited to the bottle described here but is also applicable to cases where similar processes are involved. It might be that for other applications some simplifications as used here can not be justified, the general approach however remains similar. One aspect that has not thoroughly been examined in the present thesis is the time-dependent material behavior. This effect might be of significant importance for other applications than the one described here.

Summary

The present thesis describes the physical (solubility and permeability), the mechanical (structural behavior) and the chemical (oxidation) processes which are very often relevant to a thin-walled package. Initially a study has been carried out which identified the relevant requirements for the involved package, here being a plastic bottle for edible oil. These requirements are based on experimental work and consist of empty and filled compression testing and vacuum resistance testing. Subsequently, these experiments have been modeled with Finite Element Analysis (FEA). The latter required several special numerical adaptations for the deformation induced internal pressure and solubility effects which play a significant role during vertical compression of filled bottles.

Each of the processes as mentioned above have been examined by many researchers, however a model which combines structural behavior, permeability and solubility effects and oxidation of the contents can hardly be found in literature. If it is desired to optimize a complete structure then it is however necessary to take all these processes into account. In the present thesis such a model is described, moreover the model is general applicable and can be used to determine the behavior of the package and to a certain extent the behavior of the contents as a function of time. The mechanical behavior of the package required for this can be determined in a quasi-static way with the help of FEA. The amount of dissolved gas is determined using Henry's law. The influence of the permeability effect is determined by the gas pressures, while the oxidation is determined by the oxygen gas pressure and an initial oxidation speed. Accurate oxidation data is however scarce. If such accurate data is required one could set up experiments for this, if not approximate data may be used. An explicit integration scheme has been used to determine the behavior of the package as a function of time.

Applying this model to the round bottle indicated that permeability effects could be neglected in the present setting. Moreover, it has been indicated that the mechanical behavior of the structure can be simplified to a piece-wise linear volume pressure relation. This simplification originates from the fact that all initial present oxygen reacts in a relatively short period of time with the contents. Hereafter the behavior of the structure is fully determined by the nitrogen pressure. Since time dependent behavior of the package has not been taken into account, the situation after disappearing of all oxygen is investigated as a static problem. The piece-wise linear behavior of the involved structure can easily be identified with a linear FE analysis and a buckling FE analysis. The latter has been exploited during optimization of the involved structure.

During analysis of the optimization problem, sensitivity analysis has been used to identify the most important design variables of the structure. Hereafter, an optimal design was looked for, making use of the Multipoint-Approximation Method (MAM). For the present bottle the optimization led to a bottle where weight savings up to 46% can be achieved. The origin of these weight savings comes however not directly from the optimization analysis itself. Most potential weight savings have been 'created' during the definition of the constraints. In common practice the constraints are mostly based on history or experience while in this thesis the constraints are derived from buckling requirements.

Samenvatting

In dit proefschrift worden de fysische (oplosbaarheid en permeabiliteit), de mechanische (het constructief gedrag) en de chemische processen beschreven welke vaak relevant zijn voor dunwandige verpakkingen. In eerste instantie is er een studie gedaan naar de relevantie van de verschillende eisen die momenteel gesteld worden aan de verpakking, hier een plastic fles voor eetbare oliën. Deze eisen zijn gebaseerd op experimentele resultaten zijnde: compressietesten op lege en op gevulde flessen en vacuümproeven. Vervolgens zijn bovenstaande tests gesimuleerd met behulp van de eindige-elementenmethode. Het simuleren van de door vervorming geïnduceerde druk in de fles en de oplosbaarheidseffecten vereiste verscheidene speciale numerieke wijzigingen in de analyse code.

Vele onderzoekers hebben de boven genoemde processen reeds bestudeerd, echter een model welke het mechanisch gedrag, de oplosbaarheid, de permeabiliteit en de oxidatie van de inhoud combineert is niet eerder gerapporteerd. Indien het gewenst is een dergelijke constructie te optimaliseren dan dienen al deze aspecten in overweging genomen te worden. In dit proefschrift wordt dit algemeen toepasbare model beschreven en toegepast om het tijdsafhankelijke gedrag van de verpakking en tot op zekere hoogte van de inhoud te bepalen. Het mechanische gedrag van de verpakking dat hiervoor benodigd is kan op een quasi-statische manier benaderd worden met behulp van de eindige-elementenmethode. De hoeveelheid opgelost gas wordt bepaald met de wet van Henry. De invloed van permeabiliteit wordt bepaald door de gas drukken terwijl de oxidatie afhangt van de zuurstofdruk en de initiële oxidatiesnelheid. Nauwkeurige data met betrekking tot oxidatie is echter schaars. Indien dergelijke data gewenst is dan dient men hiertoe experimenten uit te voeren. Als dit niet het geval is dan kan gebruik worden gemaakt van benaderende gegevens. Een expliciete integratie methode is gebruikt om het tijdsafhankelijke gedrag van de verpakking te bepalen.

Toepassing van dit model op de ronde fles leidde tot de conclusie dat permeabiliteitseffecten hier verwaarloosd kunnen worden. Bovendien is aangetoond dat het mechanische gedrag van deze constructie benaderd kan worden met een gedeelde lineaire volume-druk afhankelijkheid. Deze benadering komt voort uit het feit dat reeds in een korte periode alle initieel aanwezige zuurstof reageert met de inhoud. Hierna wordt het gedrag van de structuur volledig bepaald door de stikstof-druk. Sinds tijdsafhankelijk materiaal gedrag van de verpakking niet in het model is opgenomen kan deze situatie als statisch beschouwd worden. Deze stuksgewijze lineaire volume-druk relatie van de verpakking kan reeds voor de vervaardiging hiervan eenvoudig afgeleid worden met behulp van de eindige elementen methode. Tijdens optimalisatie is hiervan uitvoerig gebruikt gemaakt.

Met de formulering van het optimalisatie-probleem is er gebruikt gemaakt van gevoeligheidsanalyses voor de identificatie van de relevante ontwerpvariabelen. Hierna is er getracht een optimaal ontwerp te vinden met behulp van de 'Mutipoint-Approximation' Methode (MAM). Voor de hier genoemde fles leidde dit tot een gewicht besparing van maximaal 46%. De oorsprong van deze gewicht besparing is vooral te wijten aan de definitie van de randvoorwaarden. Het is in de praktijk gebruikelijk deze randvoorwaarden of eisen te baseren op historie en ervaring. Echter in dit proefschrift zijn de randvoorwaarden gebaseerd op echte relevante 'knik'-eisen.

Acknowledgements

First of all I would like to thank Unilever Research in Vlaardingen, The Netherlands, for their support. It has been a great experience to work with Unilever in many ways. Special thanks I want to give to Duilio Sgorbani, who gave me a lot of support, and Wim Agterof, with whom I had fruitful discussions about the adopted models for gas-fluid interaction. I hope the results of the presented work will be used in applications and will be a basis for further research.

Furthermore, I would like to thank Fred van Keulen for his supervision and extensive guidance in the world of engineering mechanics. We had a lot of discussions about 'fundamental-science' and 'applied-science', which always let to the conclusion that they need to coexist.

I thank my family for their continuous support. Having family in and from a country which is in many ways very different from the Netherlands enriched my life significantly. I hope the latter is true visa-versa.

Ronald van Dijk,

July 2001

Curriculum Vitae

The author, was born on Januari 6, 1971 in Maassluis, the Netherlands. The examination for Atheneum B at Develsteincollege was passed in 1989. In the same year he subscribed to the education at the Faculty of Industrial Design Engineering where together with colleague students he organised the workshop 'Quality of Life' in 1993. In 1994 he spend 3 months in Nikolaev, Ukraine on a student exchange program in order to obtain practical and personal experience.

His graduation work was done in 1995 at the Food Packaging Unit of Unilever Research, Vlaardingen, The Netherlands and involved the optimization of plastic bottles for edible oil. His graduation was followed by a temporary contract at Unilever Research.

Inspired by the scientific drive of Fred van Keulen he felt the need of a more scientific approach to packaging. Therefore in 1996, he started a PhD study entitled 'The Optimization of Plastic Packaging' which was fully sponsored by Unilever Research. During this period he had the pleasurable experience to be able to practice his scientific knowledge and to audit his research at several industrial clients of Unilever.

At November 1-st 2000, he joined MSC.Software in Gouda, The Netherlands.

Other publications, which have not been used in this thesis, of the author are:

- A Finite Rotation Shell Element Taking into account Pneumatic Effects, R. van Dijk and F. van Keulen, Ices'98 Conference, 6–9 Oct. 1998, Atlanta, USA;
- Accurate design sensitivities for closed-filled structures, R. van Dijk, H. de Boer and F. van Keulen, 3-rd World Congress on Structural and Multidisciplinary Optimization, 17–21 May, 1999, Niagara Falls/Amherst, New York;
- Influence of Material Properties of a Tub on its Top Load Strength, R. van Dijk, J. Hunter and E. Deerenberg, Packaging Technology and Science, [page 193-202], Vol.12(4), 1999;

Bibliography

[1] M.A. Akgün, J.H. Garcelon, and R.T. Haftka. Fast exact static structural reanalysis in relation to the Sherman-Morrison-Woodbury equation. *In proceedings:ISSMO/NASA/AIAA First Internet Conference on Approximation and Fast Reanalysis Techniques in Engineering Optimization, June 14-27, 1998.*, 1998.

[2] O. Akiho. *Container having collapse panels with longitudinally extending ribs.* US patent 4.805.788, Tokyo, date of patent: 21-2-1989. Yoshino Kogyosho Co. Ltd.

[3] A.C. Alberghini. *Hot fill container with enhanced label support.* US patent 5.054.632, Atlanta, date of patent: 8-10-1991. Sewell Plastics.

[4] Anonimous. Inner cap prevents hot fill panelling. *Packaging News*, 6(5), 1988.

[5] Anonimous. Hot-filling. *Food Marketing and Technology*, 6(4):56–58, 1992.

[6] K.J. Bathe. *Finite Element Procedures.* Prentice-Hall, New Jersey, 1996.

[7] D.T. Berry. Formulation and experimental verification of a pneumatic element. *Int. J. Num. Meth. Eng.*, 39:1097–1114, 1996.

[8] N.D. Bhakuni, A.B. Trageser, S. Sundaresan, and K. Ishii. Structural optimization methods for aluminium beverage can bottoms. *In proceedings: ASME 1991*, 1:265–271, 1991.

[9] J. Booij and F. van Keulen. Consistent formulation of a triangular finite rotation shell element. *In proceedings: DIANA Computational Mechanics'94*, pages 235–244, 1994. Eds. G.M.A. Kusters and M.A.N. Hendriks.

[10] R.A. Bucklin, I.J. Ross, and G.M. White. The influence of grain pressure on the buckling load of thin walled bins. *Transactions of the ASEA*, 28(6):2011–2020, 1985.

[11] Firestone Industrial Products Company. *Firestone Airstroke Actuators and Airmount Isolators. Engineering Manual and Design Guide (MEMDG 997).* Firestone, Carmel, Indiana, 1997.

[12] G.R. Conrad. *Ovalized label panel for round hot filled plastic containers.* US patent 4.946.053, Vernon, Ind., date of patent: 7-8-1990. General Electric Company.

[13] M.J.R. Dack. *Solutions and Solubilities Part I.* John Wiley & Sons, New York, 1975.

[14] H. de Boer and F. van Keulen. Accurate semi-analytical design sensitivities. *Int. J. for Solids and Structures*, 37:6961–6980, 2000. 46-47.

[15] R.W. DiRaddo and A. Garcia-Rejon. Experimental and theoretical investigation of the inflation of variable thickness parisons. *Polymer Engineering and Science*, 34(13), 1994.

[16] D.D. Cerny *et al. Non-panelling container.* US patent 4.381.061, Muncie, Ind., date of patent: 26-4-1983. Ball Corporation.

[17] S. Hirata *et al. Biaxially drawn polyester vessel having resistance to heat distortion and gas barrier properties and process for preparation thereof.* UK patent GB 2.218.395, Tokyo, 1990. Toyo Seikan Kaisha Ltd.

[18] W.N. Collette *et al. Hott fill container.* US patent 4.863.046, Norwalk, Conn., date of patent: 5-9-1989. Continental Pet Technologies.

[19] Y. Hayashi *et al. Pressure resistant bottle shaped container.* US patent 4.877.141, Tokyo, date of patent: 31-10-1989. Yoshino Kogyosho Co. Ltd.

[20] M. Esslinger and B. Geier. Calculated postbuckling loads as lower limits for the buckling loads of thin-walled circular cylinders. *Buckling of Structures*, pages 274–290, 1976.

[21] C.D. Evans, G.R. List, H. Moser, and J.C. Cowan. Long term storage of soybean and cottonseed salad oils. *Journal of the American Oil Chemists' Society*, pages 218–222, 1973.

[22] S. Fishman, V. Rodov, J. Peretz, and S. Ben-Yehoshua. Model exchange dynamics in modified-atmosphere packages of fruits and vegetables. *Journal of Food Science*, 60:1078–1083, 1995.

[23] S. Flügge. *Encyclopedia of Physics; Thermodynamics of gases.* Springer-Verlag, Berlin, 1958.

[24] P.G.T. Fogg and W. Gerrard. *Solubility of Gases and Liquids.* John Wiley & Sons, New York, 1991.

[25] Y.C. Fung and E.E. Sechler. Buckling of thin-walled circular cylinders under axial compression and internal pressure. *Journal of Aeronautical Sciences*, 24(5):351–356, 1957.

[26] L.H. Going. Oxidative deterioration of partially processed soybean oil. *The Journal of the American Oil Chemists' Society*, 45:632–634, 1968.

[27] G.H. Golub and C.F. Van Loan. *Matrix Computations.* The John Hopkins University Press, Baltimore, 1989.

[28] T.I. Gombosi. *Gaskinetic Theory.* Cambridge University Press, Cambridge, 1994.

[29] W.S. Goree and N.A. Nash. Elastic stability of circular shells stabilized by a soft elastic core. *Proceedings of the Society for Experimental Stress Analysis*, 19(1):142–149, 1962.

[30] R.T. Haftka, Z. Gürdal, and M.P. Kamat. *Elements of Structural Optimization.* Kluwer Academic Publishers, Dordrecht, 1990.

[31] W.W. Hager. Updating the inverse of a matrix. *SIAM review*, 31(2):221–239, 1989.

[32] H. Hamada and T. Okumura ane E. Ohno. Optimum analysis method for thermoforming process by numerical approach. *In proceedings: Antec'95, Boston, Massachusetts*, 1:800–804, 1995.

[33] L.A. Harris. The stability of thin-walled unstiffened circular cylinders under axial compression including the effects of internal pressure. *Journal of Aeronautical Sciences*, 24(8):587–596, 1957.

[34] W. Herlitze, K. Becker, and R. Heiss. Berechnung einer kunststoffverpackung für sauerstoff-fempfindliche lebensmittel. *Verpackungs-Rundschau*, 7:51–54, 1973.

[35] H.D. Hibbit. Some follower forces and load stiffness. *Int. J. Numer. Methods Eng.*, 14:937–941, 1979.

[36] Karlsson & Sorensen Hibbit' *Abaqus Theory Manual Version 5.5.* Hibbit Karlsson & Sorensen, PawTucket, USA, 1995.

[37] M.H. Hilder. The solubility of water in edible oils and fats. *The Journal of the American Oil Chemists' Society.*, 45:703–707, 1968.

[38] M.H. Hilder. Oil storage, transport and handling. *In proceedings: Lipid Technology and Applications, Dekker, New York.*, 1:169–198, 1997.

[39] T.J.R. Hughes. *The Finite Element Method.* Prentice-Hall, New Jersey, 1987.

[40] Y.H. Hui. *Bailey's industrial oil and fat products.* John Wiley & Sons, New York, 1996.

[41] T. Ishitani and T. Inoue. Changes in oxygen concentration and volume of gas-flushed plastic pouches during storage. *Packaging Technology and Science*, 5:69–77, 1993.

[42] A.K. Kiritsakis. *Olive Oil.* American Oil Chemists' Society, 1990.

[43] I.M. Kolthof and P.J. Elving. *Treatise on Analytical Chemistry.* John & Wiley Sons, New York, 1983.

[44] N.C. Lee. *Plastics blow molding handbook.* Van Nostrand Reinhold, New York, 1990.

[45] T.S. Lee, H.R. Kwon, and J.U. Ha. Estimation of pressure and volume changes for packages of kimchi, a korean fermented vegetable. *Packaging Technology and Science*, 5:15–32, 1997.

[46] K. Loganathan, S.C. Chang, R.H. Gallagher, and J.F. Abel. Finite element representation and pressure stiffness in shell stability analysis. *Int. J. Numer. Methods Eng.*, 14:1413–1429, 1979.

[47] H.A. Mang. Symmetricability of pressure stiffness matrices for shell with loaded free edges. *Int. J. Numer. Methods Eng.*, 15:981–990, 1980.

[48] J.E. Mark. *Physical Properties of Polymers Handbook.* American Institute of Physics, 1996.

[49] J. Miltz, N. Passy, and C.H. Mannheim. Mass transfer from and trough packaging materials. *Packaging Technology and Science*, 5:49–52, 1992.

[50] J. Penzkofer. Untersuchungen zum einbeulen zylindrischen kunststoff-flaschen. *Verpackungsrundschau*, 34(9):61–68, 1983.

[51] C. Pfeiffer, M. d'Aujourdhui, J. Walter, J. Nüssli, and F. Escher. Auslegung von lebensmittelverpackungen computerunterstützte simulation der haltbarkeit. *Verpackungs-Rundschau*, 7:30–33, 1995.

[52] Metal Box p.l.c. *Heat-treatment of thermoplastic tubular articles.* GB patent 2 179 585 A, 1987.

[53] V.M. Ramm. *Absorbtion of Gases.* Israel Program for Scientific Translations, Jerusalem, 1968.

[54] E. Riks. Buckling analysis of elastic structures: A computational approach. *Advances in Applied Mechanics*, 34:373–384, 1997.

[55] D.V. Rosato. *Blow Molding Handbook.* Hanser/Gardner Publications Inc., Cincinnati, 1988.

[56] R.J. Ryder and J.A. Buttermore. *Packaging Encyclopedia.* Cahner, Des Plaines, IL, USA, 1989.

[57] K. Scheizerhof and E. Ramm. Displacement dependent pressure loads in nonlinear finite element analysis. *Computers & Structures*, 18(6):1099–1114, 1984.

[58] P. Seide. The stability under axial compression and lateral pressure of circular-cylindrical shells with a soft elastic core. *Journal of the Aerospace Sciences*, 29(7):851–862, 1962.

[59] J.L. Szanja. *In proceedings: SPE 39th Annual Technical Conf.*, pages 750–752, 1981.

[60] M.S. Talasila and A. Huyghebaert. Interaction of packaging materials and vegetable oils: oil stability. *Food Chemistry*, 64:451–459, 1999.

[61] P.C. Talasila and A.C. Cameron. Prediction equations for gases in flexible modified-atmosphere packages of respiring produce are different than those for rigid packages. *Journal of Food Science*, 62:926–930, 1997.

[62] J.M.T. Thompson and G.W. Hunt. *A General Theory of Elastic Stability*. John Wiley & Sons, London, 1973.

[63] V.V. Toropov, F. van Keulen, V. Markine, and H. de Boer. Refinements in the multi-point approximation method to reduce the effects of noisy structural responses. *In proceedings: 6th AIAA/NASA/ISSMO Symposium on Multidisciplinary Analysis and Optimization, Bellevue WA, September 4-6, A Collection of Technical Papers*, 2:941–951, 1996. AIAA-96-4087-CP, ISBN 1-56347-218-X.

[64] D. Tsiourvas, J. Pagidas, and A. Stassinopoulos. Development of plastic bottles resistant to lateral deformation. *Packaging Technology and Science*, 6:23–29, 1993.

[65] R. van Dijk. *Finite Element Optimisation of Plastic Bottles*. Graduation report TU-Delft, Faculty of Industrial Design Engineering, Delft, 1995.

[66] R. van Dijk. Fea as a design tool. *Packaging Today Europe*, 1(2):40–44, 1997.

[67] R. van Dijk, J.C. Sterk, F. van Keulen, and D. Sgorbani. Lateral deformation of plastic bottles; experiments, simulations and prevention. *Packaging Technology and Science*, 11:91–117, 1998.

[68] R. van Dijk and F. van Keulen. A finite rotation shell element taking into account pneumatic effects. *In proceedings: International Conference on Engineering Science 1998 (ICES'98), Atlanta, Georgia*, 1:808–813, 1998. Eds. S.N. Atluri and P.E. O'Donoghue.

[69] R. van Dijk and F. van Keulen. Simulation of closed-filled structures; permeability, solubility and chemical reactions. *In proceedings: European Conference on Computational Mechanics (ECCM'99), August 31 - September 3, 1999, Munich, Germany.*, 1999.

[70] R. van Dijk and F. van Keulen. Deformation of closed-filled packages due to oxidation, permeation and solubility effects; permeability, solubility and chemical reactions. *In proceedings: Fourth International Colloquium on Computation of Shell & Spatial Structures (IASS-IACM 2000), June 5 - June 7, 2000, Chania-Crete, Greece.*, 2000.

[71] R. van Dijk, F. van Keulen, and J.C. Sterk. Simulation of closed thin-walled structures. *Int. J. of Solids and Structures*, 37:6063–6083, 2000.

[72] F. van Keulen and J. Booij. Refined consistent formulation of a curved triangular finite rotation shell element. *Int. J. Num. Meth. Eng.*, 39:2803–2830, 1996.

[73] F. van Keulen, A. Bout, and L.J. Ernst. Nonlinear thin shell analysis using a curved triangular element. *Comp. Meth. Appl. Mech. Engng.*, 103:315–343, 1993.

[74] F. van Keulen and H. de Boer. Refined semi-analytical design sensitivities for buckling. *In proceeding: 7th AIAA/USAF/NASA/ISSMO Symposium on Multidisciplinary Analysis and Optimization*, 1:420–429, 1998.

[75] F. van Keulen and H. de Boer. Rigorous improvement of semi-analytical design sensitivities by exact differentiation of rigid body motions. *Int. J. Numer. Meth. Engng.*, 42:71–91, 1998.

[76] F. van Keulen and V.V. Toropov. New developments in structural optimization using adaptive mesh refinement and multi-point approximations. *Engineering Optimization*, 29:217–234, 1997.

[77] Centraal Bureau voor de Statistiek (ed.: N. Snijders). *Statistisch Jaarboek 2000*. Sdu Servicecentrum Uitgevers, Heerlen, The Netherlands, 2000.

[78] V.I. Weingarten, E.J. Morgan, and P. Seide. Elastic stability of thin-walled cylindrical and conical shells under combined internal pressure and axial compression. *AIAA Journal*, 3(6):1118–1125, 1965.

[79] O.C. Zienkiewicz and R.L. Taylor. *The Finite Element Method. Vol.1. Basic formulation and linear problems*. McGraw-Hill, London, 1989.

In this thesis it is illustrated how to minimize the weight of a package to the utmost extend. The example that has been referred to during the whole publication is a PET bottle for edible oil. This optimized bottle is currently in use by Unilever and material savings up to 25% have been achieved. For the optimization extensive use has been made from computer simulations. This thesis was carried out in cooperation with the Structural Optimization and Computational Mechanics group of the Faculty of Design, Engineering and Production of Delft University of Technology in The Netherlands.

This Ph.D.-project was fully sponsored by Unilever Research in Vlaardingen, The Netherlands.

This publication was also made possible by:

www.petcore.org

www.nvc.nl

www.mscsoftware.com

ISBN 90-9015084-6